UNI-AXIAL TENSION TESTING ON SYNTHETIC FIBRE REINFORCED CONCRETE

by

Lynsey Ann Poushay

Submitted in partial fulfilment of the requirements
for the degree of Master of Applied Science

at

Dalhousie University
Halifax, Nova Scotia
August 2012

DALHOUSIE UNIVERSITY

DEPARTMENT OF CIVIL AND RESOURCE ENGINEERING

The undersigned hereby certify that they have read and recommend to the Faculty of Graduate Studies for acceptance a thesis entitled "Uni-Axial Tension Testing on Synthetic Fibre Reinforced Concrete" by Lynsey Ann Poushay in partial fulfilment of the requirements for the degree of Master of Applied Science.

Dated: August 2, 2012

Supervisor _____

Readers _____

_____

DALHOUSIE UNIVERSITY

DATE: August 2, 2012

AUTHOR: Lynsey Ann Poushay

TITLE: Uni-Axial Tension Testing on Synthetic Fibre Reinforced Concrete

DEPARTMENT OR SCHOOL: Department of Civil and Resource Engineering

DEGREE: MASc CONVOCATION: October YEAR: 2012

_____

Signature of Author

To Mom, Dad, Jacqueline, Heather, Nicole, Colin, and Janelle for always doing their best to understand, even when I made it difficult for them.

TABLE OF CONTENTS

LIST OF TABLES

LIST OF FIGURES

ABSTRACT

The purpose of this research was to determine uni-axial response of synthetic fibres required for structural design. The stress versus crack opening curves, required by RILEM for structural design of fibre reinforced concrete, were determined for each fibre type investigate and were used to compare the per fibre post-crack response, the pullout curves, and the flexural response. A study of the fibre distribution was conducted in order to determine the orientation factor required to predict the number of fibres expect in the tensile specimen crack face. The orientation factor, dosage, fibre geometry, and per fibre post-crack response were determined in order to predict the resulting tensile strength of a concrete mix. The tensile strength was compared to that of steel fibre currently being used in structural applications. The synthetic fibres tested only achieve a small percentage of their ultimate tensile strength; in order to produce synthetic fibres for structural applications, the bond strengths must be improved.

LIST OF ABBREVIATIONS AND SYMBOLS USED

ACI	American Concrete Institute
AFT	Atlantic Fiber Technologies Limited
ASTM	American Society for Testing and Materials
CMOD	crack mouth opening displacement
EVA	ethylene vinyl acetate
FCM	fictitious crack model
FEM	finite element method
FPZ	fracture process zone
FRC	fibre reinforced concrete
HDPE	high density polyethylene
LVDT	linear variable displacement transducer
MAH	melaic anhydrice
PP	polypropylene
PVDF	poly(vinylidene fluoride)
RILEM	International Union of Laboratories and Experts in Construction Materials, Systems, and Structures
RSI	residual strength index
SOG	slab on grade
UTT	uni-axial tension test
w/c	water cement ratio
WST	wedge-splitting test
WWF	welded wire fabric
A_c	cross sectional area of the cylinder (mm^2)

A_f	fibre cross section (mm^2)
A_n	cross sectional area of notch cylinder (mm^2)
b	average width of the specimen (mm)
d	average depth of the specimen (mm)
D	fibre dosage (kg/m^3)
d_{eq}	equivalent fibre diameter (mm^2)
E	modulus of elasticity (GPa)
E_f	elastic modulus of fibre (GPa)
f'_c	compressive strength (MPa)
f_1	first-peak strength (MPa)
f_P	peak strength (MPa)
$f_{R,I}$	residual flexural strength (MPa)
f_t	peak tensile strength (MPa)
F_{sp}	splitting force applied during the WST (kN)
F_v	vertical force recorded during the WST (kN)
f^D_{600}	residual strength at a net deflection of L/600 (MPa)
f^D_{150}	residual strength at a net deflection of L/150 (MPa)
G_F	material fracture toughness (J)
h	depth of stiffening bars or the depth of the beam (m)
k	neutral axis depth ratio
L	beam specimen span length (mm)
M	moment (N-m)
M_{bcr}	bilinear cracking moment (N-m)
M_{cr}	moment at first cracking (N-m)

M_{cr2}	reduced cracking moment (N-m)
M_{it}	moment at intersection point (N-m)
n	total number of effective fibres in crack plane
P	applied load during UTT (kN)
P_1	first-peak load (kN)
P_P	peak load (kN)
P^D_{600}	residual load at a net deflection of L/600 (kN)
P^D_{150}	residual load at a net deflection of L/150 (kN)
T^D_{150}	toughness, taken as area under load vs. deflection curve between a net deflection of 0 and L/150 (J)
V_f	volume fraction of fibre (%)
w	crack width (mm)
w_c	critical crack width (mm)
$\bar{w}$	abscissa of the centroid of the softening area (mm),
α	orientation coefficient
β_{crit}	normalized critical tensile strain
β_{tu}	normalized ultimate tensile strain
δ	displacement (mm)
δ_1	net deflection at the first-peak load (mm)
δ_{bcr}	deflection at bilinear cracking moment (mm)
δ_P	net deflection at the peak load (mm)
δ_u	deflection at ultimate moment (mm)
ε_c	compressive strain
ε_{cr}	first cracking tensile strain

ε_{cu}	ultimate compressive strain
ε_{cy}	compressive strain at yielding
ε_{t}	tensile strain
ε_{tu}	ultimate tensile strain
ϕ	curvature (mm^{-1})
ϕ_{bcr}	bilinear cracking curvature (mm^{-1})
ϕ_{cr}	curvature at first cracking (mm^{-1})
ϕ_{it}	curvature at intersection point (mm^{-1})
Φ_{cr}	safety factor for the cracking strain
$\Phi_{cracking}$	safety factor for the cracking stress
Φ_{fibre}	safety factor for *n*
$\Phi_{post\ crack}$	safety factor for the cracking stress
κ_{h}	size-dependent safety factor
λ	normalized top compressive strain
λ_{cu}	normalized top ultimate compressive strain
λ_{tu}	normalized top compressive strain when bottom fibre reaches ultimate tensile strain
μ	normalized post peak tensile strength
ρ_{f}	density of the fibre (kg/m^3)
$\sigma(w)$	stress-crack width displacement response (mm-MPa)
$\sigma(w)_{f}$	per fibre stress-crack width displacement response (mm-MPa)
σ_1	peak tensile strength of FRC (MPa)
σ_2, σ_3,	residual tensile strength (MPa)
σ_c	compressive stress (MPa)

σ_{cy}	compressive yield stress (MPa)
σ_f	tensile strength of fibre (MPa)
σ_{FRC}	FRC tensile strength (MPa)
σ_t	tensile stress (MPa)
σ_{UTT}	tensile strength of fibre in matrix (MPa)
σ_w	tensile stress in crack opening (MPa)
ω	compressive to tensile strength ratio

ACKNOWLEDGEMENTS

Thank you to Dr. Dean Forgeron for all his supervision and guidance throughout this project. Thank you to my supervisory committee, Dr. John Newhook and Dr. George Jarjoura. Thank you to the faculty and staff of the Civil and Resource Engineering Department, especially Shelley Parker, Tanya Timmins, and June Ferguson.

Thank you to Brian Liekens for reminding me that sometimes the best solution to a problem is to take a little break. Thank you to all my friends for their patience, but especially Shannon O'Connell for knowing exactly what it is like and Kaylee Shannon for countless telephone calls and hours of advice, reassurance, and support.

Most importantly, thank you to my family who have always had complete faith in my abilities, even at times when I did not. I could not have done this without all of your love.

CHAPTER 1 INTRODUCTION

1.1 FIBRE REINFORCED CONCRETE

Concrete has the largest production value of all man-made materials. Concrete is favourable when compared to other construction materials because of its low cost, general availability of raw materials, adaptability and utilization under different environmental conditions. Because of these advantages concrete is likely to continue to dominate as a construction material for the foreseeable future.

One disadvantage of concrete is its low tensile strength and strain capacity; with a tensile strength to compressive strength ratio of approximately 1:10. As a result, the tensile strength of concrete in design is normally taken as zero and tensile reinforcing is supplied in the regions required to resist tensile loading. Traditionally, reinforcing steel in the form of reinforcing bars or welded wire fabric is used to resist tensile stresses in concrete structures.

In the past few decades a trend has emerged in the concrete industry where discrete fibre reinforcement of varying sizes, geometries, and materials types is being used as reinforcement in what is generally known as fibre reinforced concrete (FRC). The concept of adding steel fibres to concrete was first introduced early in the twentieth century. Midway through the century other materials came into use such as glass and synthetic fibres. Initially, fibres were used to prevent and control plastic and drying shrinkage induced cracking; however, it was observed that fibres had a beneficial effect on some other material properties such as flexural toughness, fatigue resistance, impact resistance, and post-crack strength.

Fibres used in FRC generally fall within two categories; micro-fibres and macro-fibres. Micro-fibres typically have diameters less than 0.25 mm and range from 1 to 50 mm in length. They are made from a variety of materials such as polypropylene, steel, and carbon. These fibres have a very high surface area which results in low workability. For this reason they are

typically added at low rates (0.1 to 0.3 % volume). Micro-fibres provide concrete with increased green strain capacity by intercepting and arresting internal shrinkage induced cracks and therefore have been shown to be an effective method of reducing the occurrence of plastic shrinkage cracking. Micro-fibres have a negligible effect on the toughness, abrasion, and impact resistance of concrete due to their low tensile capacity and the low dosage rates that are typically used (Trottier et al., 2002).

Macro-fibres are generally 0.3 to 1 mm in diameter and 25 to 60 mm long. They are made of steel or synthetic materials, such as polypropylene, polyethylene, and polymer blends. These fibres are generally added in high fiber dosages compared to micro-fibres, 0.3 to 2.0 % by volume. In general these fibres are too large and far apart from each other to have a significant effect on plastic shrinkage cracking but they do impart post-crack tensile resistance by bridging and transferring loads across cracks. The addition of macro fibers to concrete results in effects on the material properties mentioned above, flexural toughness, fatigue resistance, impact resistance, and post-crack strength (Trottier et al., 2002).

1.2 PROJECT OBJECTIVES

This research is part of a larger project to increase the use of synthetic fibres in structural applications by studying the response of commercially available and prototype fibres, produced by Atlantic Fiber Technologies Limited.

This thesis will focus on determining the uni-axial tensile response necessary for structural design incorporating FRC. In order to make the UTT procedure RILEM has proposed more widely available, the viability of a UTT completed without closed-loop feedback was investigated and adjustments made to the test setup in order to produce results comparable to a closed-loop setup. The post-crack responses of each fibre type and dosage were examined in order to determine the parameters required for synthetic fibres to be used in structural applications.

Also, methods for comparing the flexural and tensile responses of FRC were investigated. Flexural testing, such as the ASTM C1609-10 "Standard Test Method for Flexural Performance of Fiber-Reinforced Concrete", is routinely performed for quality control purposes. A reliable method of correlating the flexural load-deflection response to the stress-crack width opening ($\sigma(w)$) or stress-strain (σ–ε) response of FRC would greatly simplify the design process and eliminate the need for more complicated and expensive tensile testing.

CHAPTER 2 BACKGROUND

2.1 STRUCTURAL APPLICATIONS OF FIBRE REINFORCED CONCRETE

The term "synthetic fibre" refers to fibre contain a range of synthetic materials. A summary of the properties of typical materials can be seen in Table 2.1. In addition to these materials, other substances can be used in the production of synthetic fibres as binders which help bind together materials that normally would not blend. Melais anhydrice (MAH) is know to promote adhesion between polyolefins (Yu et al., 2009). Also, materials can be used specifically to help produce a chemical bond with the concrete, such as Ethylene vinyl acetate (EVA). Synthetic fibres typically contain more than one material; the different components and the amounts used are determined by considering the tensile and bonding properties desired as well as cost.

Table 2.1 – Summary of properties of common synthetic materials

Fibre Material	Abbrev.	σ_f (MPa)	E_f (GPa)	Relative Bond Strength	Approx. Cost (US/kg)
High Density Polyethylene	HDPE	400	5-6	Low	2
Polypropylene	PP	500-750	5-7	Low	3
Poly(vinylidene fluoride)	PVDF	350	2	High	32

In 2001 Tuf-Strand SF was developed by Trottier et al., containing 77% PP and 23% HDPE. Tuf-Strand SF is a self-fibrillating fibre produced by AFT and sold commercially by Euclid Chemical Company. Due to its commercial success and proven performance in FRC (Trottier et al., 2002), Tuf-Strand SF has been used as the main focus for this research.

2.2 STRUCTURAL APPLICATIONS OF FIBRE REINFORCED CONCRETE

The use of fibre reinforcing to partially or completely replace tradition steel rebar reinforcing in structural applications has been increasing throughout

the past three decades. Steel fibres have been used to improve the toughness, ductility, and impact resistance of concrete. Though synthetic fibres were originally developed for their beneficial effects on plastic and drying shrinkage of concrete, new high performance synthetic fibres aimed at structural applications are being developed (O'Connell, 2011). The tensile properties of these fibres and the material performance of FRC containing them in flexural testing indicate that synthetics can be used to replace steel fibres in many applications (Sorelli et al, 2006). The three main structural applications of fibre reinforced concrete are: slab on grade (SOG), elevated slab, and shotcrete.

2.2.1 Slab on Grade

Fibre reinforced concrete has been in use in industrial pavements, roads, parking areas, warehouse floors, and airport runways for well over a decade (Sorelli, et al, 2006). Guidelines for the use of steel fibre reinforced concrete in SOGs were developed in the United Kingdom in 1992 (Mobasher and Destrée, 2010). The discrete nature of traditional reinforcing bars or welded wire mesh (WWM) reinforcing can result in excessive deformations and cracking due to the heavy concentrated loads from industrial machinery and shelves often imposed on SOG. Steel fibres improve the load-carrying capacity of SOG and have been used as partial and total replacement of conventional reinforcement at relatively low fibre volumes, less than one percent (Sorelli et al., 2006).

Slabs on grade must be designed to withstand impact and fatigue loading caused by heavy industrial equipment travelling repeatedly across the slabs, often along the same travel routes. The increased ductility and toughness fibre reinforcing lends to concrete, even at low contents, makes FRC ideal for these applications (Sorelli et al., 2006).

Shrinkage of SOG resulting in joint distress and movement can result in several issues, including edge cracking, joint spalling, curling, and faulting.

Synthetic macro-fibres can be used to control the dry shrinkage cracking of SOG; total crack openings can be reduced by a factor of four compared to plain concrete (Mobasher and Destrée, 2010). The use of FRC can also reduce the curling and joint opening of slabs. Welded-wire mesh is less effective than fibres in obtaining flatter slabs and must be continuous over a crack or joint for any significant resistance (Mobasher and Destrée, 2010).

Microfibers have been used for decades to reduce plastic shrinkage cracks which form during the early plastic stage of curing and can develop into macro cracks throughout the life of the composite. Synthetic microfibers have been used to reduce plastic shrinkage by up to 90% when compared to traditional reinforcement (Senthilkumar and Natesan, 2005). The beneficial effects fibres have on shrinkage results in slabs which can have larger bay areas and reduced numbers of construction joints.

2.2.2 Elevated Slab

Steel fibres have been used to reinforce several million square meters of SOG, proving this type of reinforcing system can successfully resist high moments, shear, and punching shear stresses. The application of this type of reinforcement has been extended to pile supported and elevated floor slabs (Mobasher and Destrée, 2010).

In SOG applications where the ground is unable to support the slab, piles are used. Piles may be used when the soil-structure interaction would result in differential settlement or plastic settlement of the soil; over time, this settlement would lead to loss of contact with the ground. Piles may also be used when the ground does not have the bearing capacity required by the slab or the soil is expansive, such as swelling clay, and the slab cannot rest on the ground (Mobasher and Destrée, 2010).

Mobasher and Destrée propose a design method for elevated slabs which uses a σ–ε response of FRC, similar to the response described by RILEM (Vandewalle et al., 2003a), to determine the slabs' moment capacity.

2.2.3 Shotcrete

Shotcrete has been in use since the 1970's in a variety of applications including new construction, repair and rehabilitation of old and deteriorating structure, retaining walls, for slope stabilization and in tunnel lining. The most common use of fibre reinforced shotcrete is in the design of tunnel lining.

Installing WWM as reinforcement on the irregular surface of tunnel lining is difficult and time consuming. The WWM cannot always be fitted close to the tunnel surface and the shotcrete must fit through the reinforcing to fill the gaps resulting in inefficient use of material and voids. When fibres are used to replace the WWM, less material is required to obtain better coverage. Fibre reinforced shotcrete has become popular because of its economic and structural competitiveness that often new tunnel construction makes use of the material (Bernard, 2002).

Tunnel lining design is a complicated process due to the variety of groundwater, rock, and soil conditions. Damage from water leakage and freeze/thaw cycles is common as well as high local deformations and displacements due to earth loads and rock burst. The effects of fibre reinforcing on the mechanical properties of shotcrete, including increased crack resistance, fibre bridging of cracks, and toughness, make it ideal to resist these types of loadings (Won et al., 2009).

2.3 FRACTURE TOUGHNESS OF FIBRE REINFORCED CONCRETE

The addition of fibre reinforcement changes the brittle crack behaviour of concrete to create a more ductile material. The concrete is capable of absorbing more energy during fracture due to the post crack bridging effect of fibres. This enhances the performance of concrete under static, fatigue, impact, and impulse loadings. The energy absorption of FRC is described as the fracture "toughness".

In 1976, Hillerborg suggested the fictitious crack model (FCM) to explain crack formation in plain concrete. The FCM was initially intended to be applied to FEM analysis but can easily be adapted to other numerical and analytical models and has become a widely used model in fracture mechanics because of its versatility and simplicity (Vandewalle et al., 2002). Later, this model was adapted to cracking mechanics in FRC (Hillerborg, 1980).

Hillerborg (1980) found that in the case of plain concrete the stress-crack mouth opening displacement ($\sigma(w)$) curve takes the shape shown in Figure 2.1. A cohesive force generated in the process zone and by aggregate interlock is observed in plain concrete. In general, a great decrease in stress occurs for *w*-values below 0.02-0.1 mm and some residual stress remains up to the critical crack width, w_c.

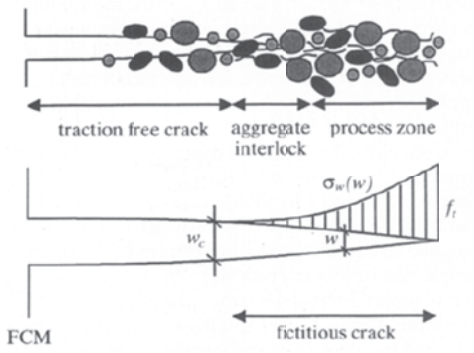

Figure 2.1 – Features and $\sigma(w)$ curve of plain concrete (Vandewalle et al., 2002)

Where:

w is the crack width (mm),

w_c is the crack width when σ is zero (mm),

f_t is the peak tensile strength (MPa) and

$\sigma_w(w)$ is stress-crack width displacement response (mm-MPa)

The material fracture toughness, G_F, represents the energy absorbed per unit area of crack and is regarded as a material fracture parameter for plain concrete. The area underneath the curve denotes G_F and can be expressed as:

$$G_F = \int_0^{w_c} \sigma(w)dw \qquad [2.1]$$

Where:

w is the crack width (mm) and

w_c is the crack width when σ is zero (mm)

The σ(w) curve for FRC, seen in Figure 2.2, is greatly influenced by the addition of fibres. A theoretical analysis of the curve was also proposed but it requires many assumptions and estimations to be made with respect to the initial length of the fracture process zone (FPZ), the bond-slip relationship of different fibre types, the orientation of the fibres bridging the crack, and the behaviour of oblique fibres in the FPZ. The action of fibres is very complex and does not result in any specific critical crack width at which to limit the fracture toughness, G_F. For these reasons it is best to determine the σ(w) curve experimentally rather than theoretically (Hillerberg, 1980).

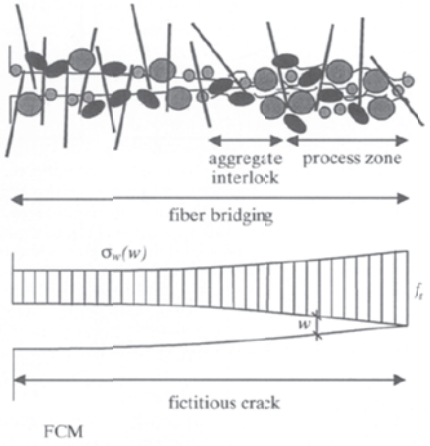

Figure 2.2 - Features and σ(w) curve of fibre reinforced concrete (Vandewalle et al., 2002)

2.4 RILEM STRESS-STRAIN DESIGN METHOD

The RILEM Technical Committee 162-TDF has proposed a σ–ε design method in order to incorporate the benefits of fibre reinforcement into structural applications. This method relies on the determination of the σ–ε relationship of the material in both compression and tension, as shown in Figure 2.3. Once this relationship has been determined it can be applied to the typical reinforced concrete beam cross-section as shown in Figure 2.4 (Vandewalle et al., 2003a). The σ–ε or σ(w) relationships can describe the contribution of fibre in FRC. These relationships can be determined using simplified design models or direct experimental determination.

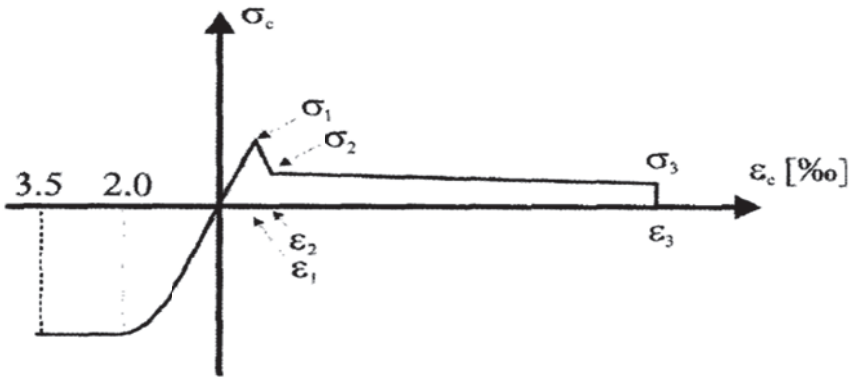

Figure 2.3 - σ–ε diagram (Vandewalle et al., 2003a)

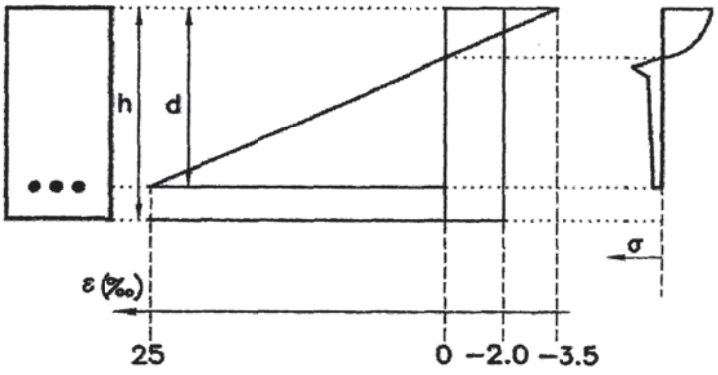

Figure 2.4 - Cross sectional stress and strain distribution (Vandewalle et al., 2003a)

Where:

σ_1 is the peak tensile strength (MPa),

σ_2, σ_3 are the post crack residual strengths at ε_2, ε_3 (MPa),

ε_1 is the peak tensile strain,

ε_2 is ε_1 + 10%,

ε_2 is 25% and

h is depth of stiffening bars or the depth of the beam (m)

2.5 Stress-Crack Mouth Opening Displacement Relationship

In order to describe the $\sigma(w)$ curve of plain concrete, the fictitious crack model was proposed by Hillerborg (1976). In FRC, the fibres bridge the crack and provide a closing force similar to the cohesive force observed in plain concrete; because of this, the $\sigma(w)$ curve can be used to describe the residual force provided by the fibres (Hillerborg, 1980). This model has proven very applicable to the description of fracture in FRC and has been widely adopted by researchers (Vandewalle et al., 2002). However, the FCM approach must be modified when applied to FRC due to fibre bridging being closely related to fibre debonding and pullout. The fibre bridging effect on $\sigma(w)$ curve can be seen in Figure 2.2.

The $\sigma(w)$ relationship of FRC can be defined by the separate contributions of the concrete and fibre, shown in Figure 2.5. Observed in crack openings up to crack openings of about 0.1-0.2 mm, the $\sigma(w)$ curve is the result of both the concrete and fibre contributions combined. For larger crack openings the relationship is mainly defined by the fibre bridging action. The $\sigma(w)$ curve can be defined by several simplified relationships. Most commonly used are the multi-linear, bi-linear, and free-form relationships.

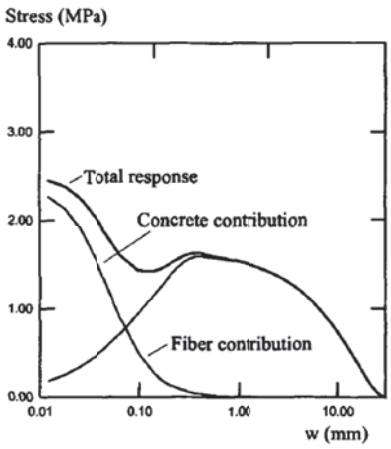

Figure 2.5 - Conceptual theoretical modeling of σ(w) relationships showing concrete and steel fibre contributions (logarithmic scale) (Vandewalle et al., 2002)

2.5.1 Multi-linear Relationship

The σ(w) relationship in steel FRC can be realistically described with a multi-linear function.

$$\sigma_w = \sigma_i - \alpha_i w \;\; for\; w_{i-1} < w \leq w_i = \frac{\sigma_{i+1} - \sigma_i}{\alpha_{i+1} - \alpha_i} \qquad [2.2]$$

$$w_0 = 0;\; \sigma_1 = f_t;\; \alpha_1 > 0 \qquad [2.3]$$

Where:

w_0 is a crack width of 0 (mm),

f_t is the peak tensile strength (MPa) and

α_1 is the verticle portion of the slope between w_0 and w_1

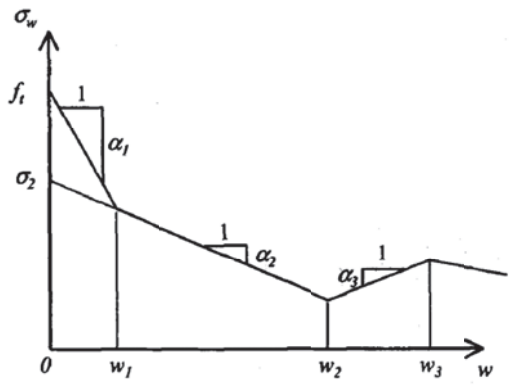

Figure 2.6 - Multi-linear σ(w) relationship (Vandewalle et al., 2002)

As shown in Figure 2.6, the slopes can be either positive or negative but it is assumed that after softening occurs the tensile strength is never reached again (Vandewalle et al., 2002).

2.5.2 Bi-linear Relationship

A general bi-linear function has proven very useful to describe the σ(w) relationship in concrete and other materials. This relationship is characterized using four parameters; the tensile strength, f_t, the fracture energy, G_F, the abscissa of the centroid of the softening area, w, and the horizontal intercept, w_1 of the initial linear portion. A general bi-linear relationship can be seen in Figure 2.7.

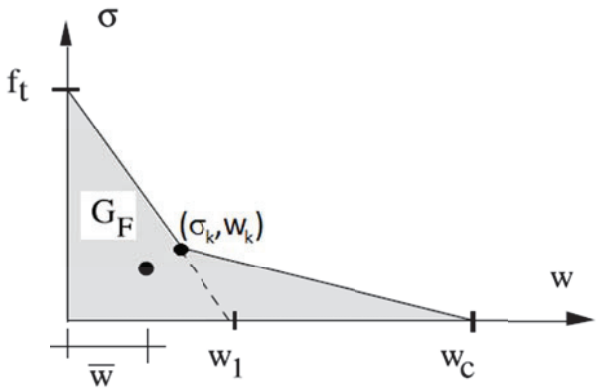

Figure 2.7 - General bi-linear softening curve, the centroid of the shaded area is marked with a dot (Elices et at., 2002)

Elices et at. (2002) determined these parameters using the split-cylinder or prism test and the three-point bending test. Whereas the peak load occurs before much softening takes place in the body of uncracked specimens, the peak load-specimen size curve of the split-cylinder test and the three point bending test can be used to determine f_t and w_1. The G_F and w were both determined using the three-point bending test; using the area under the complete load-displacement curve and the far post-peak trend of this curve, respectively. This results in the following relationships:

$$\sigma_w(w) = f_t(1 - w/w_1) \;\; for \;\; 0 \leq w \leq w_k \qquad [2.4]$$

$$\sigma_w(w) = \sigma_k \left(\frac{w - w_c}{w_k - w_c} \right) \;\; for \;\; w_k \leq w \leq w_c \qquad [2.5]$$

Where (σ_k, w_k) are the coordinates of the kink point, given by:

$$w_k = w_1 \frac{w_c - 2\,G_F/f_t}{w_c - w_1} \qquad [2.6]$$

$$\sigma_k = f_t \frac{2\,G_F/f_t - w_1}{w_c - w_1} \qquad [2.7]$$

And w_c, the critical opening, can be obtained from the quadratic equation:

$$w_c^2 - w_c \frac{6\bar{w}\,G_F/f_t - 2w_1\,G_F/f_t}{2\,G_F/f_t - w_1} + \frac{6\bar{w}w_1\,G_F/f_t - 4w_1\,(G_F/f_t)^2}{2\,G_F/f_t - w_1} = 0 \qquad [2.8]$$

Where:

$\bar{w}$ is the abscissa of the centroid of the softening area (mm),

G_F is the fracture energy (J),

f_t is the peak tensile strength (MPa) and

w_1 is the horizontal intercept of the initial linear portion (mm)

RILEM (2002) provides the following general description of the bi-linear relationship based on Figure 2.8:

$$\sigma_w(w) = \sigma_1 - \alpha_1 w \ \ for \ \ 0 \le w \le w_1 = \frac{\sigma_2 - \sigma_1}{\alpha_2 - \alpha_1};\ \alpha_1 > 0;\ \sigma_1 = f_t \qquad [2.9]$$

$$\sigma_w(w) = \sigma_2 - \alpha_2 w \ \ for \ \ w_1 < w \le w_c = \frac{\sigma_2}{\alpha_2};\ \alpha_2 > 0 \qquad [2.10]$$

Where:

α_1 is the verticle portion of the slope between w_0 and w_1 and

α_2 is the verticle portion of the slope between w_1 and w_c

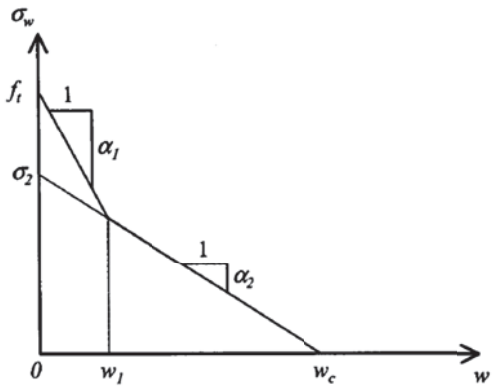

Figure 2.8 - Bi-linear σ(w) relationship (Vandewalle et al., 2002)

2.5.3 Free-form Relationship

Stang et al. (1995) proposed an empirical model for determining σ(w) relationship. After the FRC has reached a maximum stress, σ_m^u, the stress transferred over the crack, σ_a, for any given crack opening, *w*, can be expressed by Equation 2.11. Two parameters are used to describe the relationship; a parameter corresponding to the crack opening at which the stress has dropped to half of the maximum stress, w_0, and a parameter used to describe the shape of the softening process, *p* (Stang et al., 1995).

$$\sigma_a = \frac{\sigma_m^u}{1 + (w/w_0)^p} \qquad [2.11]$$

The two parameters, related to the post-peak behaviour, can be modified to allow the model to be applied to a variety of FRC. In Figure 2.9 the influence of the shape parameter for a fixed value of w_0 is shown.

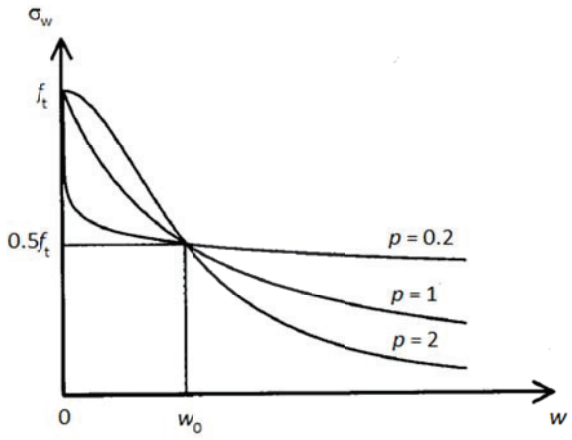

Figure 2.9 - Free-form σ(w) relationship showing influence of parameter p for a fixed w_0 (Vandewalle et al., 2002)

2.6 EXPERIMENTAL DETERMINATION OF STRESS-CRACK OPENING DISPLACEMENT RELATIONSHIP

The experimental determination of the σ(w) curve can be completed in two ways; (i) verification of the simplified relationships presented in the previous section via indirect methods and (ii) direct determination of the relationship. Neither method has been accepted as a standard test (Vandewalle et al., 2002).

2.6.1 Indirect Methods

Indirect determination of the σ(w) curve requires an inverse analysis of the test output, most commonly in the form of a load-crack mouth opening displacement (CMOD) curve. The goal of this analysis is to minimize the difference between an analytical curve and the test results in order to determine the material parameters. The three point bending test and the wedge-splitting test are described in the following sections, followed by a description of the inverse analysis conducted on the results of these tests conducted by Löfgren et al. (2005).

Bending Test

A standard test method for the three-point bending test has been recommended by the RILEM Technical Committee 162-TDF (2000). The test specimen is a concrete beam of 150 x 150 mm cross section and minimum length of 550 mm with a notch cut as shown in Figure 2.10.

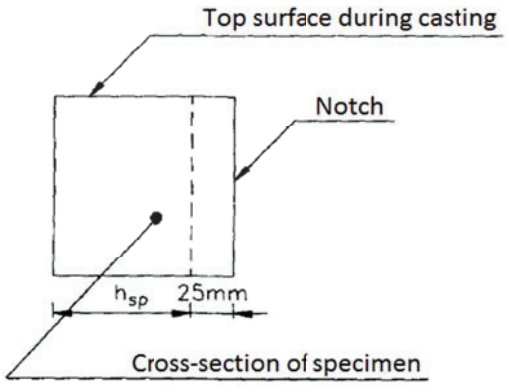

Figure 2.10 - Beam cross section with position of sawn notch illustrated (Vandewalle et al., 2000)

The test setup and loading procedure is shown in Figure 2.11. The beam is supported on two roller supports 30 mm in diameter which are free to rotate. The setup must allow for horizontal movement during loading which eliminates transmission of any horizontal forces on to the test specimen. The testing machine must be capable of producing a constant rate of deflection in the specimen. This is most easily achieved through the use of a closed loop system, using the specimen deflection as feedback. A test machine which only produces a constant rate of load is not capable of producing an accurate curve after the peak load. The setup must be stiff enough and fast enough to avoid instability in the deflection measurements.

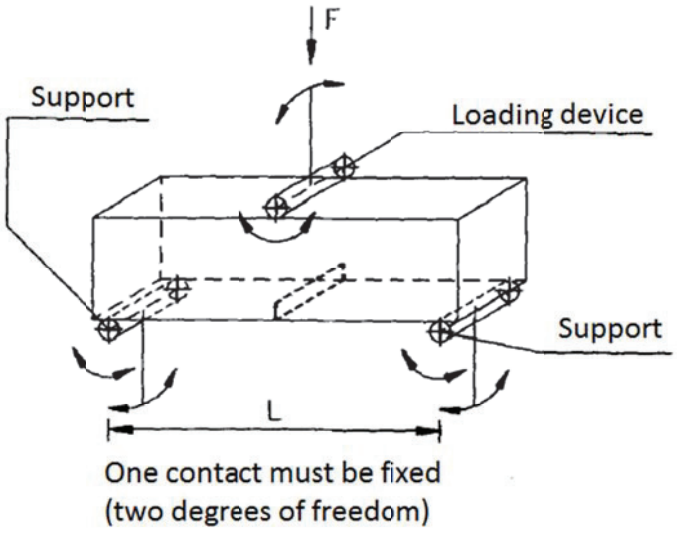

Figure 2.11 - Position of the load and supports of the beam specimen (Vandewalle et al., 2000)

The measuring apparatus must be capable of accurately measuring the mid-span deflection excluding any deformation occurring in the machine or specimen supports. The deflection is measured on both sides of the specimen in the RILEM setup as can be seen in Figure 2.12.

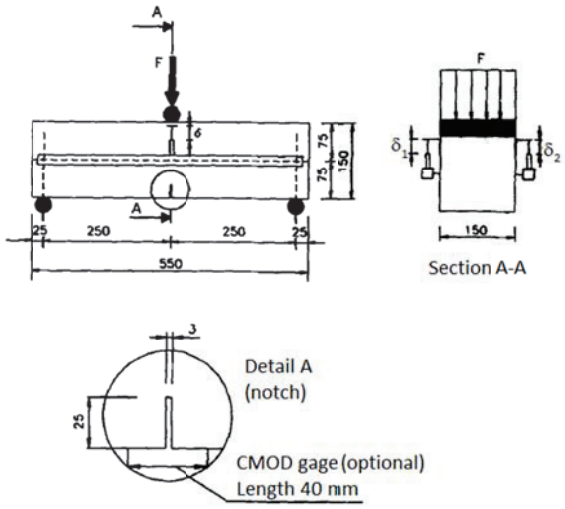

Figure 2.12 - Arrangement of displacement monitoring gauges (Vandewalle et al., 2000)

In order to determine the $\sigma(w)$ curve, the CMOD must be measured. The test can also be performed under CMOD control instead of deflection control.

When this method is used to determine the σ–ε curve, RILEM requires size-dependent safety factors to be applied. When experimental results were compared with design predictions made before the introduction of the safety factors, the design method resulted in severe overestimations of carrying capacities. The origin of this size effect is not fully understood; it may be due to discrepancies in material properties between batches, a size effect intrinsic to the method, or a combination of both (Vandewalle et al., 2003a).

Wedge-Splitting Test

The wedge-splitting test (WST) was originally proposed by Linsbauer and Tschegg (1986) and was further developed by Brühwiler and Wittmann. The primary benefit of the WST is that it does not require sophisticated test equipment; the test can be performed stably on a mechanical testing apparatus with a constant crosshead displacement (Löfgren et al., 2008).

The specimen geometry and loading procedure are shown in Figure 2.13; the specimen is prepared with a cast groove in order for the wedge device to apply a splitting load. Also, a starter notch is cut into the specimen in order to avoid any wall effects on the test results. Steel platens with roller bearings, placed partly on top of the specimen and partly in the groove, allow a wedge device to apply a splitting force, F_{sp}.

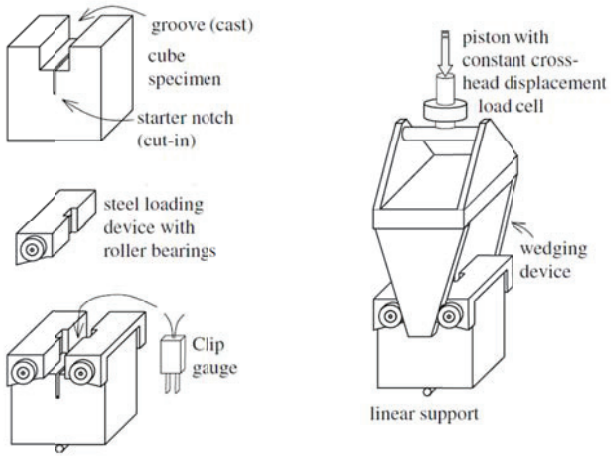

Figure 2.13 - Schematic of the WST specimen and testing arrangement (Löfgren et al., 2008)

During the test, two parameters are recorded; the load in the vertical direction, F_v, and the CMOD. The CMOD is the deflection measured in the groove at the level of the roller bearings. The relationship between the vertical and the splitting force is shown schematically in Figure 2.14 below (Löfgren et al., 2008).

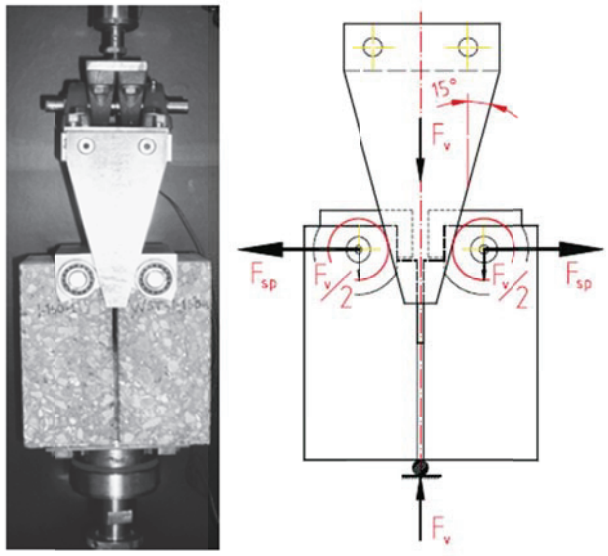

Figure 2.14 - Experimental setup for the WST (Löfgren et al., 2008)

Method of Inverse Analysis

Löfgren et al. (2005) conducted inverse analysis on both the bending and wedge-splitting tests. A Matlab® program was developed by Østergaard (2003) based on a cracked hinge model that assumed a bi-linear σ–ε relationship and was proposed by Olesen (2001). The analysis is performed in three phases: the modulus of elasticity is determined (phase I), the tensile strength and first slope of the curve, α_1 (from Figure 2.8) are determined (phase II), and the remaining parameters, α_2 and σ_2, are determined (phase III). For each phase an optimization procedure was conducted and the analysis performed until there was less than 1.0% difference between two subsequent iterations.

Löfgren et al. (2005) also conducted inverse analysis assuming a poly-linear σ–ε relationship using the finite element program DIANA. The crack was assumed to be a discrete crack with non-linear interface elements and plane stress conditions. Outside the crack the concrete was assumed to have linear elastic and isotropic behavior. Since no automatic procedure was used in the FEM analysis, the σ(w) curve was manually changed until a curve that fitted the test results was obtained.

The inverse analysis of FRC can be very complicated because there is no unique solution for any given curve. If the σ(w) curve being determined is complex and requires many parameters to describe it, the iteration of the estimation can become difficult and time consuming; however, simple relationships requiring few parameters may not be able to converge to a good solution. Though researchers have proposed different solutions to overcome some of the problems, the non-uniformity of fibre orientation and distribution across the specimen height continues to cause issues.

2.6.2 Direct Method

The σ–ε relationship can also be determined using a direct test, most commonly the UTT. The σ(w) curve can be determined directly from the test

data and does not require complicated analysis as noted for the previously mentioned test methods. The UTT, however, is very time-consuming and requires sophisticated testing equipment. Test results can be affected by machine-specimen interactions when a testing machine of insufficient stiffness is used (Löfgren et al., 2005).

Uni-axial Tension Test

RILEM Technical Committee 162-TDF has proposed a standard test method for the UTT (Vandewalle et al., 2001). The recommended procedure is a displacement controlled test on a notched cylindrical specimen which can be performed on plain concrete or any FRC that exhibits strain softening behaviour. The specimens can either be cast or cored from an existing structure. The standard specimen has a diameter and height of 150 mm and a cut notch as shown in Figure 2.15. The maximum acceptable aggregate size and fibre length are 32 mm and 60 mm, respectively.

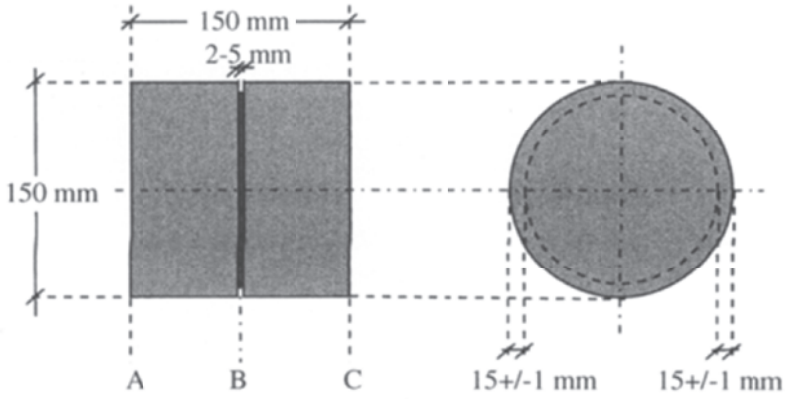

Figure 2.15 - Schematic of the standard test specimen for the uni-axial tensile testing. Planes A, B, and C are parallel (Vandewalle et al., 2001)

RILEM requires the test to be conducted in a closed loop mechanical testing machine using the average notch displacement as the feedback signal or, alternatively, another setup which will ensure a stable post-crack response. Hinge joints allowing for the free rotation of the specimen ends can reduce initial bending stress; however, as the crack forms the stress field across the

specimen is not uniform (Wang et al., 1990). In order to obtain a true uni-axial test, RILEM specifies fixed connections which control specimen end rotation. Any misalignment or eccentricity introduced when the specimen is affixed to the end fixtures may introduce unknown stress to the specimen or may cause bending to occur. In order to eliminate rotation of the specimen, both ends of the cylinder must be clamped to the test machine; however, pre-stressing of the specimen must be avoided (2001).

The test is run at displacement rates of 5 μm/min up to a displacement of 0.1 mm and 100 μm/min up to 2 mm. The displacement across the notch is measured by a minimum of three transducers arranged equally around the specimen, as seen in Figure 2.16. The load is measured by a load cell connected in series with the specimen.

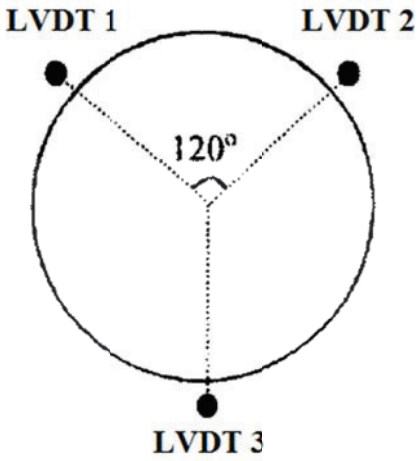

Figure 2.16 - Typical arrangement of the displacement transducers around the cylindrical specimen

The tensile and rotation stiffness of the testing apparatus is essential for performing a stable UTT. There is no way to numerically quantify the necessary tensile stiffness of the testing equipment. In order to assure the required stiffness is achieved, the test is typically preformed on a high-capacity testing machine using only a small percentage of the frame's capacity (Wang et al., 1990). The test setup must also have sufficient axial and bending stiffness. The axial stiffness cannot be expressed quantitatively

but must ensure a stable testing without snap-back in the averaged displacement measurement. The bending stiffness is considered sufficient if, at the end of the test, no individual transducer signal differs from the mean displacement by 10% or more.

The stress, σ_w, is obtained dividing the measured load, P, by the cross sectional area of the notched section, A_n

$$\sigma_w = \frac{P}{A_n} \qquad [2.12]$$

The average displacement, δ, is determined from the individual displacement readings. The crack opening, w, is calculated by subtracting the average peak displacement from the all other average displacements

$$w = \bar{\delta} - \overline{\delta_p} \qquad [2.13]$$

Where

$$\bar{\delta} = \frac{1}{n}\sum_{j=1}^{n} \delta_j \qquad [2.14]$$

The $\sigma(w)$ relationship, and thus the σ–ε relationship, can now be formed.

2.7 FRC Performance Testing

Several tests are commonly performed in order to characterize the contribution of fibre type and dosage to the performance of FRC. The American Society for Testing and Materials (ASTM) provides test methods to determine the compressive strength, first peak strength, residual strength, and toughness of FRC. These test methods and associated calculations are described in this section.

2.7.1 FRC Compressive Strength Test

The compressive strength of FRC is determined using ASTM C39-11 "Standard test Method for Compressive Strength of Cylindrical Concrete Specimens".

The specimens for compressive strength testing are commonly 100 mm diameter cylinders, with a height of 200 mm. A compressive load is applied until the load indicator shows that the load is steadily decreasing and a well-defined fracture pattern can be seen in the specimen. The fracture pattern should be noted as one of the six types in Figure 2.17 or, if it is not one of these typical patterns, a sketch or photograph and brief description of the fracture pattern should be noted.

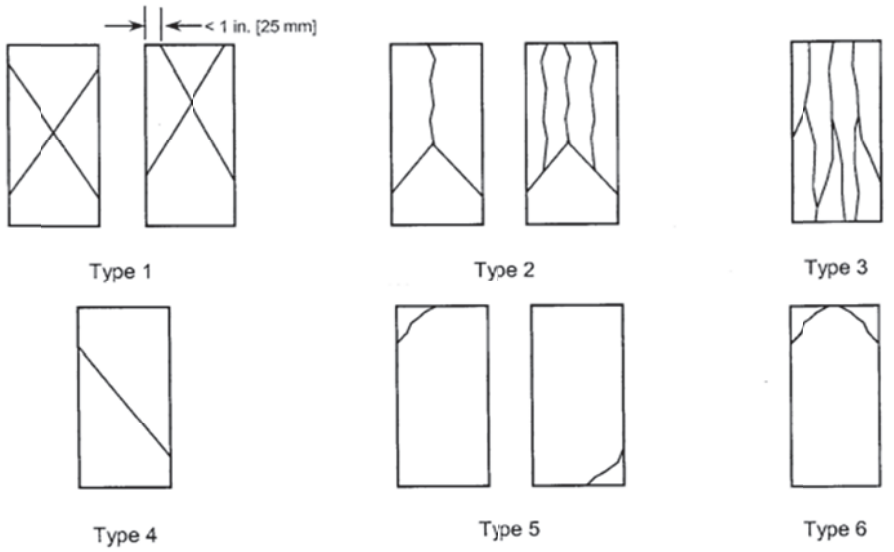

Figure 2.17 – Schematic of typical fracture patterns

In order to calculate the compressive strength, the maximum load carried by the specimen during the test is divided by the cross-sectional area. Figure 2.18 shows the testing machine with sulphur capped specimen post rupture.

Figure 2.18 – Testing machine with sample failed in compression

2.7.2 FRC Flexural Strength Tests

Flexural Performance Testing (ASTM 1609-10)

ASTM C1609-10 "Standard Test Method for Flexural Performance of Fiber-Reinforced Concrete (Using Beam With Third-Point Loading)" allows the behaviour of FRC under static flexural loading to be examined by determining the first-peak, residual strengths, and flexural toughness of the beam specimen. The results of this test method are dependent on the size of the specimen; typically rectangular beams with a 150 mm by 150 mm cross-section and span of 500 mm are used.

The test is conducted using a closed-loop, servo-controlled system in order to properly record the post-cracking response of the FRC. A typical test setup can be seen in Figure 2.19. The load and displacement versus time are recorded by a data acquisition system; the resulting load-deflection curve, shown in Figure 2.20, is used to determine specimen parameters.

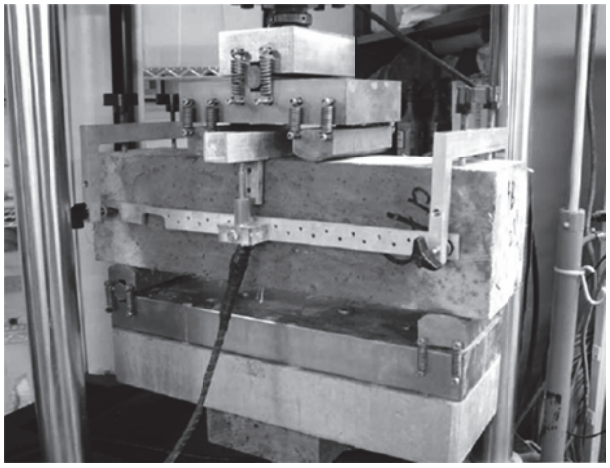

Figure 2.19 – Test setup for ASTM 1609-10

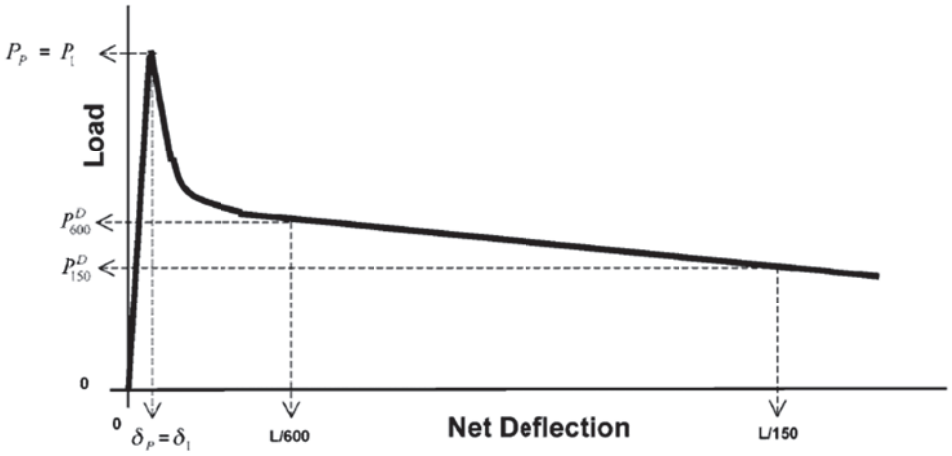

Figure 2.20 – Example of resulting load-deflection curve used to determine specimen parameters

$$f_x^D = \frac{P_x^D L}{bd^2} \qquad [2.15]$$

Where:

L is the span length (mm),

b is the average width of the specimen (mm),

d is the average depth of the specimen (mm),

P_1 is the first-peak load (kN),

P_P is the peak load (kN),

δ_1 is the net deflection at the first-peak load (kN),

δ_P is the net deflection at the peak load (kN),

f_1 is the first-peak strength (MPa),

f_P is the peak strength (MPa),

P^D_{600} is the residual load at a net deflection of L/600 (kN),

f^D_{600} is the residual strength at a net deflection of L/600 (MPa),

P^D_{150} is the residual load at a net deflection of L/150 (kN),

f^D_{150} is the residual strength at a net deflection of L/150 (MPa) and

T^D_{150} is toughness, taken as area under load vs. deflection curve between a net deflection of 0 and L/150 (Joules)

Residual Strength Testing (ASTM 1399-10)

A method for determining the residual strength of FRC is described by ASTM C1399-10. The typical specimen is a 100 x 100 x 350 mm rectangular beam which is first cracked in a standard manner using a steel plate to help control the rate of deflection. The plate is then removed and the cracked beam is reloaded to obtain the post-crack load-deflection curve. A schematic of a typical test setup is shown in Figure 2.12.

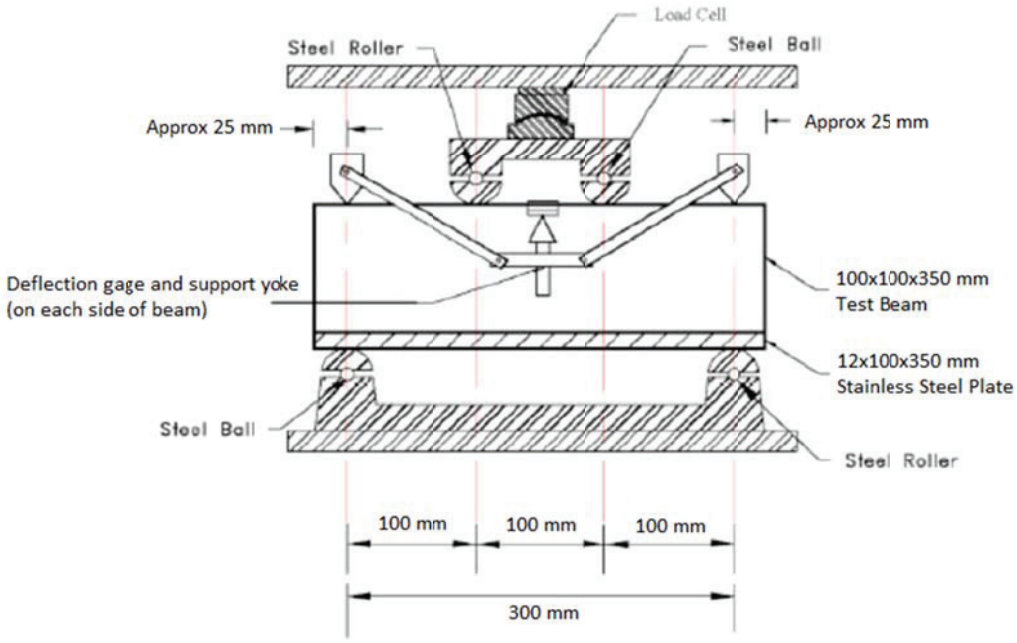

Figure 2.21 – Schematic of test setup for ASTM 1399-10

The load-deflection curve is created using the data stored by a data acquisition system. The residual strength index (RSI) is calculated with Equation 2.16

$$RSI = \frac{P_{avg} L}{bd^2} \qquad [2.16]$$

Where:

L is the sample length (mm),

b is the sample width (mm),

d is the sample height (mm),

RSI is the residual strength index (MPa) and

P_{avg} is the average load corresponding to 0.5, 0.75, 1.00 and 1.25 mm deflection (N)

Flexural Toughness Testing Using Round Panels (ASTM 1550-10)

The flexural toughness of FRC can be characterized using ASTM 1550-10 "Standard Test Method for Flexural Toughness of Fiber Reinforced Concrete (Using Centrally Loaded Round Panels)" and is expressed as the energy absorbed between the onset of loading and selected values of central deflection of a round panel.

The standard requires specimen dimensions of 800 mm in diameter and 75 mm thickness; specimens that do not comply with the target thickness and diameter can be scaled as long as the actual dimensions fall within given limits. The molded round panels are supported on three symmetrically arranged pivots and subjected to a central point load. A servo-controlled testing machine with feed-back loop is used to apply a constant rate of deflection up to 40 mm central deflection, measured relative to the pivot supports. Figures 2.22 and 2.23 illustrate the suggested test setup and measurement method.

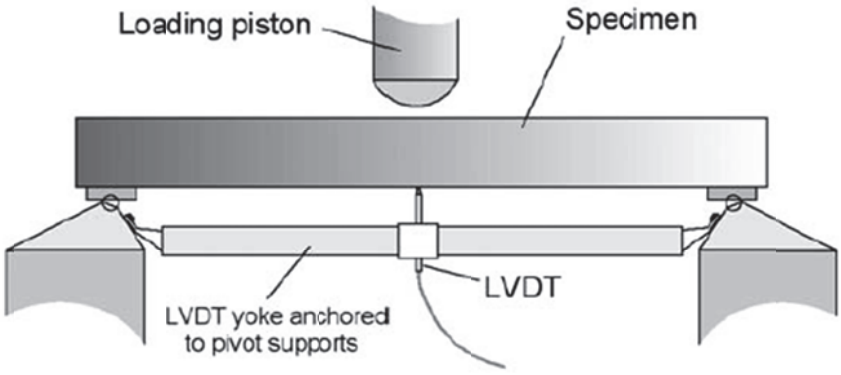

Figure 2.22 – Schematic of suggested method of deflection measurement of ASTM 1550-10

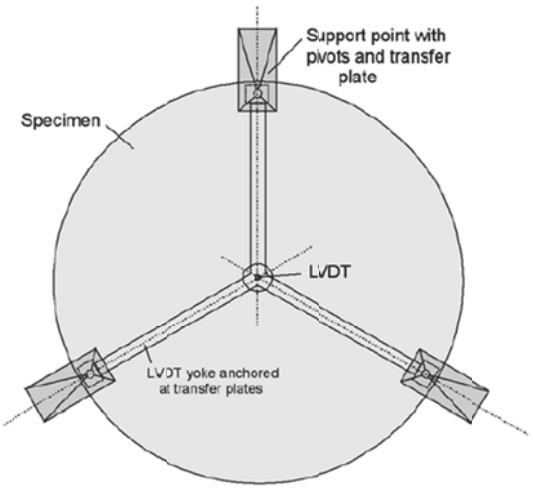

Figure 2.23 – Schematic of the plane view of suggested test setup for ASTM 1550-10

A data acquisition system is used to record the load-deflection of the round panel. This data is corrected for extraneous deformations of the concrete to create a load-net deflection curve. The area under this curve between 0 and 40 mm of central deflection provides the energy absorption, or toughness, in J. The peak load and any radial cracks in the round panel are also reported.

2.8 THE EFFECT FIBRE DISTRIBUTION ACROSS THE CRACK PLANE

The toughness of a concrete specimen and the $\sigma(w)$ relationship are directly influenced by the number of fibres bridging the crack. The size of specimens as well as the casting procedure affects the number and orientation of the fibres across the crack plane. The RILEM TC 162-TDF completed a round robin analysis of the UTT which included a fibre counting program; it was found that the total number of fibres in the crack plane had coefficients of variation ranging from 30% to 50% (Vandewalle et al., 2003c). Löfgren et al. (2008) noted that the RILEM uni-axial tensions specimens may have as little as half the expected amount of fibres in the crack plane, significantly affecting the test results. This was attributed to the casting and vibration process of the cylindrical moulds, which tends to orient the fibres parallel to the fracture plane.

Although not required, RILEM recommends that the uniformity of fibre distribution be recorded for each specimen included in the test report (Vandewalle et al.,2001).

2.9 Correlation of Tensile and Flexural Responses of FRC

Although the UTT is a more direct method to determine the $\sigma(w)$ relationship of FRC, flexural tests are simpler to conduct and are routinely used for quality control purposes. A reliable method to correlate the tensile and flexural response would allow the $\sigma(w)$ relationship to be determined without requiring additional testing or the sophisticated test setup for the UTT. Several methods have been proposed to correlate the tensile response of FRC to the three and four-point beam tests that are commonly conducted. The RILEM $\sigma-\varepsilon$ design method proposes a simple correlation and Soranakkom and Mobasher (2008) have developed a more complicated closed-form solution.

2.9.1 RILEM Stress-Strain Design Method

The $\sigma-\varepsilon$ design method proposed by RILEM (Vandewalle et al., 2003a) allows for the tensile response of FRC to be approximated using parameters determined from the compression and flexural responses. The compressive strength, f'_c, determined using ASTM C39-11 "Standard test Method for Compressive Strength of Cylindrical Concrete Specimens" is used to calculate the modulus of elasticity, E;

$$E = 9500{f'_c}^{1/3} \quad [2.17]$$

The peak tensile stress, σ_1, and the residual flexural strengths, σ_2 and σ_3, are calculated using the load-deflection or load-CMOD curves determined from the three-point bending test, described by RILEM (2000);

$$\sigma_1 = 0.7 f_P (1.6 - d) \quad [2.18]$$

Where:

f_P is the first peak strength (MPa) and

d is the depth of stiffening bars or the depth of the beam (m).

The residual tensile stress is determined from the residual flexural strength, $f_{R,i}$;

$$\sigma_2 = 0.45 f_{R,1} \kappa_h \quad [2.19]$$

$$\sigma_3 = 0.37 f_{R,4} \kappa_h \quad [2.20]$$

Where

$$\kappa_h = 1.0 - 0.6 \frac{h - 125}{475} \quad [2.21]$$

And the residual flexural strength is calculated using the ASTM C1609-10 "Standard Test Method for Flexural Performance of Fiber-Reinforced Concrete";

$$f_{R,i} = \frac{3 F_{R,i} L}{2 b h^2} \quad [2.22]$$

Where:

b is the width of the beam (mm),

h is the height of the beam (mm),

L is the beam span (mm) and

$F_{R,i}$ is the load recorded at $\delta_{R,I}$ (N).

The residual flexural tensile strengths, $f_{R,1}$ and $f_{R,4}$, are defined the following mid span deflections;

$$\delta_{R,1} = 0.46\,mm \quad [2.23]$$

$$\delta_{R,4} = 3.00\,mm \quad [2.24]$$

The corresponding strains are calculated as:

$$\varepsilon_1 = \sigma_1/E \quad [2.25]$$

$$\varepsilon_2 = \varepsilon_1 + 0.1\% \quad [2.26]$$

$$\varepsilon_3 = 25\% \quad [2.27]$$

The design method was originally developed without the application of a size-dependent safety factor, κ_h. This resulted in an overestimation of the carrying capacity of structural elements when the design method was applied on experimental beam specimens of various sizes. The safety factor was defined in order to compensate for this affect; however, the origin of this size effect is not fully understood.

2.9.2 Soranakom and Mobasher's Closed-form Solution

Soranakom and Mobasher (2007) developed a closed-form solution to relate the post peak flexural and tensile responses of FRC. The moment-curvature and load-deflection relationships were determined in closed-form to develop a procedure for back-calculation of material properties from load-deflection tests.

A generalized fibre reinforced concrete model, seen in Figure 2.24, was used; all strains in the model are normalized with respect to the first cracking strain, ε_{cr}; the tensile limit, $\varepsilon_{tu}=\beta_{tu}\varepsilon_{cr}$, the compressive yield strain, $\varepsilon_{cy}=\omega\varepsilon_{cr}$, and the ultimate compressive strain, $\varepsilon_{cu}=\lambda_{cu}\varepsilon_{cr}$. The parameter μ represents the ratio of the post peak tensile stress, which remains constant, and the cracking stress. The classic beam theory, which ignores shear deformation, is used to derive the moment-curvature diagram of a rectangular beam. The top compressive strain, $\lambda = \varepsilon_c/\varepsilon_{cr}$, occurs in three stages: $0< \lambda <1$, $1< \lambda <\omega$, and $\lambda >\omega$, shown in Figure 2.25.

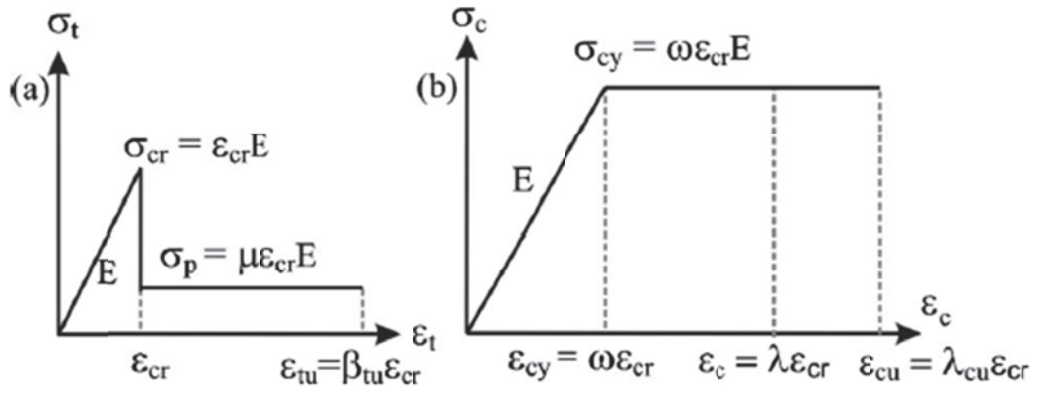

Figure 2.24 – Fibre reinforced concrete model; (a) tension model; (b) compression model (Soranakom and Mobasher, 2007)

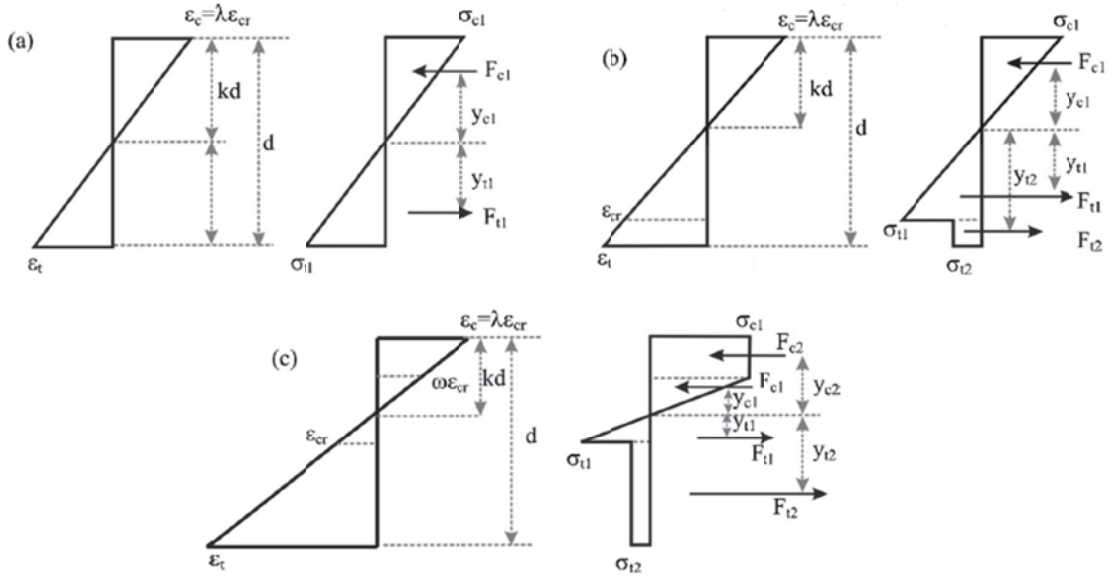

Figure 2.25 – σ–ε diagram at three stages of normalized top compressive strain λ: (a) 0< λ <1; (b) 1< λ <ω; and (c) λ >ω (Soranakom and Mobasher, 2007)

The moment and curvature at any strain level are normalized with respect to the values at cracking, (M_{cr},ϕ_{cr}), and expressed as (M',ϕ'). These normalized values are calculated using the closed-form solution presented in Table 2.2.

Table 2.2 – Neutral axis depth ratio, normalized moment, and curvature for each stage top compressive strain

Stage	K	M'	ϕ'
$0<\lambda<1$	$\frac{1}{2}$	$\frac{\lambda}{2k}$	$\frac{\lambda}{2k}$
$1<\lambda<\omega$	$\frac{2\mu\lambda}{\lambda^2+2\mu(\lambda+1)-1}$	$\frac{(2\lambda^3+3\mu\lambda^2-3\mu+2)k^2}{\lambda^2}-3\mu(2k-1)$	
$\lambda>\omega$	$\frac{2\mu\lambda}{-\omega^2+2\lambda(\omega+\mu)+2\mu-1}$	$\frac{(3\omega\lambda^2+\omega^3+3\mu\lambda^2-3\mu+2)k^2}{\lambda^2}-3\mu(2k-1)$	

In order to determine the predicted load-deflection response of a beam in three- or four-point bending, the ultimate top compressive strain, λ_u, is calculated as the smaller of λ_{cu} (from Figure 2.24) or λ_{tu}:

$$\lambda_{tu}=\begin{cases}\sqrt{2\mu\beta_{tu}-2\mu+1} & for\ \beta_{tu}\le\beta_{crit}\\ \dfrac{2\mu\beta_{tu}-2\mu+\omega^2+1}{2\omega} & for\ \beta_{tu}>\beta_{crit}\end{cases} \qquad [2.28]$$

Where:

$$\beta_{crit}=\frac{(\omega^2+2\mu-1)}{2\mu} \qquad [2.29]$$

Once λ_u is determined, the normalized ultimate moment, $M'_{u,}$ can be calculated by the expressions given in Table 2.2. The intersection point of the two straight lines in the bilinear, deflection softening moment-curvature relationship, seen in Figure 2.26, is calculated using equation 2.30 and the normalized reduced cracking moment M'_{cr2} at ϕ'_{bcr} can be interpolated linearly.

$$M'_{it}=0.7425M'_{u}+0.1739 \quad and \quad \phi'_{it}=M'_{it} \qquad [2.30]$$

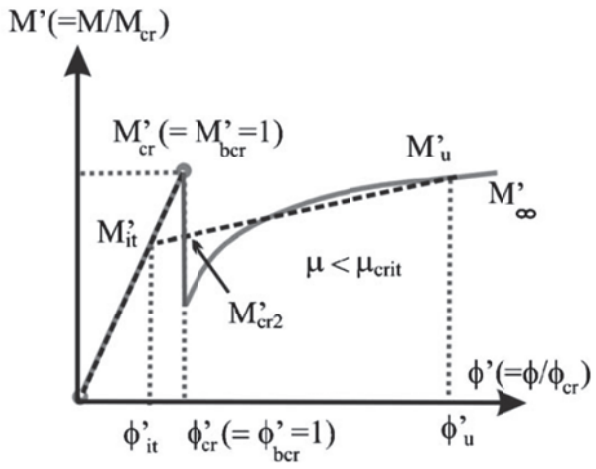

Figure 2.26 – Normalized deflection softening moment-curvature diagram (Soranakom and Mobasher, 2007)

Once the moment-curvature relationship has been determined, the *M* and ϕ values can be substituted into equations 2.31, 2.32, and 2.33 to determine the load-deflection relationship for either a three- or four-point bending test. The moment and curvature distribution of a four-point bending test, obtained by static equilibrium, is shown in Figure 2.27. The two curvature patterns are required to derive the midspan deflection.

$$P_i = \frac{2M_i}{L/3} \quad [2.31]$$

$$\delta_{bcr} = \frac{23}{216} L^2 \phi_{bcr} \quad [2.32]$$

$$\delta_u = \frac{5L^2\phi_u}{72} + \frac{M_u L^2 \phi_{bcr}}{27 M_{bcr}} \quad [2.33]$$

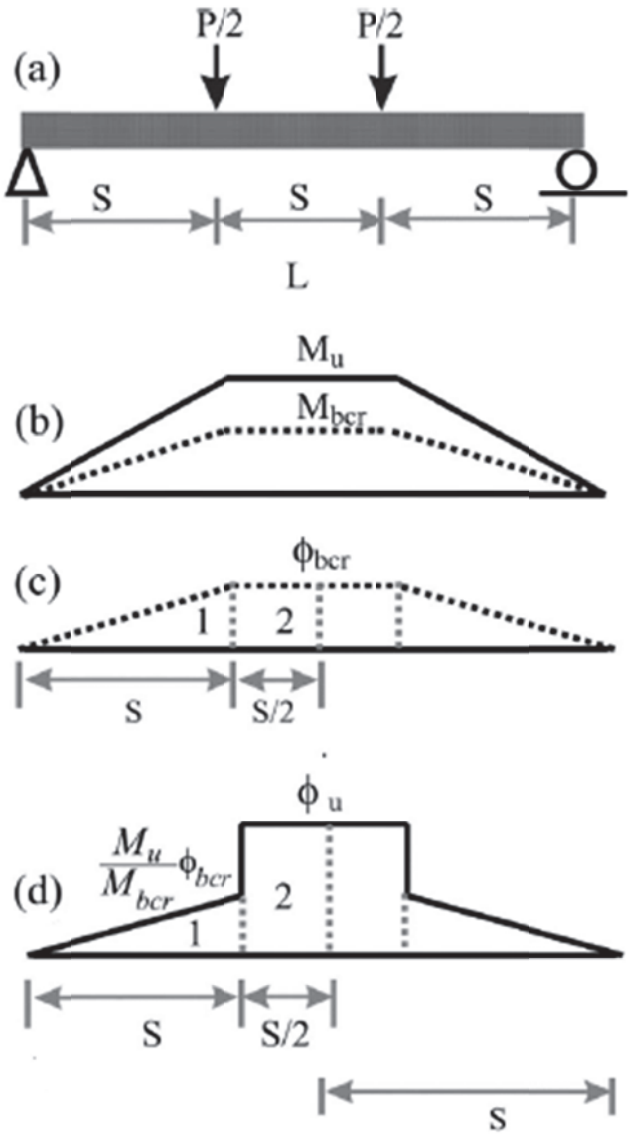

Figure 2.27 – Four-point bending test: (a) setup; (b) moment distribution; (c) curvature distribution at first bilinear cracking; (d) curvature distribution at ultimate moment (Soranakom and Mobasher, 2007)

CHAPTER 3 TESTING PROGRAM

The tensile response of FRC was determined by the UTT. More common performance testing was conducted on specimens cast with the same FRC mixes used in the UTT test in order to provide parameters to compare the tensile and flexural response. Eight of the mixes used the Tuf-Strand SF production fibre. Dosages of 1.8 kg/m^3, 3.0 kg/m^3, and 4.6 kg/m^3 were cast using both the mix truck and drum mixer methods. In addition, dosages of 2.4 kg/m^3 and 6.9 kg/m^3 were cast using a mix truck. Prototype fibres, developed concurrently with the uni-axial tension testing program, were also used in the mixes. Prototype fibres containing 100% HDPE, HDPE with 3% PVDF, HDPE with 5% PVDF and 10% MAH, HDPE with 11% PVDF and 20% MAH, 80% PP, 10% HDPE, and 1% EVA as well as 100% HDPE were cast at a dosage of 3.0 kg/m^3 in the drum mixer. Finally, another prototype fibre, HDPE with 10% EVA, was cast at three dosages (1.8 kg/m^3, 3.0 kg/m^3, and 4.6 kg/m^3) and two different fibre lengths (38 mm and 50 mm). The properties of these fibres can be seen in Table 3.1. The test and casting procedures followed are described below.

Table 3.1 – Tensile properties of fibres

Fibre Type	σ_f (Mpa)	E_f (Gpa)	Width (mm)	Thickness (mm)	d_{eq} (mm)
Tuf Stran SF	646	9.53	1.05	0.34	0.65
HDPE, 10% EVA (1.5")	595	5.67	1.55	0.29	0.738
HDPE, 10% EVA (50 mm)					
HDPE, 3% PVDF	749	7.01	1.42	0.25	0.659
HDPE, 5% PVDF, 10% MAH	779	9.25	1.26	0.26	0.636
HDPE, 11% PVDF, 20% MAH	559	5.79	1.51	0.29	0.727
80% PP, 10% HDPE, 10% EVA	718	10.93	1.31	0.25	0.633
100% HDPE	673	6.13	1.39	0.25	0.651

3.1 CASTING OF SPECIMENS

Each of the eight different fibre types and dosage was mixed and cast in a separate batch. Each batch provided concrete for the uni-axial tension testing and the performance testing; four beams for ASTM C1399-10, five beams for ASTM C1609-10, three cylinders for ASTM C39-10, one or three round panels for ASTM C1550-10, and three to four cylinders for the UTT.

The concrete was cast in three batches by two different methods. The Tuf-Strand SF production fibre and prototype fibres being investigated at Dalhousie University, both produced by AFT in Sydney, Nova Scotia, were tested. The concrete was cast from a ready mix truck as well as on site at Dalhousie University in a 0.180 m^3 drum mixer. A breakdown of the fibre type, dosages, casting method and concrete compressive strength can be seen in Table 3.2.

Table 3.2 – Sample mixture information

Fibre Type	Fibre Dosage (kg/m^3)	Casting Method	f'_c (MPa)
TUF-STRAND SF	1.8	mix truck	36.2
	2.4		31.5
	3.0		32.2
	4.6		27.7
	6.9		28.1
	1.8	drum mixer	40.9
	3.0		43.5
	4.6		41.6
HDPE, 10% EVA (1.5")	1.8		39.7
	3.0		39.3
	4.6		42.0
HDPE, 10% EVA (50 mm)	1.8		36.4
	3.0		41.8
	4.6		39.6
HDPE, 3% PVDF	3.0		41.9
HDPE, 5% PVDF, 10% MAH			41.7
HDPE, 11% PVDF, 20% MAH			42.5
80% PP, 10% HDPE, 10% EVA			45.1
100% HDPE			44.9

When using the drum mixer, the fine and coarse aggregate were added to the drum first and mixed for 30 second. The cement was added and mixed for one minute. Water was then added and mixed for three minutes.

In both mixing methods, slump and density measurement tests were performed according to ASTM C143-10 "Standard Test Method for Slump of Hydraulics-Cement Concrete" and ASTM C138-10 "Standard Test Method for Density (Unit Weight), Yield, and Air Content (Gravimetric) of Concrete". Both methods of measurement were performed before fibres were added to the concrete. These measurements were taken to ensure the concrete achieved the desired slump and density ranges of 150-175 mm and 2350-2400 kg/m^3, respectively.

Once the fibres were added, Eucon SPC High Range Water Reducer-Superplasticizer was added to improve the workability of the concrete. The superplasticizer was added based on visual inspection and previous experience. After the addition of the fibres, the concrete was mixed for four minutes to allow typical fibre surface damage to occur. Another slump test was performed and a washout sample was taken. Washout samples were collected by filling a bucket with fresh FRC, flushing it with water, and separating a handful of fibres to be stored. The purpose of the sample is to visibly inspect the fibres for fibrillation after mixing. An example of a washout sample can be seen in Figure 3.1.

Figure 3.1 – Example of a washout sample

All beam, cylinder, and round panel specimens were cast in accordance with their respective standards. Samples were placed on a vibrating table and cast in two lifts. They were then covered in plastic and allowed to cure for 24 hours before being removed from their forms. All samples were allowed to cure in a moist curing room at 100% relative humidity for a minimum of 28 days, until testing was completed.

3.2 FRC Performance Testing

3.2.1 FRC Compressive Strength Test

The compressive strength testing was conducted according to ASTM C39-10. Three 100 mm x 200 mm cylinder specimens were taken for each FRC mix.

The specimens were capped using a sulfur compound to ensure a smooth level surface when the load was applied. The specimens were tested after 28 days using the Fomey testing machine, pictured in Figure 2.18.

3.2.2 Flexural Performance Test

Five 150 mm x 150 mm x 550 mm beam specimens were cast for each mix and tested for flexural strength according to ASTM C1609-10. Testing was performed after 28 days using an Instron 8501 machine, pictured in Figure 3.2, with a 100 kN load cell. The test was run and data collected using the "Wave Maker" program.

The width and depth of each specimen was measured in three locations and the average used as the true cross section measurements. After the test was complete, each specimen was separated and photographed; the fibres across the crack plane were counted and recorded in order to compare the fibre distribution in the cylindrical and beam moulds.

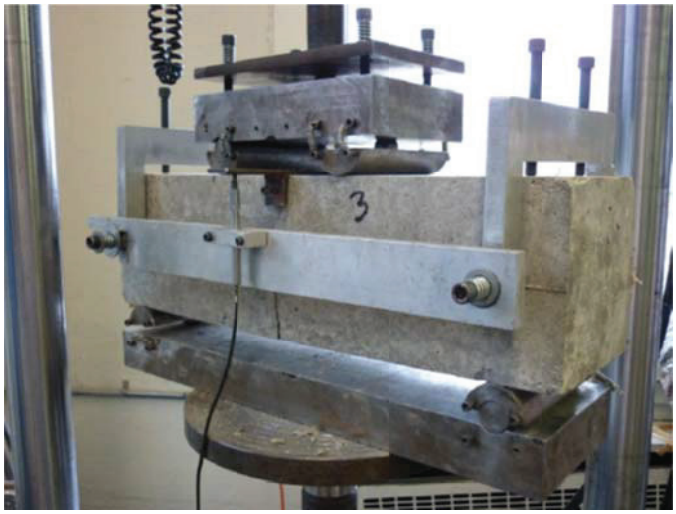

Figure 3.2 – Test set up for ASTM C1609-10

Flexural toughness testing using round panels was not conducted during this testing program.

3.2.3 Uni-Axial Tension Test

The UTT conducted for this experimental program was based on the test proposed by RILEM Technical Committee 162-TDF (Vandewalle et al., 2001). Notched cylindrical specimens (150 mm in height and diameter, 15 mm deep notch at mid-height) were glued to fixtures which provided a fixed connection to the testing machine which applied the uni-axial tension load.

There were some changes made to the RILEM test procedure. The UTT is intended to be conducted under closed-loop conditions; however, the testing system required to obtain closed-loop conditions with feedback is very sophisticated and expensive and this type of setup was not available. Instead of a displacement rate controlled by sample strain feedback, the actuator displacement was controlled. In order to account for this change in procedure, changes were made to the stiffness of the test setup described in Section 3.1.1.

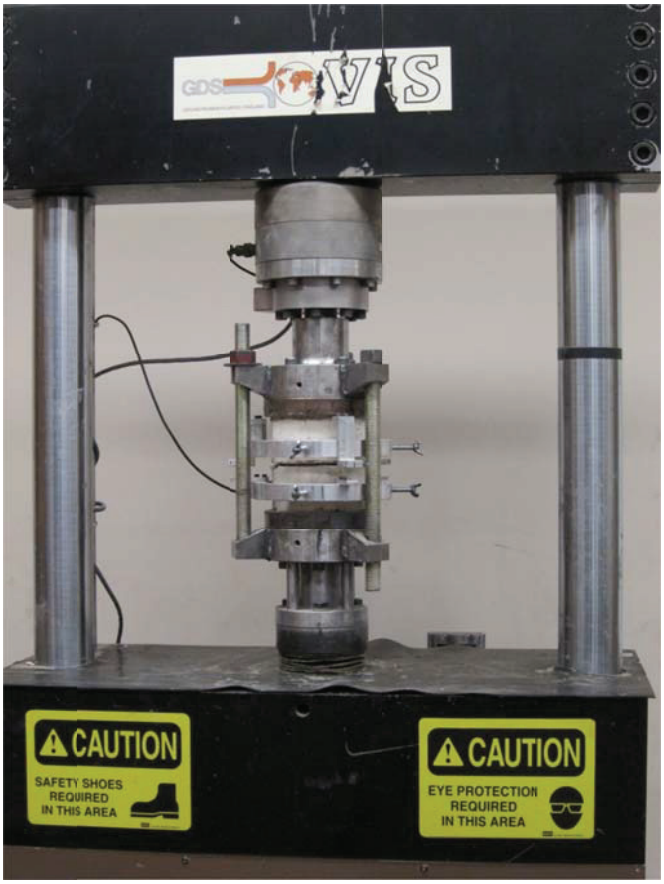

Figure 3.3 – UTT specimen in testing machine

The test was run at an actuator displacement rate of 100 μm/min up to a displacement of 0.1 mm, then 500 μm/min up to 10 mm of displacement. The load and LVDT readings were recorded using National Instruments LabVIEW 2010 software. Once the tensile tests were completed, each specimen was separated and photographed; the fibres across the crack plane were then counted and recorded. An example of a cylinder cross section can be seen in Figure 3.4. The diameter and notch depth were measured at three locations, equally spaced around the specimen, and averaged to determine the true cross section measurements.

Figure 3.4 – Example of cylinder cross section with specimen number (bottom) and fibre count (top)

The focus of this test program was to determine the uni-axial tensile response of synthetic FRC while the RILEM procedure was developed with steel FRC in mind. Because of the different moduli of synthetic fibres, there is a measurable tensile response at larger crack openings when compared to steel fibres. Though the RILEM standard suggests a test running until 2 mm of displacement, this test program ran until 10 mm of displacement, the limit of the LVDTs used.

Equipment Stiffness Requirements

The UTT were performed on a GDS VIS machine with a mechanical, screw driven actuator. The capacity of the load cell was 250 kN. The maximum expected cylinder strength was 45 kN, using only 20% of the test set up's capacity. The stiffness of the test set up and fixtures were determined by examining the UTT data; if, at the end of the test, any individual transducer signal differs from the mean displacement by 10% or more the specimen is rejected, according to the RILEM recommendation (2001). A complete list of accepted and rejected UTT specimens can be found in Appendix A; 80% of the tests achieved the required stiffness. It was noted in several cases that the reason for specimens failing to meet this requirement was that bolts connecting the fixture to the machine had become loose. When these tests

were excluded, 90% of the specimens met the requirement when the fixtures were properly attached.

Connection Fixtures

The design of the testing fixtures was governed by the connections required by the testing machine, the load cell, and the plates affixed to the specimens. Specimens were glued to 25 mm thick steel plates, 180 mm in diameter. A schematic of the bottom fixture can be seen in Figure 3.5; Section "A" shows the bolt pattern of the steel plates and Section "B" shows the bolt pattern required to attach the fixture to the machine actuator. The load cell required a 38 mm threaded connection; a schematic of the top fixture can be seen in Figure 3.6. Both fixtures were designed to be fit flush and square against the load cell and testing machine. In order to provide sufficient stiffness, the specimen plates were connected to the fixtures through 50 mm of steel. An additional 50 mm were left as a spacer to allow room for the bolts, with ribs left in to provide additional bending resistance and stiffness.

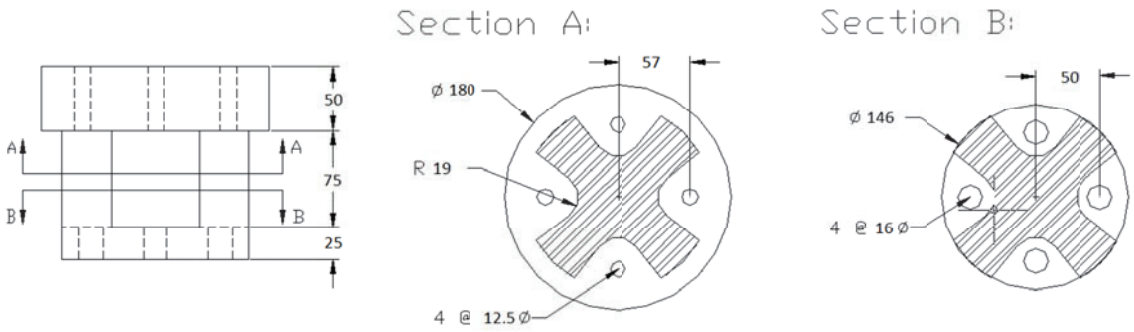

Figure 3.5 – Schematic of the bottom testing fixture (dimensions in mm)

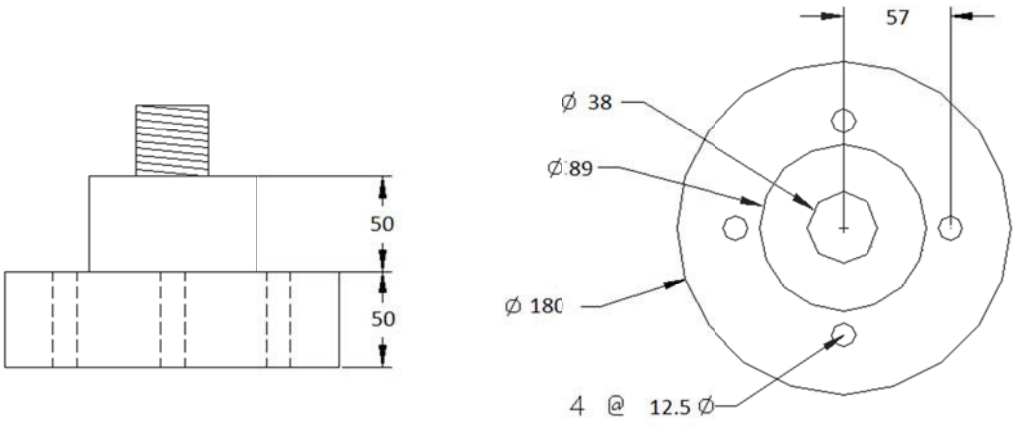

Figure 3.6 – Schematic of the top testing fixture (dimensions in mm)

Steel Bar Reinforcement of Test Setup

As noted, the UTT was not conducted using a closed-loop feedback. The test setup is not capable of detecting the softening of the concrete prior to cracking and the displacement rate of the actuator remains constant instead of adjusting with the strain. When the first UTTs were conducted it was obvious that this would have an effect on the test results. The strain induced in the sample and the test fixtures was released once the crack began to form in the specimen. This resulted in a loud "clunk" sound as well as visible "jump" in the crack opening as the strain was released into the crack.

There were three main concern with this "jump" and the lack of closed-loop testing; i) the results may be producing an artificially high cracking strain ii) the tensile response of the fibres immediately after the crack was being lost (seen in Figure 3.7); and, iii) the fibres may be damaged and their post-crack resistance affected.

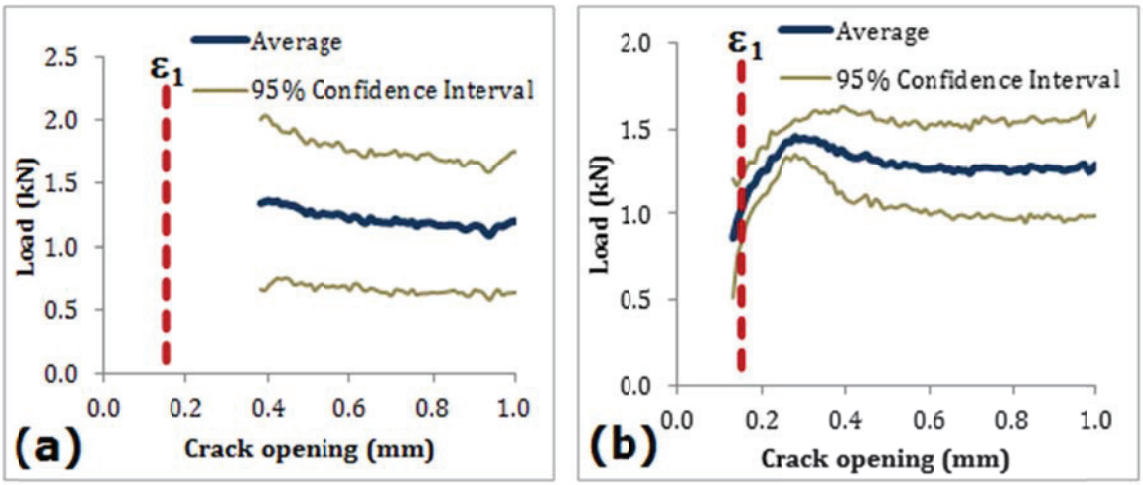

Figure 3.7 – Post-crack response of (a) specimens tested without stiffening bars and (b) specimens tested with stiffening bars used during the pre-crack phase and removed for the post-crack phase; the location of ε_1 is shown in each case

In order to limit these effects, three 25 mm diameter steel bars were spaced evenly around the specimen in order to provide increased stiffness to the specimen during the pre-cracked portion of the test. After cracking, the specimen was unloaded, the steel bars removed, and the test restarted in order to obtain a "post-crack" response. The placement of the reinforcing bars can be seen in Figure 3.8.

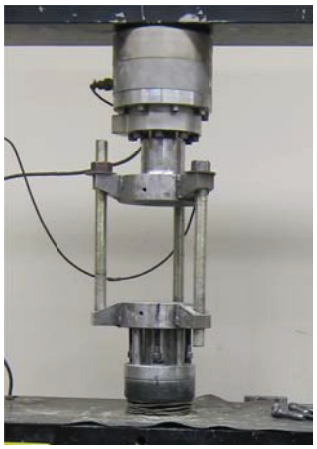

Figure 3.8 – Empty test setup with reinforcing bars

The tensile response of the test setup with the steel stiffening bars was recorded. This response was subtracted from the total response in order to identify the pre-cracking response of the concrete specimen on its own without the additional tensile response of the bars, show in Figure 3.9. In all specimen sets, at least one specimen was tested without bars for a comparison.

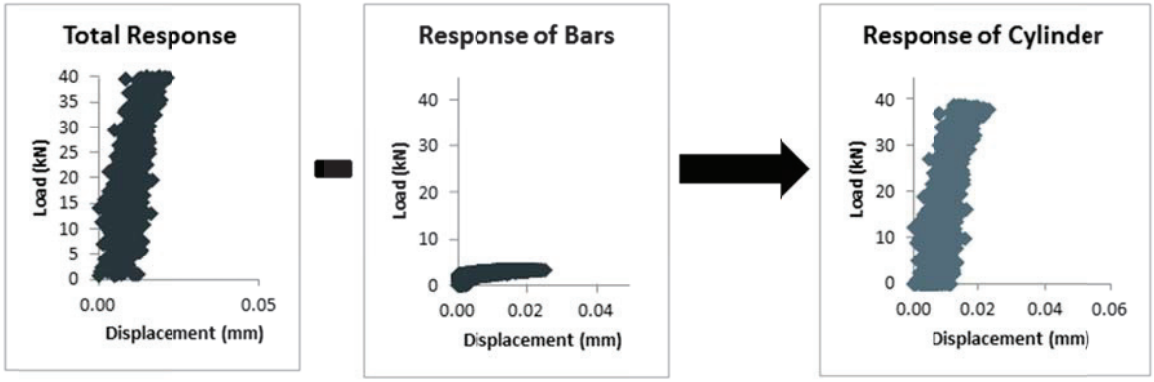

Figure 3.9 – Pre-crack response of concrete specimen, determined from the total response and the response of test set up with stiffening bars

Preparation of Cured Cylindrical Specimens

Specimen geometry seen in Figure 3.10 has been suggested by RILEM TC 162-TDF (2001). Hordijk et al. (1987) investigated the effect of specimen length on the specimen stiffness. They concluded that in order to reduce specimen rotation a length to width ration of 1:1 was preferable. This testing program prepared specimens according to RILEM TC 162-TDF (2001) specifications.

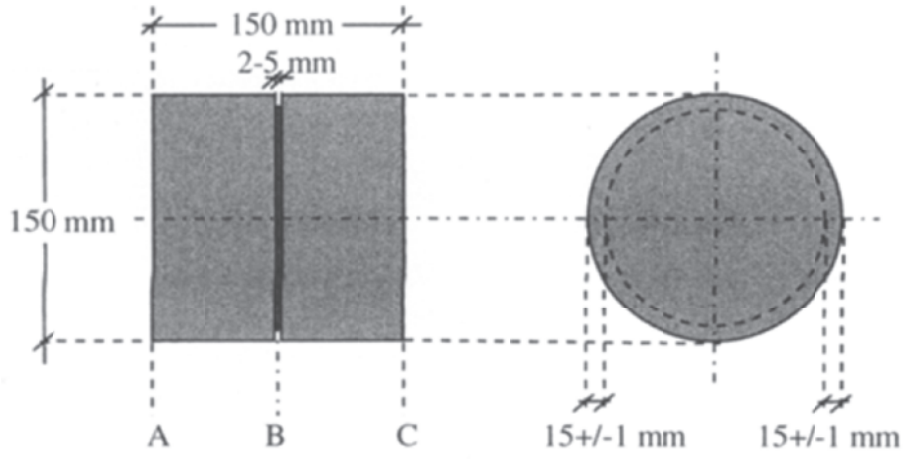

Figure 3.10 – Standard specimen geometry (Vandewalle et al., 2001)

The specimens were cast in cylindrical moulds 300 mm in length. The moulds were filled in thirds and vibrated on a vibrating table for 15 seconds for each third. The specimens were allowed to cure for 24 hours before being removed from the moulds and were then placed in curing tanks until testing.

In preparation for testing, the cylinders were cut in half to obtain the required dimensions and notched with a diamond tipped blade. The specimens were then milled in order to ensure both end surfaces were square. The procedure for affixing the specimen to the test setup suggested by RILEM TC 162-TDF (2001) was followed and is represent schematically in Figure 3.11. The specimens were affixed to the steel plates using a fast setting epoxy and were allowed to set in the test machine under a small load (approximately 3 kN) to help prevent misalignment of the specimen.

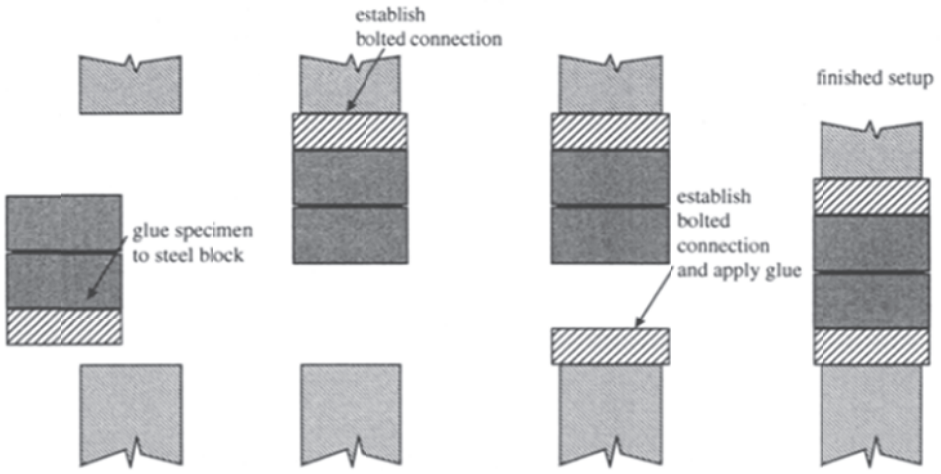

Figure 3.11 – Schematic presents the procedure for affixing the steel plates to the specimens (Vandewalle et al., 2001)

CHAPTER 4 RESULTS AND DISCUSSION

The UTT performed on the specimens produced properties for both the pre-crack (up to and including the peak tensile strength achieved by the cylinder) and the post-crack response of FRC. A total of 19 mixes were cast in order to determine the uni-axial tension response of FRC and to allow comparisons of several casting parameters. The specimens tested with stiffening bars used during the pre-crack phase and removed during the post-crack phase are denoted as specimens "cracked with stiffening bars." All specimens presented have had the additional tensile response of the stiffening bars removed from the pre-crack data. The pre-crack response of FRC is described by the peak tensile load or cracking stress; the load or stress at which the cylinder cracked. The average cracking stress of each concrete mix is listed in Table 4.1. Two specimen sets, containing 80% PP, 10% HDPE, 10% EVA and 100% HDPE, produced higher cracking stresses; these correspond to the mixes with the highest compressive strengths.

Table 4.1 – Average cracking stress of FRC

Fibre Type	Fibre Dosage (kg/m^3)	Casting Method	Peak (MPa)
Tuf-Strand SF	1.8	mix truck	2.47
	2.4		1.83
	3.0		2.01
	4.6		2.03
	6.9		1.95
	1.8	drum mixer	2.47
	3.0		2.32
	4.6		2.27
HDPE, 10% EVA (38 mm)	1.8		2.10
	3.0		1.90
	4.6		1.91
HDPE, 10% EVA (50 mm)	1.8		2.47
	3.0		1.67
	4.6		2.10
HDPE, 3% PVDF	3.0		2.40
HDPE, 5% PVDF, 10% MAH			2.41
HDPE, 11% PVDF, 20% MAH			2.57
80% PP, 10% HDPE, 10% EVA			3.22
100% HDPE			3.10

The $\sigma(w)$ response for each specimen was plotted and summary charts for each mix were created by plotting the envelope in which all specimens for that set fell as well as the average load vs. displacement $\sigma(w)$ curve and the 95% confidence interval. Plots were created for all the specimens in each set as well as just the specimens cracked using stiffening bars. An example of a summary chart is presented in Figure 4.1 below.

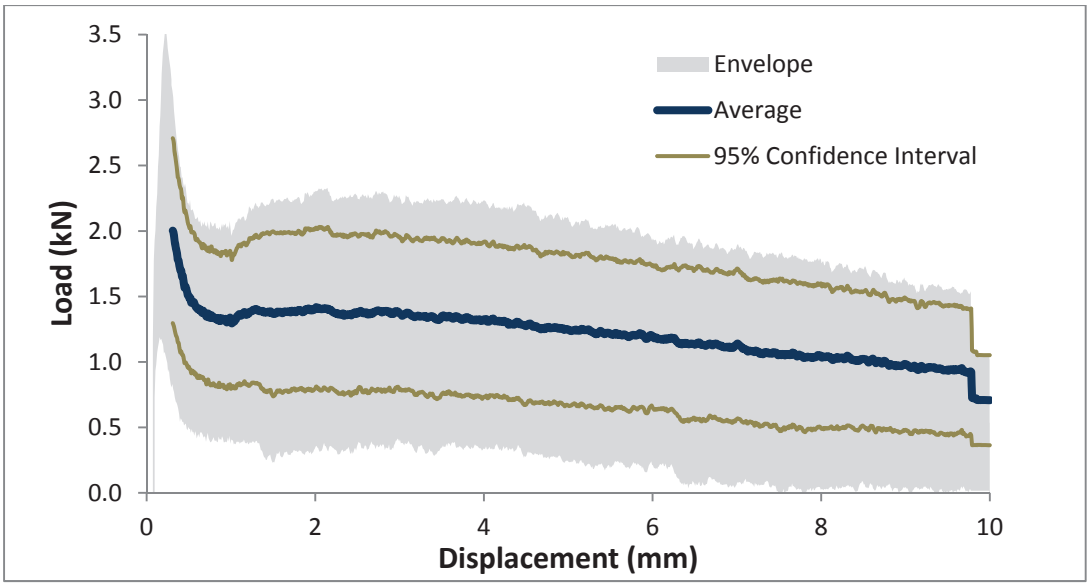

Figure 4.1 – Post-crack response of Tuf-Strand SF production fibre: 2.4 kg/m^3, cast from mix truck, all specimens.

The average curve determined for each specimen was used to create tables describing the tensile response of each mix by determining the peak, maximum and minimum loads as well as the loads at crack openings of 0.5, 1, 2, 4, 6, 8, and 10 mm. The tables are divided into three categories; all specimens, specimens cracked with steel stiffening bars and without stiffening bars. All tables and summary charts can be found in Appendix B.

4.1 Effect of Stiffening Bars on Uni-axial Tensile Tests

The increased stiffness provided by the bars had a noticeable beneficial effect during testing, the audible cracking of the specimen was reduced and occasionally completely eliminated. During visual inspection it appeared that the "jump" in the crack opening was reduced as well; this was later confirmed by the testing data. Figure 4.2 shows a plot of the cracking strain versus the cracking stress (the strain and stress at which the peak or cracking load occurred). The stresses and strains for specimens cracked with and without stiffening bars fall within the same range.

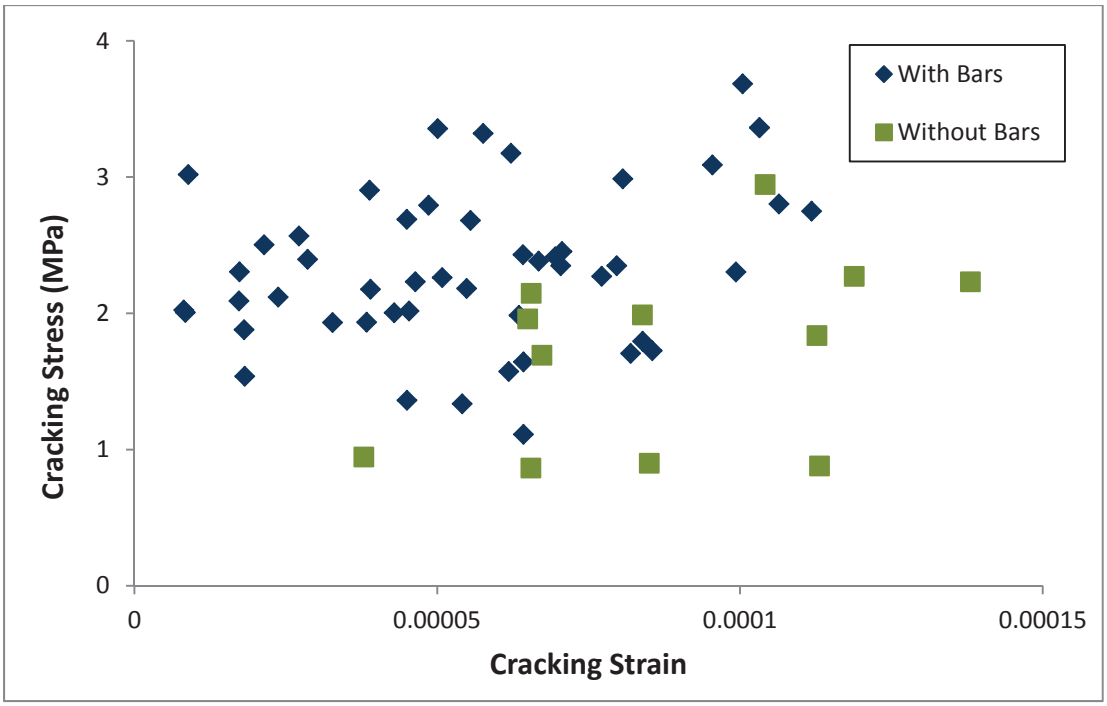

Figure 4.2 – Comparison of σ–ε at cracking, with and without stiffening bars

The gap between to cracking strain and the first recorded point of the post-crack response was also compared. Figure 4.3 plots the first post-crack strain reading versus cracking stress for the specimens. When the stiffening bars were used during the pre-crack phase, the data acquisition program was able to record the beginning of the post-crack response at significantly smaller strains. The location of ε_1 required for the RILEM σ–ε design method described in Section 2.3 is marked on the graph. Stiffening bars were required in order to record this data.

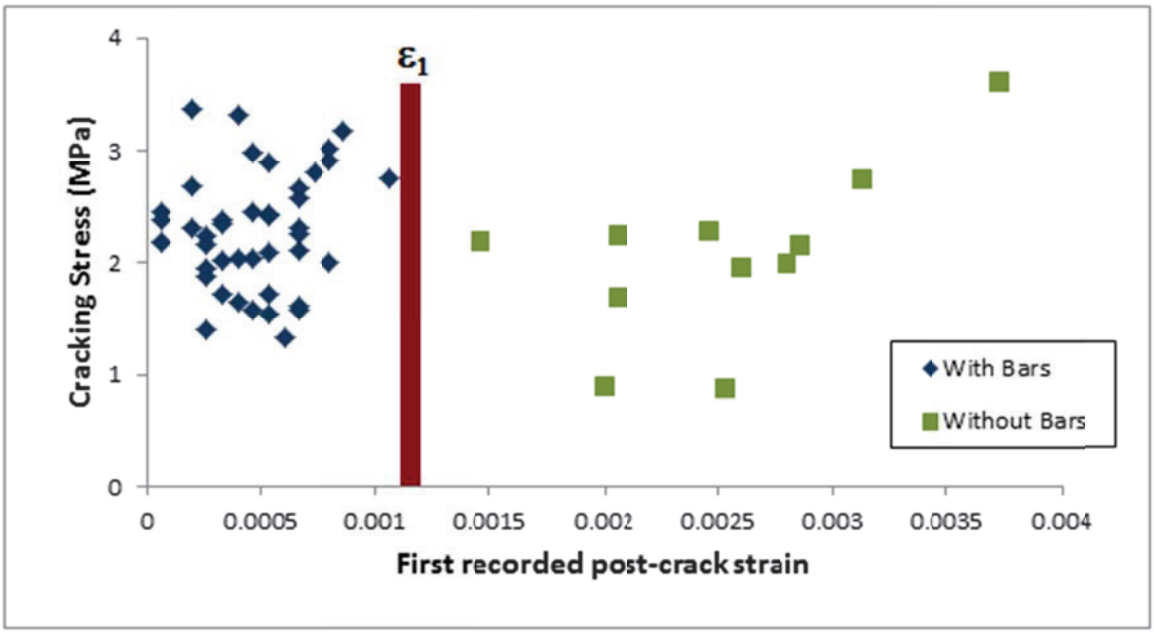

Figure 4.3 - Comparison of Tuf-Strand SF cracking stress first post-crack strain, with and without stiffening bars

The affect that the "jump" may have had on the fibres themselves was determined by comparing the $\sigma(w)$ curves, normalized to obtain the "per-fibre" response. The average post-crack response of specimens tested without stiffening bars during the pre-crack phase was slightly higher than the average response of specimens tested with stiffening bars; however, 37 samples tested with stiffening bars and only 9 samples tested without were considered and the confidence intervals of both cases overlap, as seen in Figure 4.4. This indicating that the "jump" may have little or no effect on the post-crack tensile resistance.

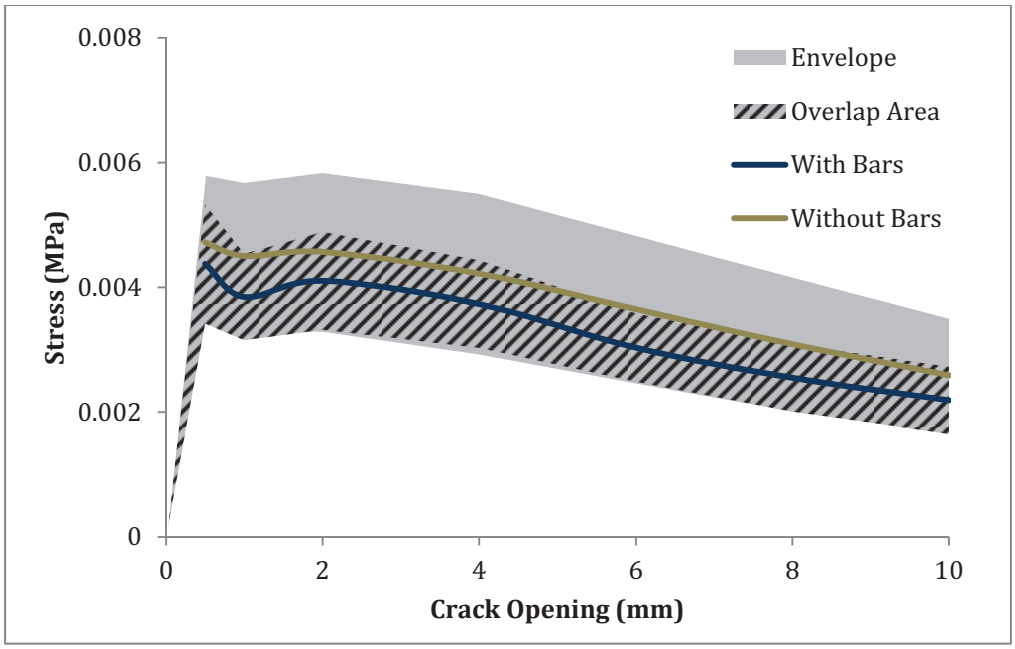

Figure 4.4 - Comparison of per-fibre Tuf-Strand SF post-crack stress displacement, with and without stiffening bars

The total effect of using stiffening bars to stiffen the specimen during the pre-crack phase to compensate for the lack of closed-loop feedback was mixed. Though the post-crack response was not affected by stiffening the pre-crack setup, the tensile response at cracking and immediately following cracking showed significant improvement. The cracking strain was reduced by 51% when stiffening bars were used, bringing the values closer to those observed in closed-loop tests. The gap between the cracking strain and the first point recorded in the post-crack phase was also reduced by 76%. The addition of the stiffening bars to the test setup allows for the evaluation of a more complete response and eliminate the concern of damage to the tensile response due to instability.

4.2 Stress-Crack Opening Relationship

4.2.1 General Post-Crack Response

The post-crack response of all specimens in each set were averaged in order to determine the $\sigma(w)$ response. The average $\sigma(w)$ plots of all the FRC mixes followed a similar shape: the response begins with an increasing slope that

ends in a maximum value at approximately 2 mm crack opening displacement. In a few instances this increasing section is preceded by a short decreasing slope. The maximum at 2 mm is followed by a decreasing slope until the end of the test. The highest point of the curve is more pronounced in some mixes than others; it is easily perceptible in all mixes except for the prototype fibre containing HDPE, 3% PVDF which produces a more consistent response than any other fibre type. Figures 4.5 and 4.6 show various fibres at 3.0 kg/m^3 dosage; the slope described above can clearly be seen.

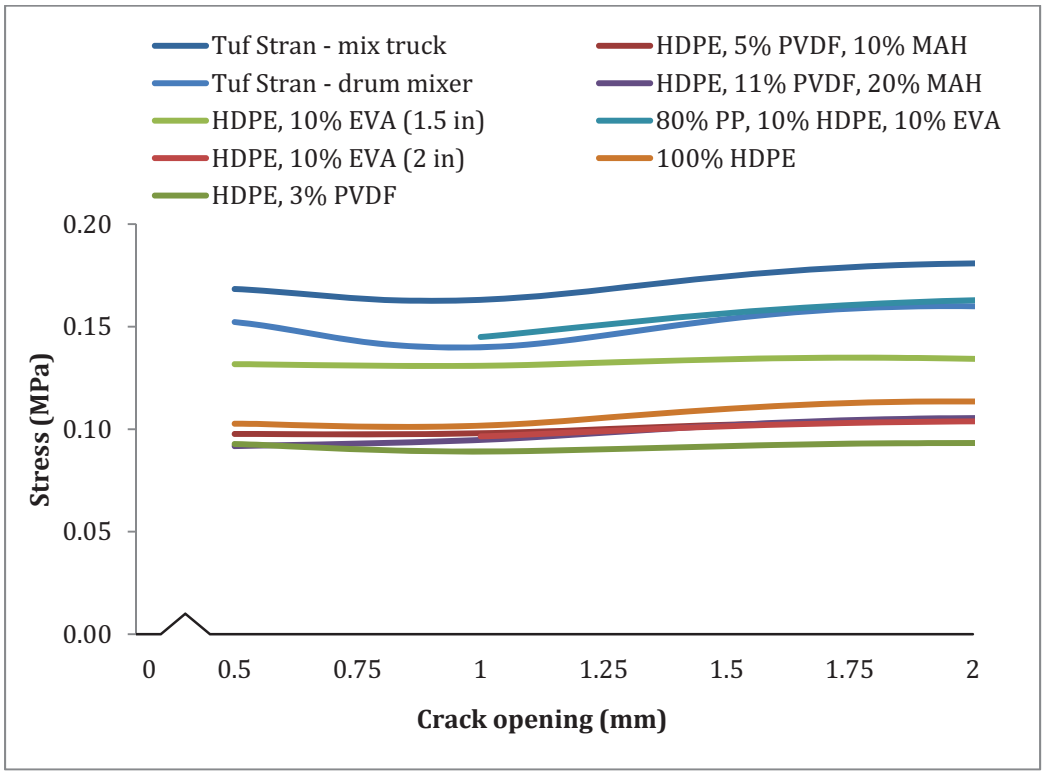

Figure 4.5 - σ(w) curve of various fibres, specimens cracked with stiffening bars, 3.0 kg/m^3 (up to 2 mm displacement)

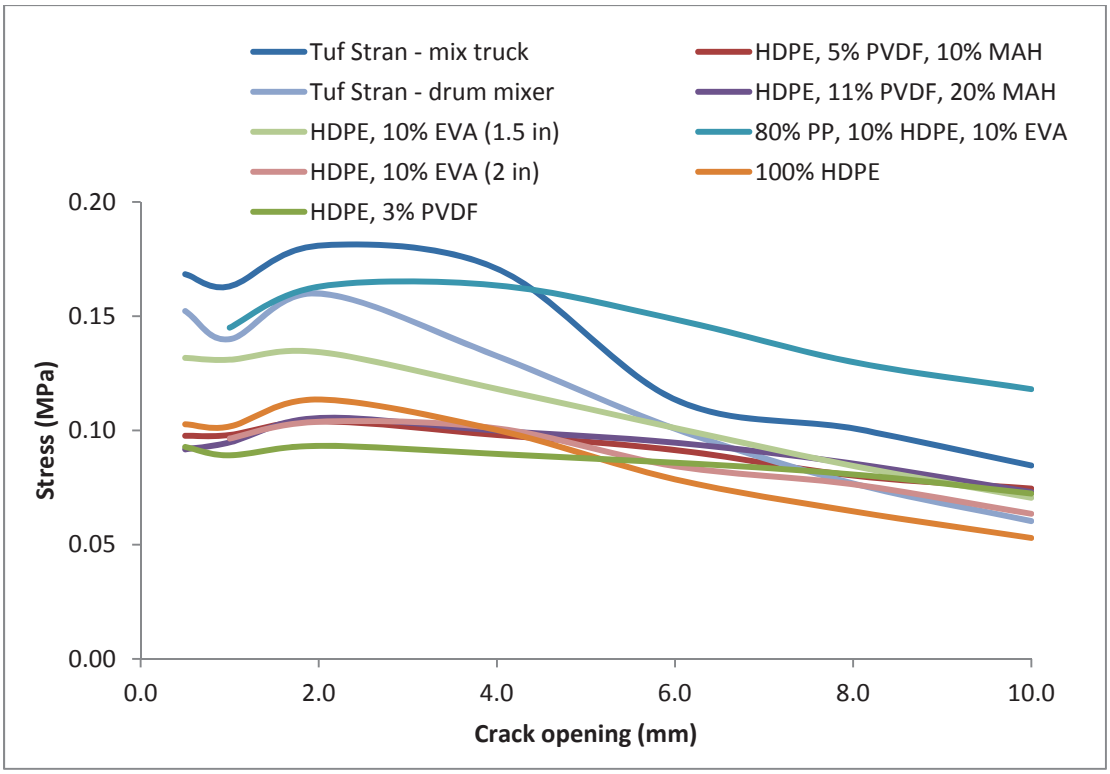

Figure 4.6 – σ(w) curve of various fibres, specimens cracked with stiffening bars, 3.0 kg/m^3 (up to 10 mm displacement)

RILEM suggests that the UTT, designed with steel fibres in mind, end after 2 mm of displacement. The synthetic fibres tested for this thesis; however, provide a resistance at displacements significantly larger than 2 mm. All tests were continued until 10 mm of displacement, the full capacity of the LVDTs used in the test setup. Though all the mixes showed a decrease in resistance at displacements greater than 2 mm, the fibre was capable of maintaining a significant amount of the resistance up to the end of the test. This translates into an increase in the toughness, G_f, of the FRC determined at maximum displacements of 2 mm and 10 mm, using Equation 2.1. Table 4.2 compares the σ and G_f determined for 2 mm and 10 mm end displacements for each fibre type.

Table 4.2 – Comparison of stress and toughnessat 2 mm and 10 mm crack openings

Fibre Type	Fibre Dosage kg/m^3	Casting Method	$f_{2.0}$ (MPa)	$f_{10.0}$ (MPa)	Decrease	$G_{2.0}$ (kJ)	$G_{10.0}$ (kJ)	Increase
Tuf-Strand SF	1.8	mix truck	0.0924	0.0726	79%	2.542	10.279	404%
	2.4		0.1195	0.0605	51%	2.565	11.183	436%
	3.0		0.1808	0.0846	47%	2.464	16.361	664%
	4.6		0.2159	0.1253	58%	4.720	21.950	465%
	6.9		0.2403	0.1208	50%	5.574	23.595	423%
	1.8	drum mixer	0.1227	0.0518	42%	2.441	9.875	405%
	3.0		0.1600	0.0603	38%	3.474	13.620	392%
	4.6		0.2963	0.1168	39%	7.869	28.288	359%
HDPE, 10% EVA (38 mm)	1.8		0.1424	0.0743	52%	3.304	14.105	427%
	3.0		0.1343	0.0705	53%	2.799	12.402	443%
	4.6		0.1708	0.0785	46%	3.032	13.971	461%
HDPE, 10% EVA (50 mm)	1.8		0.1115	0.0722	65%	2.477	11.502	464%
	3.0		0.1038	0.0635	61%	2.274	10.499	462%
	4.6		0.1399	0.0771	55%	3.167	13.485	426%
HDPE, 3% PVDF	3.0		0.0933	0.0724	78%	1.898	8.810	464%
HDPE, 5% PVDF, 10% MAH	3.0		0.1040	0.0746	72%	2.300	11.881	517%
HDPE, 11% PVDF, 20% MAH	3.0		0.1054	0.0730	69%	2.190	11.046	504%
80% PP, 10% HDPE, 10% EVA	3.0		0.1629	0.1181	72%	3.039	16.524	544%
100% HDPE	3.0		0.1135	0.0529	47%	2.350	10.004	426%

At a crack width of 10 mm, the stress is between 38% and 79% of the stress at a crack width of 2 mm; the average stress retained is 56%. The toughness at 10 mm increases between 359% and 664% compared to the toughness measured at 2 mm crack width; the average increase is 457%. This demonstrates that the fibres are able to continue providing a significant amount of resistnce past 2 mm; if the fibre performance steeply declined the toughness at 10 mm would be a similar value to the toughness at 2 mm. FRC is often used in shotcrete to reinforce tunnel lining and other applications

where they are exposed to high impact loads and large displacements. Synthetic fibres have a clear advantage over steel fibres in these applications due to their ability to maintain load resistance at crack openings 500% larger than those at which steel fibres are typically tested. A comparison of synthetic and steel fibres will be examined in more detail in Section 4.4.

4.2.2 Per Fibre Post-Crack Response

Per Fibre Response Within Concrete Matrix

AFT's Tuf-Strand SF production fibre was cast using five different dosages and two mixing methods. The average $\sigma(w)$ curves for all the mixes containing Tuf-Strand SF can be seen in Figures 4.7 and 4.8 below. In Figure 4.7 the relationship between increasing fibre dosage and post-cracking performance can be seen; as the fibre dosage increases the performance improves. An obvious exception; however, is the performance of the specimen set containing 4.6 kg/m^3 cast in the drum mixer. This mixture resulted in the best performance even though a mixture containing 6.9 kg/m^3 was also cast. The literature suggests that for disparities such as this, the number of fibres crossing the crack plane should be considered (Vandewall et al., 2003c). The relationship between fibre performance and the average number of fibres found in the crack plane for each specimen set is shown in Figure 4.8; similarly to Figure 4.7, the performance increased as the number of fibres increased. The specimen set containing 4.6 kg/m^3 cast in the drum mixer had the largest number of fibres crossing the crack plane. The UTT specimens were cast downward into a cylindrical mould, tamped, and vibrated. ASTM casting guidelines were followed but human interaction can affect the distribution and orientation of fibres, particularly in mixes with higher fibre dosages and lower workability. The average number of fibres found in the crack plane of each specimen set are shown in Table 4.3.

Table 4.3 – Average number of fibres counted in crack plane for each specimen set

Fibre Type	Fibre Dosage (kg-m$^{3)}$	Casting Method	Average No. Of Fibers
Tuf Strand SF	1.8	mix truck	24.6
	2.4		35.4
	3.0		38.3
	4.6		54.4
	6.9		70.3
	1.8	drum mixer	33.5
	3.0		42.6
	4.6		91.7
HDPE, 10% EVA (38 mm)	1.8		40.0
	3.0		53.0
	4.6		70.0
HDPE, 10% EVA (50 mm)	1.8		26.7
	3.0		33.0
	4.6		47.0
HDPE, 3% PVDF	3.0		15.0
HDPE, 5% PVDF, 10% MAH	3.0		21.0
HDPE, 11% PVDF, 20% MAH	3.0		21.3
80% PP, 10% HDPE, 10% EVA	3.0		36.0
100% HDPE	3.0		26.0

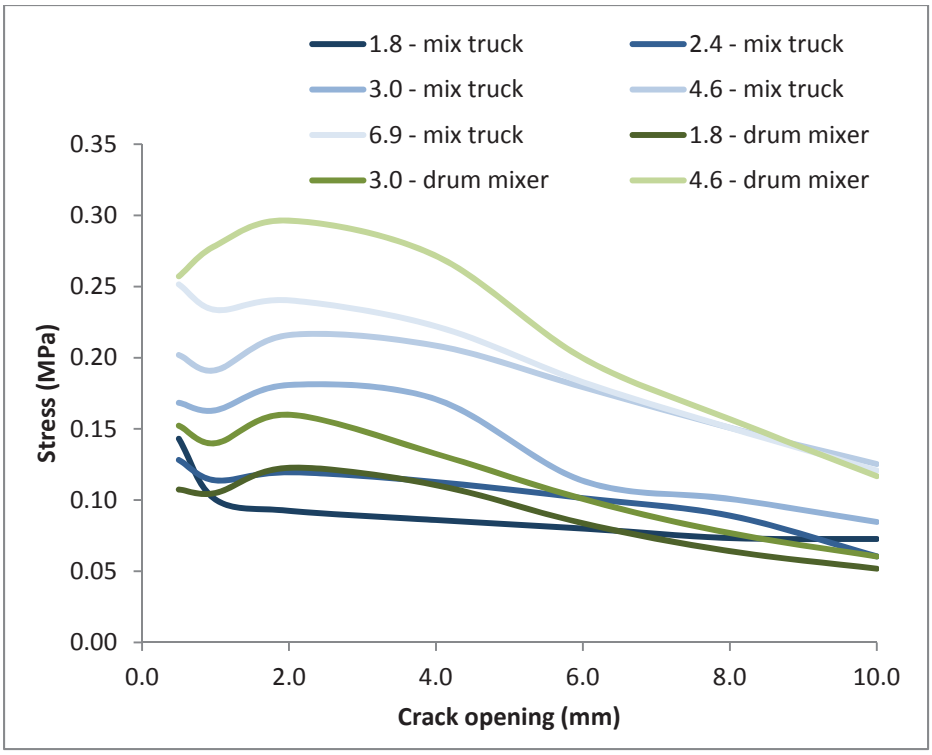

Figure 4.7 – σ(w) curve for Tuf-Strand SF at various dosages

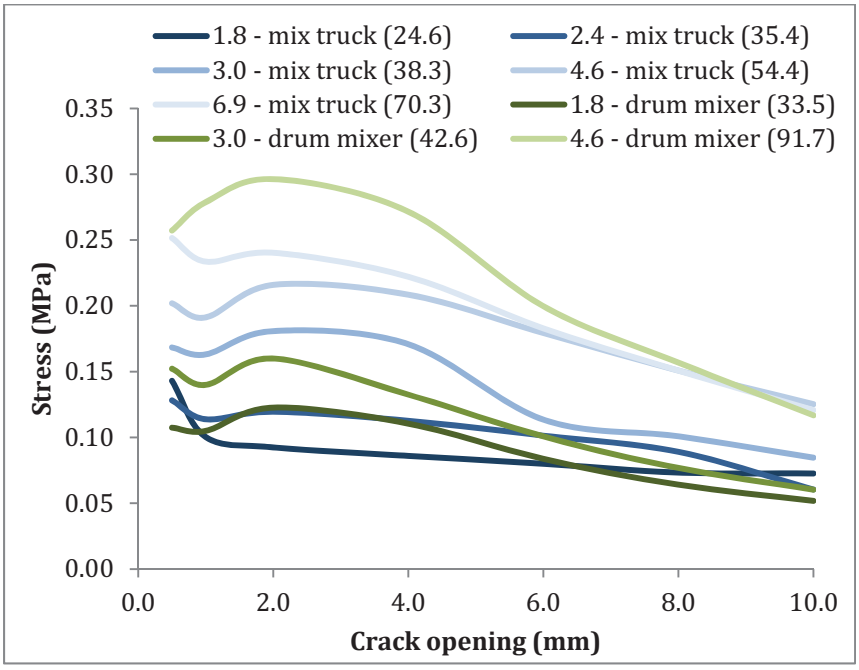

Figure 4.8 - σ(w) curve for Tuf-Strand SF by various dosages, average number of fibres crossing the crack plane in parenthesis

The results from each data set were divided by the average number of fibres found crossing the crack plane in order to determine a "per fibre" post-crack response. The per fibre response of the Tuf-Strand SF fibres, shown in Figure 4.9 below, show consistent pre fibre performance regardless of fibre dosage.

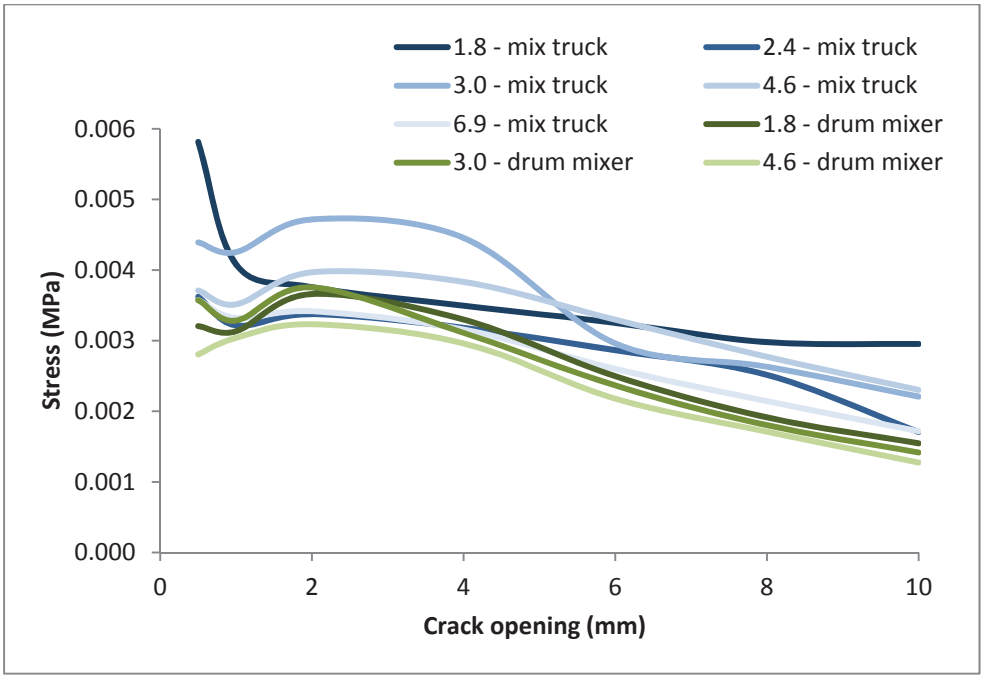

Figure 4.9 – σ(w) curve for Tuf-Strand SF, per fibre performance.

In order to further investigate the per fibre performance of the Tuf-Strand SF production fibre, the per fibre performance of each individual sample was determined. The σ(w) response and the toughness of each sample, expressed per fibre, can be seen in Figures 4.10 and 4.11 below. The Tuf-Strand SF fibre shows that regardless of dosage or casting methods, there is a consistent per fibre performance.

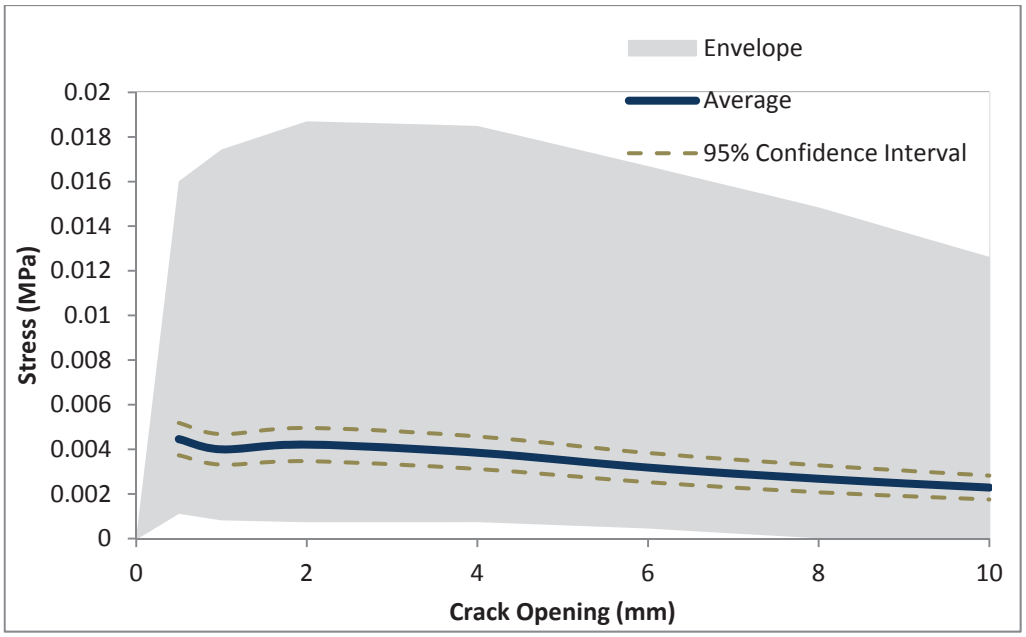

Figure 4.10 – Post-crack response of Tuf-Strand SF, per fibre performance of all specimens

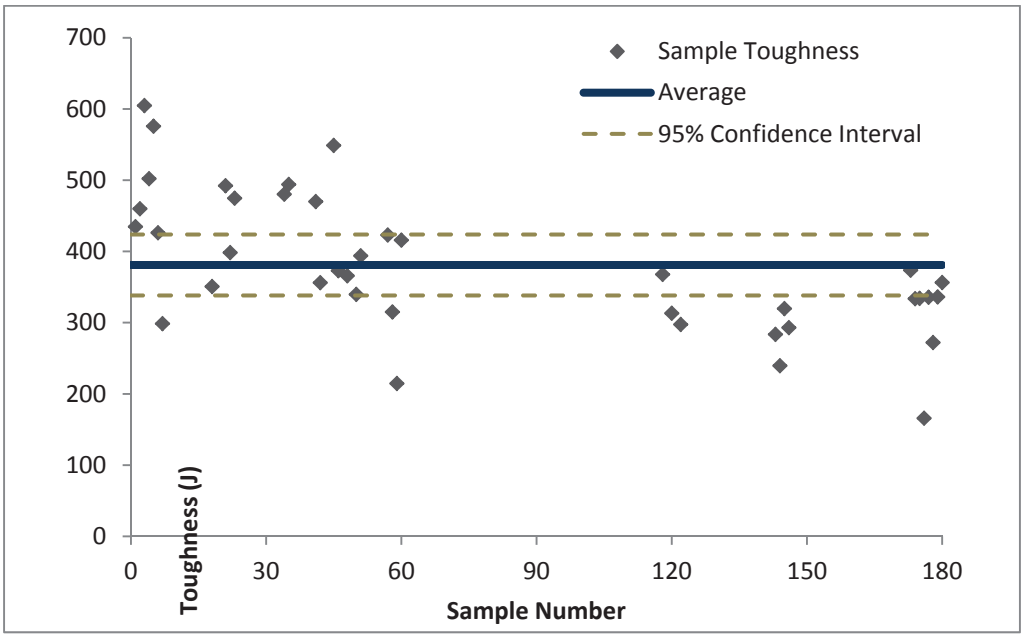

Figure 4.11 – Per fibre toughness of Tuf-Strand SF, all specimens

The per fibre performance for each specimen of the prototype fibres were plotted as well and can be found in Appendix C. The results show that each fibre type can be reliably described by the per fibre performance.

Comparison of Per Fibre Response and Prototype Fibre Testing Data

O'Connell (2011) completed a testing program at Dalhousie University to determine the tensile strength and pullout response of Tuf-Strand SF and the prototype fibres used in this study. The per fibre response was adjusted to reflect the stress over the fibre cross sectional area in order to compare the UTT results with O'Connell's data. The fibre tensile strength was compared to the maximum stress that occurs in each fibre over the course of the UTT. The strain at which the maximum stress occurs was also determined. The fibres reach between 7% and 25% of their ultimate stress during the UTT. The strain at maximum corresponds to the percentage of the ultimate stress obtained except in two cases: Tuf-Strand SF and 80% PP, 10% HDPE, and 10% EVA . Both of these fibres are expected to fibrillate when mixed with concrete, this may account for the difference.

Table 4.4 – Comparison of UTT response and tensile strength data

Fibre Type	$\sigma_{UTT, max}$	σ_f	$\%\sigma_f$	E_f	$\varepsilon_{UTT, max}$
Tuf-Strand SF	159	646	25%	9.53	1.7%
HDPE, 10% EVA (38 mm)	39	595	7%	5.67	0.7%
HDPE, 10% EVA (50 mm)	52	595	9%	5.67	0.9%
HDPE, 3% PVDF	108	749	14%	7.01	1.5%
HDPE, 5% PVDF, 10% MAH	135	779	17%	9.25	1.5%
HDPE, 11% PVDF, 20% MAH	75	595	13%	5.79	1.3%
80% PP, 10% HDPE, 10% EVA	117	718	16%	10.77	1.1%
100% HDPE	118	673	18%	6.13	1.9%

The post-crack response of each fibre was also compared to the pullout curves. An example of this can be seen in Figure 4.12. The pullout testing was conducted on two embedment lengths (25.4 mm and 22.2 mm) and five pullout angles (0°, 15 °, 30 °, 45 °, and 60 °) with a constant actuator rate of 5 mm/min (O'Connell, 2011). The UTT was conducted at a rate of 0.1 mm/min up to 1 mm of displacement and 0.5 mm/min until completion of the test. Synthetic fibres are sensitive to loading rate which makes a direct

comparison of the two tests difficult. Comparing the curves for each can give some measure of how a single fibre performs in pullout testing versus the individual fibre response in a concrete matrix. In most cases the UTT post-crack response most closely corresponded with the pullout curve for 15° inclination, 22.2 mm embedment length. The two exceptions were Tuf-Strand SF and 80% PP, 10% HDPE, and 10% EVA, again this was likely due to the lack of fibrillation in the pullout fibres. The comparison of the average and maximum stress can be found in Table 4.5. The full set of curves can be found in Appendix D.

Table 4.5 – Comparison of average and maximum stress of UTT and pullout test results

Fibre Type	$\sigma_{average}$			σ_{max}		
	UTT	Pullout	Test Details	UTT	Pullout	Test Details
Tuf-Strand SF	118	110	60 deg - 25.4 mm	148	126	60 deg - 25.4 mm
HDPE, 10% EVA (38 mm)	31	76	15 deg - 25.4 mm	39	100	15 deg - 22.2 mm
HDPE, 10% EVA (50 mm)	47			52		
HDPE, 3% PVDF	89	100	15 deg - 22.2 mm	108	114	15 deg - 22.2 mm
HDPE, 5% PVDF, 10% MAH	117	114	15 deg - 22.2 mm	135	141	15 deg - 22.2 mm
HDPE, 11% PVDF, 20% MAH	66	107	15 deg - 22.2 mm	75	133	15 deg - 22.2 mm
80% PP, 10% HDPE, 10% EVA	105	110	30 deg - 22.2 mm	117	115	30 deg - 22.2 mm
100% HDPE	91	95	15 deg - 22.2 mm	118	120	15 deg - 22.2 mm

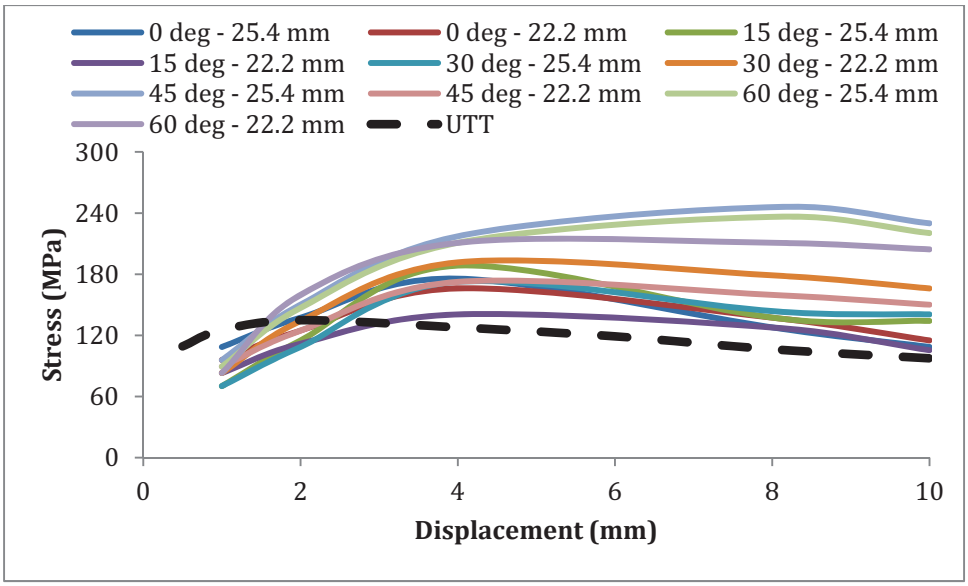

Figure 4.12 – Pullout curves and per fibre post-crack response of prototype fibre containing HDPE, 5% PVDF, and 10% MAH

4.3 Fibre Distribution in Crack Plane

The number of fibres crossing the crack plane of the tension specimens has been noted in the literature as an important factor affecting the post-crack response of FRC. When designing for industry, the amount of fibre added to concrete is dosed by weight, typically in kg/m^3. In order to predict the tensile response of FRC , the relationship between the prescribed fibre dosage of the specimens and the number of fibres observed in each specimen must be examined.

4.3.1 Experimental Determination

The number of fibres crossing the crack plane were counted and recorded for each UTT and ASTM C1609 specimen in order to examine the fibre distribution. The full set of specimen fibre counts can be found in Appendix E. The Student *t*-distribution, used to examine a normally distributed population of a small sample size with an unknown standard deviation, was applied to the fibre data. The *t*-distribution is similar to the normal distribution; it is

symmetrical and bell-shaped but it has heavier tails resulting in values that are more prone to fall far from the means.

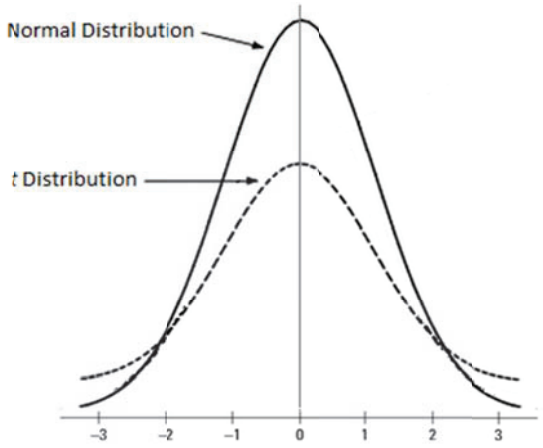

Figure 4.13 – Comparison of Normal and Student *t* Distributions

The mean, the 95% confidence interval, and the upper and lower limits for each set of specimens were calculated and presented in Table 4.6 and Table 4.7. There is a broad scope of scatter found in the fibre counts for each set. There is a lot of variation in the 95% confidence interval among data sets and the means of the UTT specimens vary with the different casting methods. For example, the Tuf-Strand SF fibre cast in the drum mixer at 4.6 kg/m^3 results in the highest mean even though Tuf-Strand SF was also cast at a dosage of 6.9 kg/m^3 by the mix truck. Also, the mean values for 1.8 kg/m^3, 3.0 kg/m^3 and 4.6 kg/m^3 specimen sets mixed in the drum mixer are all larger than the same dosages cast from the mix truck, but not by a consistent amount.

Table 4.6 – Experimental fibre distribution of UTT specimens

Fibre Type	Fibre Dosage (kg/m^3)	Casting Method	Mean	95% Conf. Interval	Lower Limit	Upper Limit
Tuf-Strand SF	1.8	mix truck	23	7.3	16	31
	2.4		35	5.8	29	40
	3.0		43	13.5	30	57
	4.6		55	5.2	50	60
	6.9		70	8.3	62	79
	1.8	drum mixer	34	8.8	25	42
	3.0		47	15.5	31	62
	4.6		81	17.7	63	99
HDPE, 10% EVA (38 mm)	1.8		34	8.8	25	42
	3.0		49	5.7	43	54
	4.6		80	18.9	61	99
HDPE, 10% EVA (50 mm)	1.8		28	6.2	22	34
	3.0		33	6.9	26	40
	4.6		50	9.6	40	60
HDPE, 3% PVDF	3.0		21	4.3	17	25
HDPE, 5% PVDF, 10% MAH	3.0		23	4.3	19	27
HDPE, 11% PVDF, 20% MAH	3.0		27	9.3	18	36
80% PP, 10% HDPE, 10% EVA	3.0		36	16.3	20	52
100% HDPE	3.0		29	8.2	21	37

Table 4.7 - Experimental fibre distribution of ASTM C1609 specimens

Fibre Type	Fibre Dosage (kg/m^3)	Casting Method	Mean	95% Conf. Interval	Lower Limit	Upper Limit
Tuf-Strand SF	1.8	mix truck	71	8.8	62	80
	2.4		91	21.8	69	113
	3.0		105	10.5	95	116
	4.6		120	26.6	93	146
	6.9		204	25.1	179	229
	1.8	drum mixer	70	10.9	59	81
	3.0		81	16.6	64	97
	4.6		113	12.4	101	126
HDPE, 10% EVA (38 mm)	1.8		64	9.2	55	73
	3.0		81	4.1	77	85
	4.6		130	49.7	80	180
HDPE, 10% EVA (50 mm)	1.8		55	17.6	37	72
	3.0		88	10.0	78	98
	4.6		108	21.6	86	130
HDPE, 3% PVDF	3.0		74	13.2	61	87
HDPE, 5% PVDF, 10% MAH	3.0		75	27.0	48	102
HDPE, 11% PVDF, 20% MAH	3.0		56	6.7	50	63
80% PP, 10% HDPE, 10% EVA	3.0		64	16.4	48	80
100% HDPE	3.0		106	10.2	95	116

4.3.2 Theoretical Determination

The number of steel fibres expected in the crack plane can be reliably determined theoretically (Dypont and Vandewalle, 2005). The total number of effective fibres, *n*, is calculated using the fibre dosage by volume fraction and an orientation factor;

$$n = \alpha \frac{V_f}{A_f} A_s \qquad [4.1]$$

Where:

α is the orientation coefficient,

V_f is the fibre volume fraction (%),

A_f is the fibre cross section (mm^2), and

A_s is the specimen cross section (mm^2)

The orientation factor, α, depends on the fibre's ability to rotate in the concrete. In the case of the UTT specimen cylindrical moulds, there are two areas to consider shown in Figure 4.14; Area 1: bulk condition in which the fibre can rotate freely which and Area 2: one boundary condition parallel to the direction of orientation. The notch cut into the specimens reduces the area with one boundary condition but does not eliminate it completely. In the case of the ASTM C1609 150 mm beam moulds, there are three areas to consider, shown in Figure 4.15; Area 1 and 2 previously described, and Area 3: two boundary conditions parallel to the direction of orientation. The α for the three conditions are 0.5, 0.6 and 0.84 for steel fibres in Areas 1, 2 and 3 respectively.

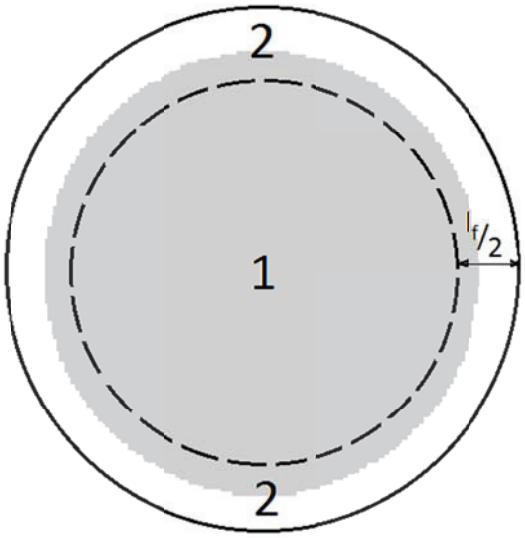

Figure 4.14 – UTT specimen cross section showing bulk condition (Area 1) and one boundary condition (Area 2); the shaded area shows cross section after the notch has been cut

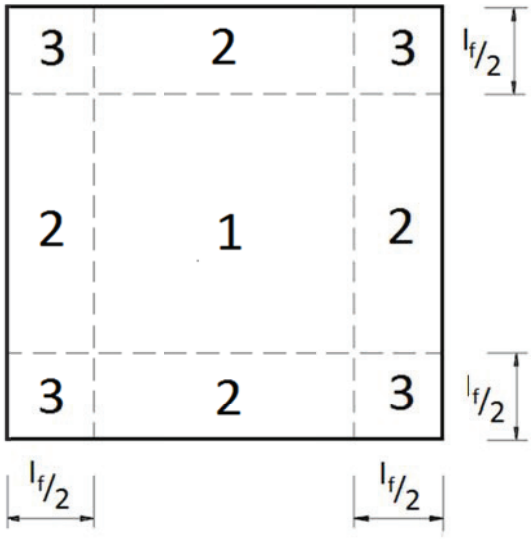

Figure 4.15 – ASTM C1609 specimen cross section showing bulk condition (Area 1), one boundary condition (Area 2), and two boundary conditions (Area 3)

The α previously described have been determined for steel fibres; however, no studies have been completed using synthetic fibres. In the case of steel fibres, the α is dependent on the assumption that the fibres remain straight. Synthetic fibres are less stiff and more flexible than steel and it cannot be

assumed that the fibres remain straight when cast in concrete. The experimental and theoretical mean fibre counts for each specimen set were compared in order to determine the orientation factors.

Table 4.8 – Means and orientation factors of UTT specimens

Fibre Type	Casting Method	Fibre Dosage (kg/m^3)	Experimental Mean	Theoretical Mean (no α)	α
Tuf-Strand SF	mix truck	1.8	23	69	0.339
		2.4	35	92	0.376
		3.0	43	115	0.377
		4.6	55	176	0.313
		6.9	70	264	0.267
	drum mixer	1.8	34	69	0.487
		3.0	47	115	0.406
		4.6	81	176	0.461
HDPE, 10% EVA (38 mm)		1.8	34	53	0.629
		3.0	49	89	0.548
		4.6	80	136	0.590
HDPE, 10% EVA (50 mm)		1.8	28	52	0.540
		3.0	33	87	0.379
		4.6	50	133	0.376
HDPE, 3% PVDF		3.0	21	102	0.207
HDPE, 5% PVDF, 10% MAH		3.0	23	108	0.213
HDPE, 11% PVDF, 20% MAH		3.0	27	69	0.393
80% PP, 10% HDPE, 10% EVA		3.0	36	117	0.308
100% HDPE		3.0	29	103	0.282

Table 4.9 - Means and orientation factors of ASTM C1609 specimens

Fibre Type	Casting Method	Fibre Dosage (kg/m^3)	Experimental Mean	Theoretical Mean (no α)	α
Tuf-Strand SF	mix truck	1.8	71	133	0.538
		2.4	91	177	0.516
		3.0	105	221	0.477
		4.6	120	353	0.338
		6.9	204	508	0.401
	drum mixer	1.8	70	133	0.530
		3.0	81	221	0.365
		4.6	113	353	0.321
HDPE, 10% EVA (38 mm)		1.8	64	100	0.637
		3.0	81	167	0.483
		4.6	130	256	0.508
HDPE, 10% EVA (50 mm)		1.8	59	100	0.584
		3.0	89	167	0.532
		4.6	113	256	0.440
HDPE, 3% PVDF		3.0	74	202	0.366
HDPE, 5% PVDF, 10% MAH		3.0	75	216	0.350
HDPE, 11% PVDF, 20% MAH		3.0	56	153	0.367
80% PP, 10% HDPE, 10% EVA		3.0	64	210	0.442
100% HDPE		3.0	106	239	0.304

The Student *t*-distribution was used to determine the α for each type of fibre and cross section. In Table 4.10, the orientation factors for each fibre type and specimen geometry were compared to the steel values for cylindrical specimens, α_C=0.532, and for beam specimens, α_B=0.584. In the cases of the Tuf-Strand SF and HDPE, 10% EVA fibres, the orientation factors for each geometry vary similarly from the steel values. The prototype fibres provided fewer samples to determine the orientation factor; however, this trend can also be seen in the fibre containing 100% HDPE.

Table 4.10 – Orientation factor for each fibre type and geometry, compared with steel values

Fibre Type	α_{UTT}	α_{UTT}/α_C	α_{ASTM}	α_{ASTM}/α_B
Tuf-Strand SF	0.378	71%	0.436	75%
HDPE, 10% EVA (1.5")	0.490	92%	0.519	89%
HDPE, 10% EVA (2")	0.470	88%	0.543	93%
HDPE, 3% PVDF	0.207	39%	0.366	63%
HDPE, 5% PVDF, 10% MAH	0.213	40%	0.350	60%
HDPE, 11% PVDF, 20% MAH	0.393	74%	0.367	63%
80% PP, 10% HDPE, 10% EVA	0.308	58%	0.442	76%
100% HDPE	0.282	53%	0.304	52%

Each fibre type results in a unique α value. The orientation factor, elastic modulus, tensile strength, and equivalent diameter of each fibre type were examined for both specimen geometries. There was no clear relationship between the α and the other fibre properties.

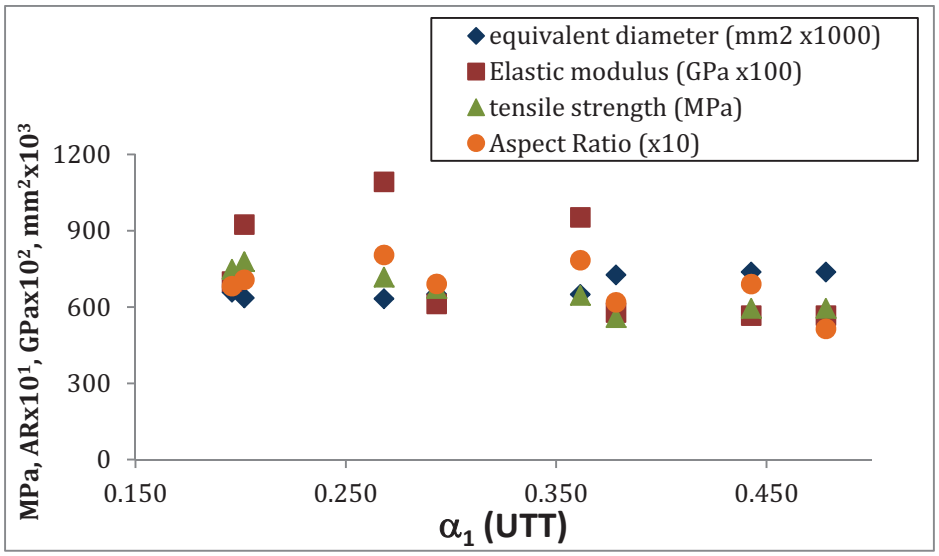

Figure 4.16 – Fibre strength, elastic modulus, and dimensions versus the orientation factor of Area 1 (UTT mould)

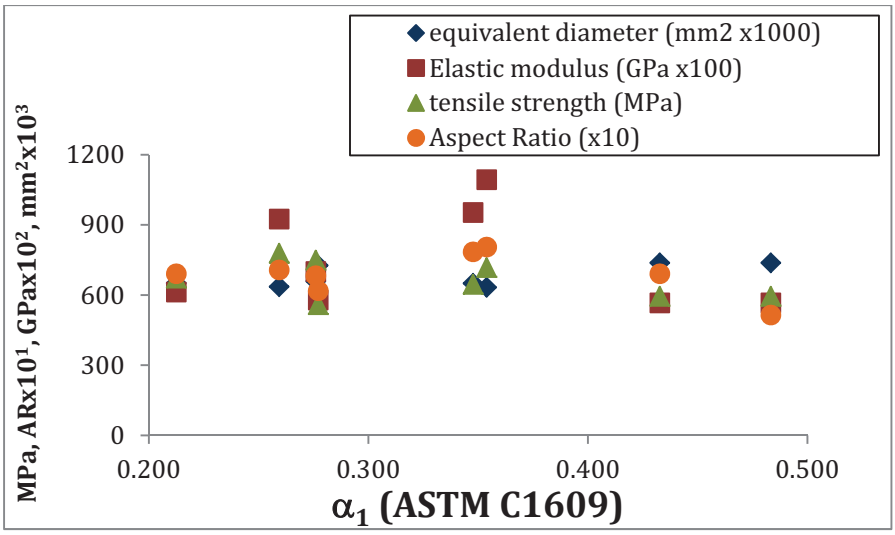

Figure 4.17 - Fibre strength, elastic modulus, and dimensions versus the orientation factor of Area 1 (ASTM C1609 mould)

The theoretical mean fibre count for each specimen set was determined using equation 4.1 with α values determined in Tables 4.8 and 4.9 and can be seen in Table 4.11. These means were used in order to compare the tensile and flexural responses of FRC in the next section.

Table 4.11 – Experimental and theoretical mean fibre counts for all specimen sets

Fibre Type	Fibre Dosage (kg/m$^{3)}$	Casting Method	UTT		ASTM C1609	
			Exper.	Theor.	Exper.	Theor.
Tuf-Strand SF	1.8	mix truck	23	26	71	54
	2.4		35	35	91	72
	3.0		43	44	105	90
	4.6		55	68	120	143
	6.9		70	101	204	206
	1.8	drum mixer	34	26	70	54
	3.0		47	44	81	90
	4.6		81	68	113	143
HDPE, 10% EVA (38 mm)	1.8		34	26	64	54
	3.0		49	43	81	91
	4.6		80	67	130	139
HDPE, 10% EVA (50 mm)	1.8		28	24	59	49
	3.0		33	41	89	82
	4.6		50	63	113	126
HDPE, 3% PVDF	3.0		16	21	74	67
HDPE, 5% PVDF, 10% MAH	3.0		21	23	75	68
HDPE, 11% PVDF, 20% MAH	3.0		20	27	56	51
80% PP, 10% HDPE, 10% EVA	3.0		36	33	64	87
100% HDPE	3.0		26	32	106	64

4.4 COMPARISON OF STEEL AND SYNTHETIC FRC PERFORMANCE

The use of steel fibres is currently more common in industry than the use of synthetics. In order to judge the viability of synthetic fibres in structural FRC applications, their post-crack response was compared to that of steel fibres. The tensile response of a typical structural steel FRC mix from the literature was considered; a mix containing Dramix RC 80/60 BN fibres at 50 kg/m^3. The UTT per fibre results for each fibre were multiplied by the number of fibres theoretically expected to cross the crack plane. A mixture of 4.6 kg/m^3 was compared because it represents a higher fibre volume while maintaining workability in the wet mix. The 4.6 kg/m^3 mix results in 0.5% fibre by

volume with Tuf-Strand SF and similar volumes with the prototype fibres, detailed in Table 4.12.

Table 4.12 – Fibre amount by volume in 4.6 kg/m^3 mix

Fibre Type	Fibre Volume
Tuf-Strand SF	0.50%
HDPE, 10% EVA (38 mm)	0.51%
HDPE, 10% EVA (50 mm)	0.51%
HDPE, 3% PVDF	0.47%
HDPE, 5% PVDF, 10% MAH	0.46%
HDPE, 11% PVDF, 20% MAH	0.44%
80% PP, 10% HDPE, 10% EVA	0.51%
100% HDPE	0.48%

The steel and synthetic post-crack responses can be seen in Figure 4.18. In all cases the synthetic fibres underperformed the steel mix; however, it was noted in Section 4.2.2 that the synthetic fibres are only achieving 7% to 25% of their ultime tensile strength. The performance of each fibre type can be found in Table 4.5; fibres with better bonding, such as Tuf-Strand SF which bonds through fibrillation, are capable of using more of their ultimate strength. Figure 4.19 shows the post-crack responses of the same synthetic fibre mixes if 50% of their ultimate tensile strenghtes are being used. This indicates that in order for synthetic fibres to be competitive with steel in structural applications, improvements are need to the bonding strengths in synthetics.

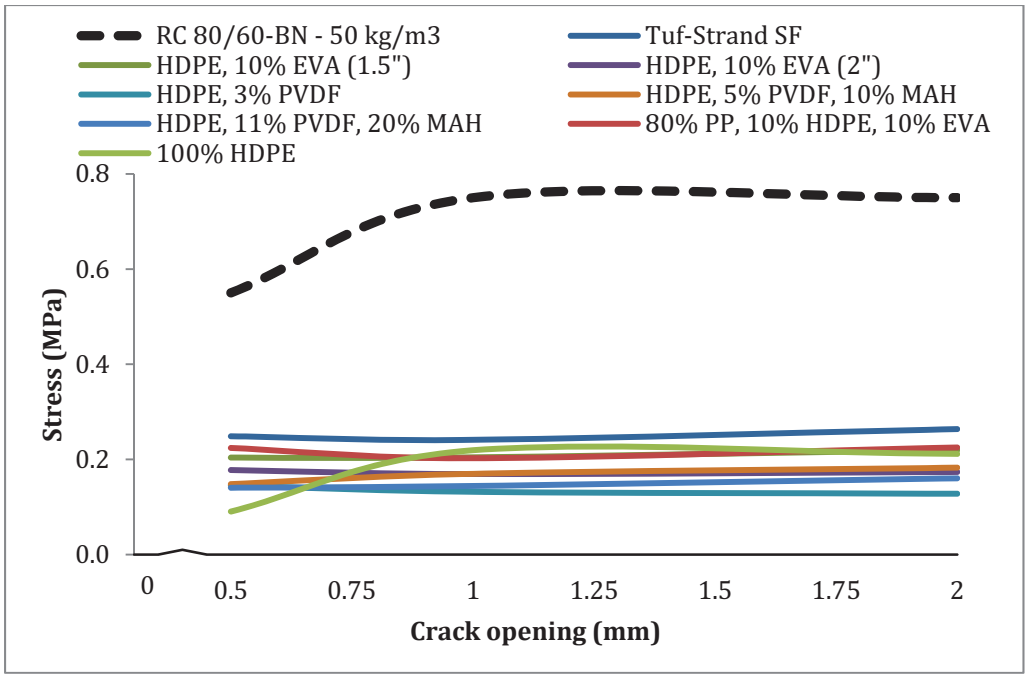

Figure 4.18 – Post-crack response of RC 80/60 BN at 50 kg/m³ and synthetic fibre at 4.6 kg/m³

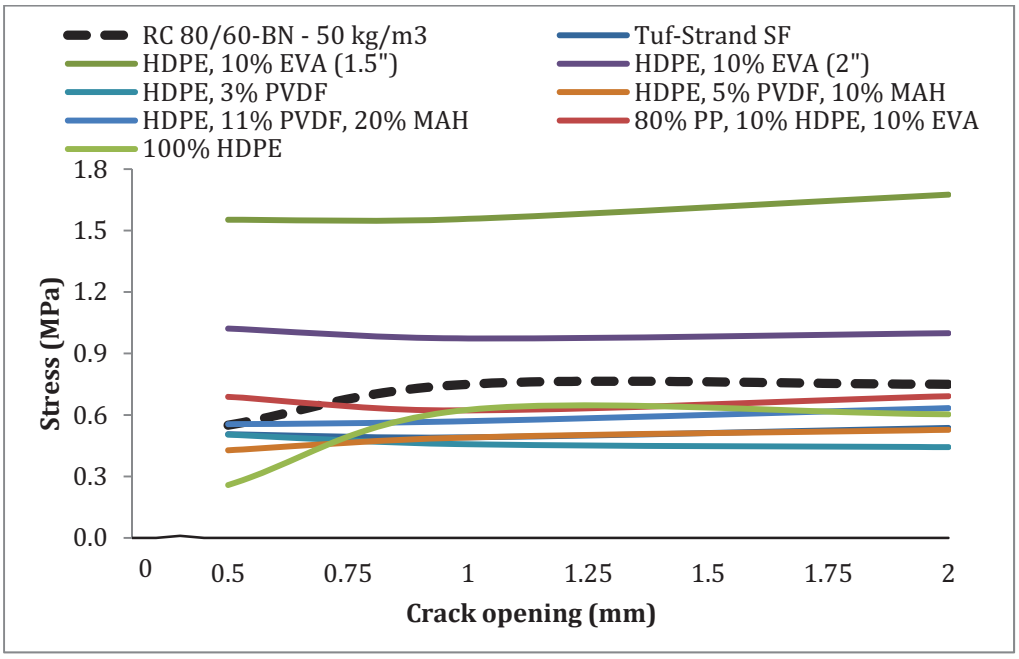

Figure 4.19 - Post-crack response of RC 80/60 BN at 50 kg/m³ and synthetic fibre at 4.6 kg/m³, at 50% σ_f

4.5 Correlation of Tensile and Flexural Responses of FRC

Specimens for UTT and ASTM C1609-10 four-point bending tests were cast from each concrete batch allowing for direct comparison of tensile and flexural data for each FRC mix. The UTT per fibre results for each fibre were multiplied by the number of fibres theoretically expected to cross the crack plane. Two methods, described in Section 2.8, were considered for this research; the simple approach proposed by the RILEM σ–ε design method and a more complicated closed-form solution proposed by Soranakkom and Mobasher (2008).

4.5.1 RILEM Stress-Strain Design Method

The predicted σ–ε relationship was determined from the ASTM C1609-10 data and plotted with UTT σ–ε curve for each data set. The method was designed using the load-deflection or load-CMOD curves determined from the three-point bending testl however, the ASTM C1609-10 "Standard Test Method for Flexural Performance of Fiber-Reinforced Concrete" is much more commonly performed in North America. An example of the comparison of both curves can be seen in Figure 4.20; curves for all data sets can be found in Appendix F.

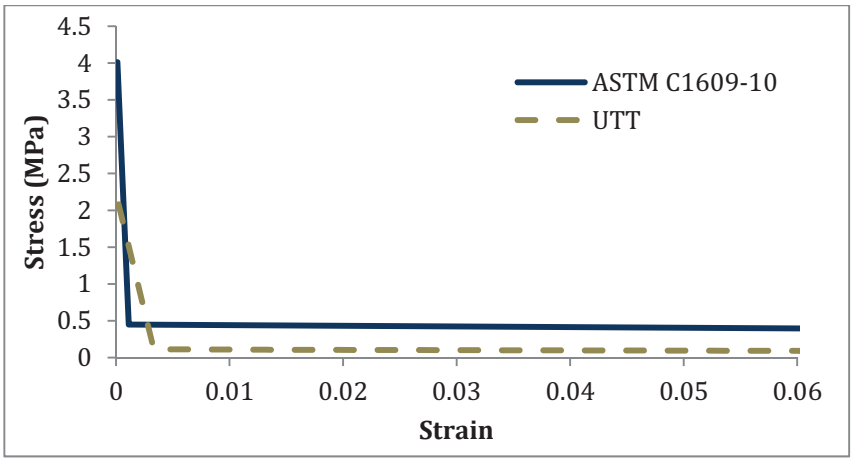

Figure 4.20 – Comparison of σ–ε responses: Tuf-Strand SF, 1.8 kg/m^3, cast from mix truck

The relationship proposed by RILEM results in a σ–ε curve with the same shape as the UTT results; however, in every case the flexural data overestimates the tensile response of FRC. The cracking and post-crack stress values determined from the flexural data need to be reduced by a factor, Φ, in order to agree with UTT response. The factor required for each data set can be found in Table 4.13. The Student *t*-distribution was applied to determine the mean and lower and upper limits of Φ for the Tuf-Strand SF production fibre and the HDPE, 10% EVA prototype fibres, shown in Table 4.14. There was not enough data available to determine these values for the rest of the prototype fibres.

Table 4.13 – Factors for RILEM σ–ε response, all data sets

Fibre Type	Fibre Dosage (kg/m^3)	Casting Method	$\Phi_{cracking}$	$\Phi_{post\text{-}crack}$
Tuf-Strand SF	1.8	mix truck	0.52	0.24
	2.4		0.37	0.28
	3.0		0.42	0.34
	4.6		0.45	0.54
	6.9		0.50	0.49
	1.8	drum mixer	0.42	0.31
	3.0		0.42	0.35
	4.6		0.49	0.47
HDPE, 10% EVA (38 mm)	1.8		0.53	0.26
	3.0		0.61	0.32
	4.6		0.39	0.32
HDPE, 10% EVA (50 mm)	1.8		0.42	0.20
	3.0		0.44	0.26
	4.6		0.56	0.36
HDPE, 3% PVDF	3.0		0.53	0.23
HDPE, 5% PVDF, 10% MAH	3.0		0.42	0.21
HDPE, 11% PVDF, 20% MAH	3.0		0.51	0.21
80% PP, 10% HDPE, 10% EVA	3.0		0.58	0.28
100% HDPE	3.0		0.52	0.30

Table 4.14 – Range of factors for RILEM σ–ε response

Fibre Type	$\Phi_{cracking}$			$\Phi_{post\text{-}crack}$		
	Lower Limit	Mean	Upper Limit	Lower Limit	Mean	Upper Limit
Tuf-Strand SF	0.41	0.45	0.49	0.29	0.38	0.47
HDPE, 10% EVA (38 mm)	0.23	0.51	0.79	0.22	0.30	0.38
HDPE, 10% EVA (50 mm)	0.29	0.48	0.66	0.08	0.28	0.47

4.5.2 Soranakom and Mobasher's Closed-form Solution

Soranakom and Mobasher (2008) completed a parametric study that indicated that the compression model has a marginal effect on the predicted flexural response; they concluded the compressive yield stress, f_{cy}, can be estimated as $0.85f'_c$. Several researchers have suggested a value of 0.004 for the ultimate compressive strain, ε_{cu} (Swammy and Al-Ta'an, 1981), (Hassoun and Sahebjam, 1985). All other parameters were determined from the UTT results and are shown in Table 4.15. The ultimate tensile strain was taken as 0.0667 for all data sets.

Table 4.15 – Parameters used in simulation of load-deflection response of FRC, all data sets

Fibre Type	Fibre Dosage (kg/m^3)	Casting Method	E (Mpa)	ε_{cr} ($x10^{-6}$)	ε_{cy} ($x10^{-6}$)	μ	ω
Tuf-Strand SF	1.8	mix truck	58692	141	646	0.063	12.1
	2.4		58692	141	562	0.084	9.8
	3.0		58692	141	575	0.105	9.0
	4.6		58692	141	494	0.160	7.9
	6.9		58692	141	502	0.240	8.9
	1.8	drum mixer	46743	106	582	0.059	9.1
	3.0		46743	106	635	0.098	10.2
	4.6		46743	106	569	0.151	10.7
HDPE, 10% EVA (38 mm)	1.8		22901	210	1426	0.022	8.3
	3.0		22901	210	1484	0.037	10.8
	4.6		22901	210	1509	0.056	7.3
HDPE, 10% EVA (50 mm)	1.8		21105	224	1395	0.028	8.3
	3.0		21105	224	1343	0.046	8.2
	4.6		21105	224	1375	0.071	10.8
HDPE, 3% PVDF	3.0		21171	301	1803	0.068	12.2
HDPE, 5% PVDF, 10% MAH	3.0		50057	90	708	0.068	10.3
HDPE, 11% PVDF, 20% MAH	3.0		127233	152	284	0.041	11.2
80% PP, 10% HDPE, 10% EVA	3.0		31374	158	1116	0.063	10.1
100% HDPE	3.0		41877	79	844	0.046	10.1

The flexural response was simulated from the UTT results for each data set. The ASTM C1609-10 four-point bending load-deflection curves and the closed-form approximation based on the average UTT response for each data set can be found in Appendix G. An example of this can be seen in Figure 4.21.

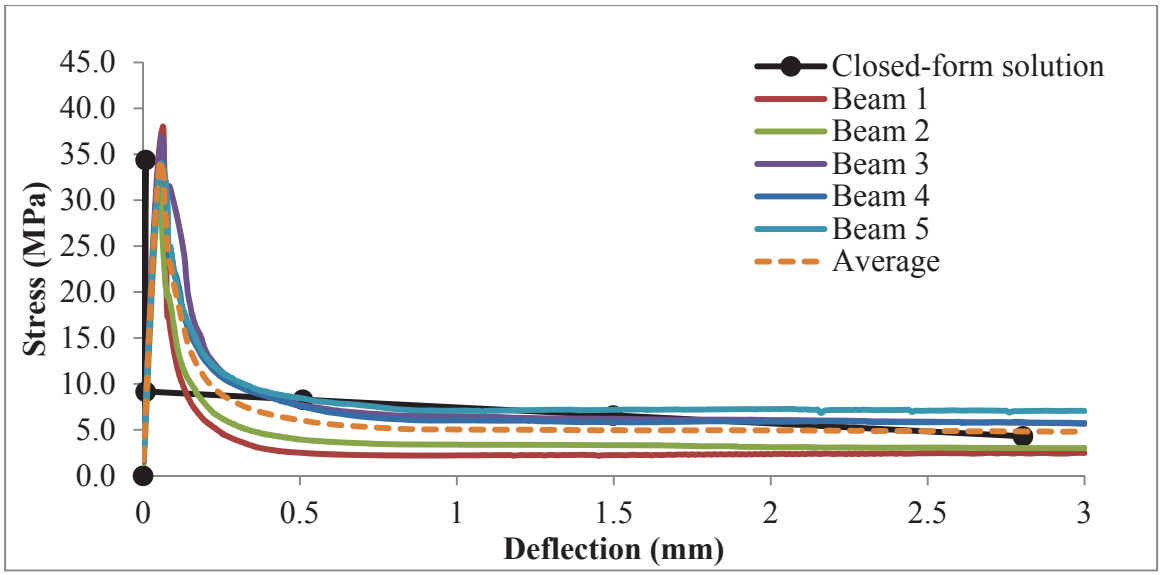

Figure 4.21 – Comparison of ASTM C1609-10 results and closed-form solution: Tuf-Strand SF, 1.8 kg/m^3, cast from drum mixer

The two parameters that have the most significant effect on the simulation of the flexural response are the normalized post crack tensile strength, μ, and the cracking strain, ε_{cr}. Soranakom and Mobasher suggest adjusting the ε_{cr} in order to obtain better agreement between the tensile simulation and the flexural data. In all cases the ε_{cr} was adjusted by a factor, Φ_{cr}, so that the predicted load at cracking corresponded to the average peak load determined by the ASTM C1609-10 test. An example of the closed-form load-deflection curve with and without the Φ_{cr} compared to the average of the four-point bending data can be seen in Figures 4.22 and 4.23.

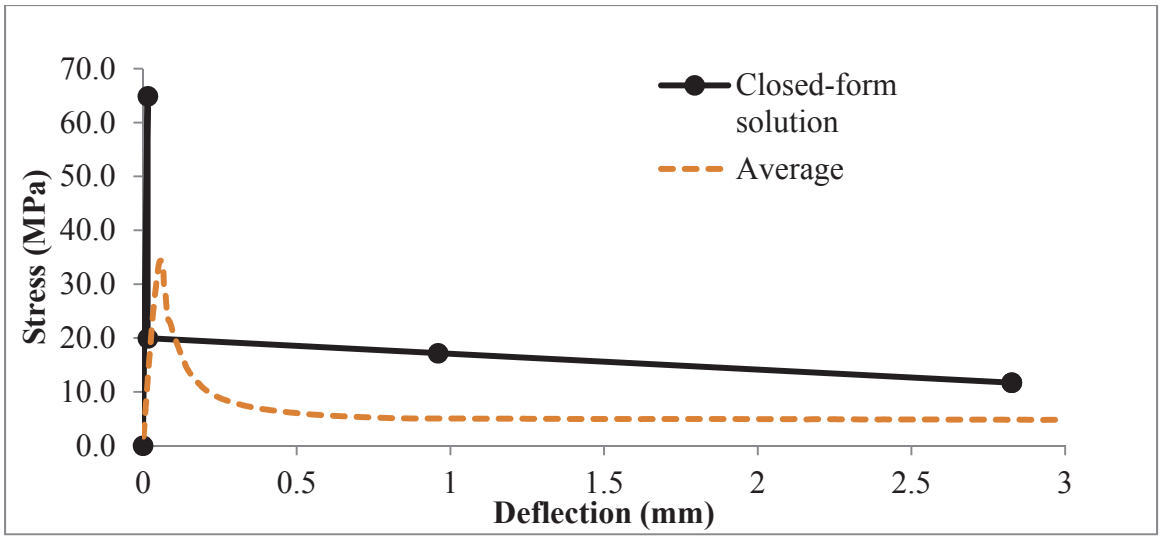

Figure 4.22 - Comparison of average ASTM C1609-10 response and closed-form solution without adjusted ε_{cr}: Tuf-Strand SF, 1.8 kg/m^3, cast from drum mixer

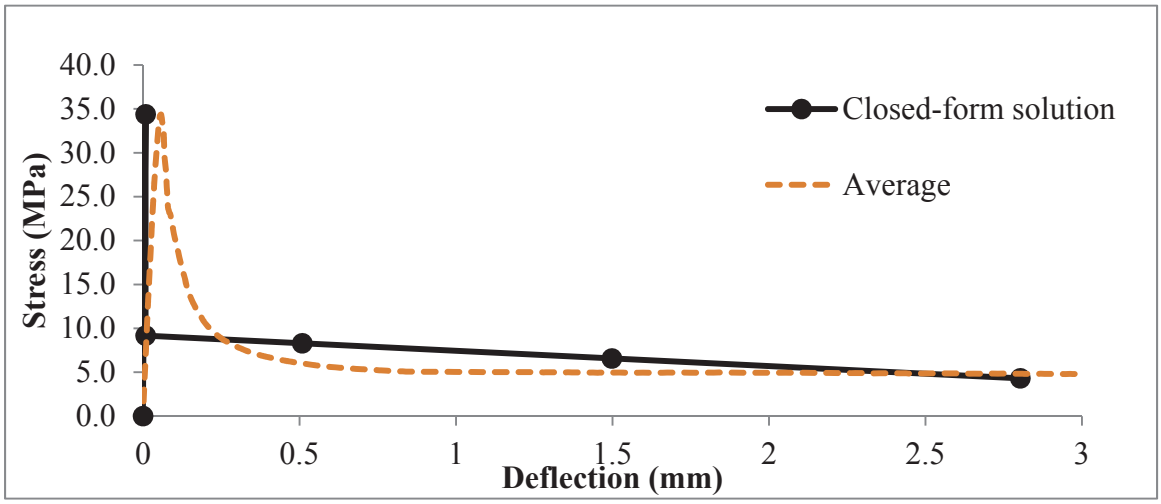

Figure 4.23 – Comparison of average ASTM C1609-10 response and closed-form solution with adjusted ε_{cr}: Tuf-Strand SF, 1.8 kg/m^3, cast from drum mixer

The post crack response used to determine the μ of each data set was based on the theoretical number of fibres expected in the crack plane for each fibre type and dosage. This parameter was not adjusted in order to compare the theoretical fibre count to the experimental four-point bending data. The theoretical fibre estimation provided good agreement with the flexural data. A safety factor, Φ_{fibre}, was determined to relate the experimental flexural data with the predicted flexural response based on tensile data.

The Φ_{cr} and Φ_{fibre} values for each data set can be found in Table 4.16. The Student *t*-distribution was applied to determine the mean, lower and upper limits of Φ for the Tuf-Strand SF production fibre and the HDPE, 10% EVA prototype fibres, shown in Table 4.17. There was not enough data available to determine these values for the rest of the prototype fibres.

Table 4.16 – Factors for the closed-form solution, all data sets

Fibre Type	Fibre Dosage (kg/m^3)	Casting Method	Φ_{cr}	Φ_{fibre}
Tuf Stran	1.8	mix truck	0.70	0.81
	2.4		0.77	1.14
	3.0		0.85	0.97
	4.6		0.87	0.94
	6.9		0.78	1.00
	1.8	drum mixer	0.84	0.96
	3.0		0.81	1.03
	4.6		0.72	1.03
HDPE, 10% EVA (38 mm)	1.8		0.81	0.84
	3.0		0.65	0.98
	4.6		0.95	1.06
HDPE, 10% EVA (50 mm)	1.8		0.80	1.01
	3.0		0.79	1.04
	4.6		0.63	1.10
HDPE, 3% PVDF	3.0		0.77	1.10
HDPE, 5% PVDF, 10% MAH	3.0		0.78	1.00
HDPE, 11% PVDF, 20% MAH	3.0		0.70	1.02
80% PP, 10% HDPE, 10% EVA	3.0		0.66	1.36
100% HDPE	3.0		0.89	1.01

Table 4.17 – Range of factors for closed-form solution

Fibre Type	Φ_{cr}			Φ_{fibre}		
	Lower Limit	Mean	Upper Limit	Lower Limit	Mean	Upper Limit
Tuf Stran	0.74	0.79	0.84	0.91	0.98	1.06
HDPE, 10% EVA (38 mm)	0.61	0.80	1.00	0.81	0.96	1.11
HDPE, 10% EVA (50 mm)	0.61	0.74	0.87	0.99	1.05	1.10

CHAPTER 5 DISCUSSION OF RESULTS

A research program was conducted in order determining the uni-axial tensile response necessary for structural design incorporating FRC. In order to make the UTT procedure RILEM has proposed more widely available, the UTT was completed without closed-loop feedback and adjustments made to the test setup in order to compensate for the lack of a closed-loop setup. In order to produce post-crack responses within the allowable deviation in 3 LVDT's using stiffening bars instead of servo control. The post-crack responses of each fibre type and dosage were examined; the per fibre performance is the same regardless of dosage. The fibre orientation factor is necessary to determine the number of fibres expected in the crack plane, which can be determined for each fibre type. The parameters required to design FRC with the prescribed tensile strength using synthetic fibres were determined. Also, methods for comparing the flexural and tensile responses of FRC were investigated. Flexural testing, such as the ASTM C1609-10 "Standard Test Method for Flexural Performance of Fiber-Reinforced Concrete", is routinely performed for quality control purposes.

5.1 Test Setup and Procedure

This study confirmed the viability of a UTT completed without closed-loop feedback. A test set up without any additional stiffening will produce the cracking and post-crack response of FRC; however, additional stiffening is easily added to the test set up and is beneficial to the testing program. Once stiffening bars were added to the test set up, the all the data required for the RILEM σ–ε design method was obtained from the UTT.

A UTT conducted with stiffening bars during the pre-crack portion reduces the cracking strain the tension specimens, more closely resembling the cracking strain of UTT performed using closed-loop feedback. The stiffening bars also preserved more of the post-crack data; the gap between the

cracking strain and the first data point of the post-crack response was reduced by 76%.

It was discovered during the testing program that the "jump" which occurs after cracking also caused the fixtures bolted into the testing machine to loosen over time. Once these became loose, the fixtures could rotate a small amount resulting in a test that no longer maintained uni-axial tension. This was observed once the test data was examined and the average displacement at 2 mm differed by more than 10% from any given LVDT reading.

5.2 Test Specimens

The specimens were cast and grouped according to fibre type and dosage. RILEM suggests at least 6 specimens in every set due to the variation in fibre distribution. Also, any specimens that did not maintain uni-axial tension, as described in the previous section, had to be discarded.

The prototype fibres were only cast with at a dosage of 3.0 kg/m^3 with 6 specimens in each set. These sets did not provide enough data to fully understand the correlation of fibre dosage and fibre distribution.

5.3 Stress-Crack Opening Displaceent Relationship

The average $\sigma(w)$ plots of all the synthetic fibres follow a similar shape: the response begins with an increasing slope that ends in a maximum value at approximately 2 mm crack opening displacement, followed by a decreasing slope until the end of the test. All fibres were tested until 10 mm of displacement, the full capacity of the LVDTs used in the test setup.

5.4 Fibre Orientation Factor

The method for determining fibre distribution in the crack plane of specimens containing steel fibres was applied to the synthetic FRC samples. A different

orientation factor was required in order to obtain correlation between the theoretical and experimental data. The synthetic fibre orientation factor is unique for each fibre type. The research showed that the α for each fibre type and boundary condition was a material property and not dependent on the casting method. No clear relationship existed between the α and any other fibre property.

5.5 Correlation of Tensile and Flexural Responses

Two methods developed to compare the tensile response with the more commonly conducted ASTM C1609 flexural response of steel FRC were applied to the study data. Both cases showed these methods are valid when applied to synthetic fibres. The closed-form solution proposed by Soranakom and Mobasher provides the best correlation and is not significantly more complicated or time consuming than the RILEM σ–ε design method.

CHAPTER 6 CONCLUSION AND RECOMENDATIONS

A research program was conducted in order determining the uni-axial tensile response necessary for structural design incorporating FRC. Each fibre type can be described by a per fibre post-crack response which is measurable up to 10 mm, the limit of the testing equipment. Adjustments were made to the fixture to allow for testing without closed-loop feedback. Finally, the parameters required to design FRC with the prescribed tensile strength using synthetic fibres were determined.

6.1 CONCLUSIONS

- In order to prevent loosing of the connections, periodic tightening of all fixture connects is required.
- Synthetic fibres are capable of maintaining a significant amount of resistance at crack widths greater than 2 mm, at least up to 10 mm. These data is useful in applications such as tunnel linnings which experience large deformations
- Each fibre type can be described by a normalized per fibre performance and the fibre distribution in the crack plane was a significant consideration.

6.2 RECOMMENDATIONS

- A load cell with a higher capacity would allow for larger stiffening bars. Enough stiffening of the test set up would likely completely eliminate the "jump" which occurs after cracking and the resulting gap in data.
- Each fibre should be cast in several fibre dosages with at least 12 cylinders in each set in order to provide enough specimens and meaningful data.
- The fibre distribution should be studied in more detail in order to determine the α with more accuracy for different fibre types and to determine if this value is related to any other fibre property.

6.3 DESIGN OF SYNTHETIC FRC

The primary goal of this research was to be able to design FRC containing synthetic fibres for structural applications. In order to do this it must be possible to prescribe the dosage required, D in kg/m^3, to obtain a specific material tensile strength, σ_{FRC} in MPa. The per fibre post-crack response, $\sigma(w)_{fibre}$, and fibre orientation factor, α_{fibre}, must be determined for the specific fibre type being used. The σ_{FRC} can be determined using the following equation:

$$\sigma_{FRC}(w) = \alpha_{fibre} \frac{A_{cylinder} D}{A_{fibre} \rho_{fibre}} \sigma(w)_{fibre} \qquad [5.1]$$

Where:

D is the fibre dosage in kg/m^3

$A_{cylinder}$ is the cross sectional area of the cylinder (mm^2),

A_{fibre} is the cross sectional area of the fibre (mm^2) and

ρ_{fibre} is the density of the fibre (kg/m^3).

Table 6.1 - Boundary condition 1 and 2 orientation factors for each fibre type

Fibre Type	α_1	α_2
Tuf-Strand SF	0.361	0.434
HDPE, 10% EVA (38 mm)	0.478	0.574
HDPE, 10% EVA (50 mm)	0.443	0.531
HDPE, 3% PVDF	0.196	0.235
HDPE, 5% PVDF, 10% MAH	0.202	0.242
HDPE, 11% PVDF, 20% MAH	0.378	0.454
80% PP, 10% HDPE, 10% EVA	0.268	0.322
100% HDPE	0.293	0.352

REFERENCES

Bekaert. (2010). *Dramix RC 65/60 BN* [Data sheet]. Retreieved from www.bekaert.com

Bernard, E. S., "Correlations in the behavior of fibre reinforced shotcrete beam and panel specimens", *Materials and Structures*, **35** (2002) 156-164.

Dupont, David and Vandewalle, Lucie, "Distribution of steel fibres in rectangular sections", *Cement & Concrete Composites*, **27** (2005) 391-398.

Hassoun, M.N. and Sahebjam, K., "Plastic hinge in two-span reinforced concrete beams containing steel fibers", *Proceedings of the American Society of Civil Engineers.* (1985) 119-139.

Hillerborg, A., Modeer, M. And Petersson, P. E., "Analysis of crack formation and crack growth in concrete by means of fracture mechanics and finite elements", *Cement and Concrete Research*. **6** (6) (1976) 773-782.

Hordijk, D. A., Reinhardt, H. W., and Cornelissen, H. A. W., "Fracture Mechanics Parameters of Concrete from Uniaxial Tensile tests as Influenced by Specimen Length", in SEM/RILEM International Concerence on Fracture of Concrete and Rock, (S. P. Shah and S. E. Swartz, Editors) (Houston, Texas) (1987) 138-149.

Linsbauer, H. N., and Tschegg, E. K., "Fracture energy determination of concrete with cube shaped specimens", *Zement und Beton*, **31** (1986) 38-40.

Löfgren, I., Stang, H., and Olesen, J. F., "Fracture Properties of FRC Determined through Inverse Analysis of Wedge Splitting and Three-Point Bending Tests", *Journal of Advanced Concrete Technology,* **3** (3) (2005) 423-434.

Löfgren, I., Stang, H., and Olesen, J. F., "The WST method, a fracture mechanics test method for FRC", *Materials and Structures*, **41** (2008) 197-211.

Mobasher, B. and Destrée, X., "Design and construction aspects of steel fiber-reinforced concrete elevated slabs", *ACI Special Publication,* **274** (2010) 95-107.

O'Connell (2011). *Development of a new high performance synthetic fiber for concrete reinforcement.* Unpublished master's thesis, Dalhousie University, Halifax, NS, Canada.

Olesen, J. F., "Fictitious crack propagation in fiber-reinforced concrete beams", *Journal of Engineering Mechanics.* **127** (3) (March 2001) 272-280.

Østergaard, L. (2003) *Early-age fracture mechanics and cracking of concrete – experiments and modeling*. Ph.D. thesis, Technical University of Denmark, Copenhagen, Denmark.

Senthilkumar, S. R. R. and Natesan, S.C., "Crack arrest properties of polypropylene fibres in cement composites", *Journal of Structural Engineering,* **32** (4) (October-November 2005) 291-295.

Soranakom, C. and Mobasher, B., "Closed-form solutions for flexural response of fiber-reinforced concrete beams"' *Journal of Engineering Mechanics*, **133** (8) (2007) 933-941.

Soranakom, C. and Mobasher, B., "Correlation of tensile and flexural responses of strain softening and strain hardening cement composites", *Cement and Concrete Composites,* **30** (2008) 465-477.

Sorelli, L. G., Meda, A., and Plizzari, G. A., "Steel Fiber Concrete Slabs on Ground: A Structural Matter", *ACI Structural Journal,* **103** (4) (July-Aug 2006) 551-558.

Swamy, R.N. and Al-Ta'an, S.A.,"Deformation and ultimate strength in flexural of reinforced concrete beams made with steel fiber concrete", *ACI Structural Journal.* **78** (5) (1981) 395-405.

Trottier, J-F, Mahoney, M. And Forgeron, D., "Can Synthetic Fibers Replace Welded-Wire Fabric in Slabs-on-Ground?", *Concrete International*. **24** (11) (2002).

Vandewalle, L. *et al.*, Recommendations of RILEM TC162-TDF: "Test and Design Methods for Steel Fibre Reinforced Concrete: Bending test (recommendation)", *Materials and Structures*. **33** (2000) 3-5.

Vandewalle, L. *et al.*, Recommendations of RILEM TC162-TDF: "Test and Design Methods for Steel Fibre Reinforced Concrete: design of steel fibre reinforced concrete using the σ-w method: principles and applications , *Materials and Structures*. **35** (2002) 262-278.

Vandewalle, L. *et al.*, Recommendations of RILEM TC162-TDF: "Test and Design Methods for Steel Fibre Reinforced Concrete: Uni-axial tension test for steel fibre reinforced concrete (recommendation)", *Materials and Structures*. **34** (2001) 3-6.

Vandewalle, L. *et al.*, Recommendations of RILEM TC162-TDF: "Test and Design Methods for Steel Fibre Reinforced Concrete: σ–ε design method (final recommendation) , *Materials and Structures*. **36** (2003a) 560-567.

Vandewalle, L. *et al.*, "Round-robin analysis of the RILEM TC 162-TDF uni-axial tensile test: Part 1", *Materials and Structures*, **36** (2003b) 265-274.

Vandewalle, L. *et al.*, "Round-robin analysis of the RILEM TC 162-TDF uni-axial tensile test: Part 2", *Materials and Structures*, **36** (2003c) 275-280.

Wang, Y., Li, V. C., and Backer, S., "Experimental Determination of Tensile Behavior of Fiber Reinforced Concrete", *ACI Materials Journal.* **87** (1990) 461-468.

Won, J.-P., Park, C.-G., Lee, S.-W., and Kim, H.-Y., "Performance of synthetic macro-fibres in reinforced concrete for tunnel linings", *Magazine of Concrete Research*. **61** (2009) 165-172.

APPENDIX A – ADDITIONAL CHARTS FOR UTT SPECIMEN STABILITY

Table A.1 – Summary of accepted and rejected UTT (1 of 5)

Fibre Type *Dosage*	Sample Number	Accepted	Rejected	Notes
Tuf Stran (Mix Truck) *1.8 kg/m^3*	1	X		
	2	X		
	3	X		
	4	X		
	5	X		
	6	X		
	7	X		
Tuf Stran (Mix Truck) *2.4 kg/m^3*	17	X		
	18	X		
	21	X		
	22	X		
	23	X		
Tuf Stran (Mix Truck) *3.0 kg/m^3*	33	X		
	34	X		
	35	X		
	36	X		
Tuf Stran (Mix Truck) *4.6 kg/m^3*	41	X		
	42	X		
	45	X		
	46	X		
	48	X		
Tuf Stran (Mix Truck) *6.9 kg/m^3*	50	X		
	57	X		
	58	X		
	59	X		
	60	X		

Table A.1 - Summary of accepted and rejected UTT (2 of 5)

Fibre Type *Dosage*	Sample Number	Accepted	Rejected	Notes
Tuf Stran (Drum Mixer) *1.8 kg/m^3*	173	X		
	174	X		
	175	X		
	176	X		
	177	X		
	178	X		
	179	X		
	180	X		
Tuf Stran (Drum Mixer) *3.0 kg/m^3*	141		X	
	143	X		
	144	X		
	145	X		
	146	X		
	147	X		
Tuf Stran (Drum Mixer) *4.6 kg/m^3*	118	X		
	119		X	Bolts in test set were loose
	120	X		
	122	X		
	123		X	Bolts in test set were loose
	124		X	Bolts in test set were loose

Table A.1 – Summary of accepted and rejected UTT (3 of 5)

Fibre Type *Dosage*	Sample Number	Accepted	Rejected	Notes
HDPE, 10% EVA (1.5") (Drum Mixer) *1.8 kg/m^3*	157	X		
	158		X	Bolts in test set were loose
	159		X	Bolts in test set were loose
	160	X		
	161	X		
	162		X	Bolts in test set were loose
	163	X		
	164	X		
HDPE, 10% EVA (1.5") (Drum Mixer) *3.0 kg/m^3*	149	X		
	153	X		
	154		X	
	156	X		
HDPE, 10% EVA (1.5") (Drum Mixer) *4.6 kg/m^3*	125	X		
	126		X	
	128	X		
	129	X		
	130	X		
	131		X	
	132		X	
HDPE, 10% EVA (2.0") (Drum Mixer) *1.8 kg/m^3*	165	X		
	166	X		
	167	X		
	168	X		
	169	X		
	171	X		
	172		X	

Table A.1 – Summary of accepted and rejected UTT (4 of 5)

Fibre Type *Dosage*	Sample Number	Accepted	Rejected	Notes
HDPE, 10% EVA (2.0") (Drum Mixer) *3.0 kg/m^3*	133		X	Bolts in test set were loose
	135	X		
	136	X		
	137		X	Bolts in test set were loose
	138	X		
	139		X	Bolts in test set were loose
	140		X	Bolts in test set were loose
HDPE, 10% EVA (2.0") (Drum Mixer) *4.6 kg/m^3*	110		X	
	111	X		
	112	X		
	113	X		
	114	X		
	115	X		
	116	X		
HDPE, 3% PVDF *3.0 kg/m^3*	73	X		
	74	X		
	75	X		
	76	X		
	77		X	
	78		X	
HDPE, 5% PVDF, 10% MAH *3.0 kg/m^3*	68	X		
	70			
	71	X		
	72	X		

Table A.1 – Summary of accepted and rejected UTT (5 of 5)

Fibre Type *Dosage*	Sample Number	Accepted	Rejected	Notes
HDPE, 11% PVDF, 20% MAH *3.0 kg/m^3*	85	X		
	88		X	
	89	X		
	90	X		
80% PP, 10% HDPE, 10% EVA *3.0 kg/m^3*	97	X		
	98	X		
	99			
	100	X		
100% HDPE *3.0 kg/m^3*	103	X		
	105	X		
	106	X		
	107	X		
	108		X	

APPENDIX B – ADDITIONAL TABLES AND PLOTS FOR UTT POST-CRACK RESPONSE

Table B.1 – Post-crack response of all specimens

Fibre Type	Fibre Dosage ($kg/m^{3)}$	Casting Method	Date Poured	No. Of Fibers	*Peak* (MPa)	*fmax* (MPa)	*fmin* (MPa)	*f0.5* (MPa)	*f1.0* (MPa)	*f2.0* (MPa)	*f4.0* (MPa)	*f6.0* (MPa)	*f8.0* (MPa)	*f10.0* (MPa)
Tuf-Strand SF	1.8	mix truck	23/06/2010	24.6	2.47	0.16	0.07	0.14	0.10	0.09	0.09	0.08	0.07	0.07
	2.4		29/06/2010	35.4	1.83	0.15	0.06	0.13	0.11	0.12	0.11	0.10	0.09	0.06
	3.0		07/07/2010	38.3	2.01	0.18	0.08	0.17	0.16	0.18	0.17	0.11	0.10	0.08
	4.6		23/08/2010	54.4	2.03	0.22	0.13	0.20	0.19	0.22	0.21	0.18	0.15	0.13
	6.9		26/08/2010	70.3	1.95	0.27	0.12	0.25	0.23	0.24	0.22	0.18	0.15	0.12
	1.8	drum mixer	08/06/2011	33.5	2.47	0.13	0.05	0.11	0.10	0.12	0.11	0.08	0.06	0.05
	3.0		31/05/2011	42.6	2.32	0.16	0.06	0.15	0.14	0.16	0.13	0.10	0.08	0.06
	4.6		25/05/2011	91.7	2.27	0.30	0.12	0.26	0.28	0.30	0.27	0.20	0.16	0.12
HDPE, 10% EVA (38 mm)	1.8		06/06/2011	40.0	2.10	0.14	0.07	-	0.13	0.14	0.13	0.11	0.09	0.07
	3.0		02/06/2011	53.0	1.90	0.14	0.07	0.13	0.13	0.13	0.12	0.10	0.08	0.07
	4.6		26/05/2011	70.0	1.91	0.17	0.08	0.16	0.15	0.17	0.15	0.12	0.10	0.08
HDPE, 10% EVA (50 mm)	1.8		07/06/2011	26.7	2.47	0.12	0.07	0.12	0.10	0.11	0.11	0.10	0.09	0.07
	3.0		30/05/2011	33.0	1.67	0.11	0.06	-	0.10	0.10	0.10	0.08	0.08	0.06
	4.6		24/05/2011	47.0	2.10	0.14	0.08	0.14	0.13	0.14	0.12	0.11	0.09	0.08
HDPE, 3% PVDF	3.0		07/10/2010	15.0	2.40	0.10	0.07	0.09	0.09	0.09	0.09	0.09	0.08	0.07
HDPE, 5% PVDF, 10% MAH	3.0		05/10/2010	21.0	2.41	0.11	0.07	0.10	0.10	0.10	0.10	0.09	0.08	0.07
HDPE, 11% PVDF, 20% MAH	3.0		18/10/2010	21.3	2.57	0.11	0.06	0.09	0.09	0.11	0.10	0.09	0.09	0.07
80% PP, 10% HDPE, 10% EVA	3.0		20/10/2010	36.0	3.22	0.17	0.11	-	0.14	0.16	0.16	0.15	0.13	0.12
100% HDPE	3.0		21/10/2010	26.0	3.10	0.12	0.05	0.10	0.10	0.11	0.10	0.08	0.06	0.05

Table B.2 – Post-crack response of specimens cracked with stiffening bars

Fibre Type	Fibre Dosgae kg/m^3	Casting Method	Date Poured	No. Of Fibers	*Peak* (MPa)	*fmax* (MPa)	*fmin* (MPa)	*f0.5* (MPa)	*f1.0* (MPa)	*f2.0* (MPa)	*f4.0* (MPa)	*f6.0* (MPa)	*f8.0* (MPa)	*f10.0* (MPa)
Tuf-Strand SF	1.8	mix truck	23/06/2010	25.00	2.44	0.18	0.07	0.15	0.11	0.10	0.09	0.09	0.08	0.08
	2.4		29/06/2010	34.50	1.86	0.15	0.05	0.12	0.11	0.11	0.11	0.10	0.08	0.05
	3.0		07/07/2010	38.33	2.01	0.19	0.06	0.16	0.15	0.17	0.16	0.09	0.08	0.06
	4.6		23/08/2010	53.25	2.04	0.22	0.12	0.20	0.19	0.22	0.21	0.18	0.15	0.12
	6.9		26/08/2010	69.40	1.89	0.27	0.12	0.25	0.23	0.24	0.22	0.18	0.15	0.12
	1.8	drum mixer	08/06/2011	34.80	2.70	0.13	0.05	0.11	0.10	0.12	0.11	0.08	0.06	0.05
	3.0		31/05/2011	35.25	2.13	0.15	0.06	0.14	0.13	0.15	0.12	0.09	0.07	0.06
	4.6		25/05/2011	82.00	2.31	0.29	0.12	0.24	0.27	0.28	0.26	0.20	0.16	0.12
HDPE, 10% EVA (38 mm)	1.8		06/06/2011	41.00	1.42	0.12	0.06	0.11	0.10	0.11	0.10	0.08	0.07	0.06
	3.0		02/06/2011	53.00	1.90	0.13	-0.01	0.11	0.11	0.12	0.11	0.09	0.08	0.07
	4.6		26/05/2011	69.67	1.94	0.17	0.08	0.16	0.15	0.17	0.15	0.12	0.10	0.08
HDPE, 10% EVA (50 mm)	1.8		07/06/2011	28.20	1.99	0.14	0.08	0.13	0.11	0.11	0.11	0.10	0.09	0.08
	3.0		30/05/2011	47.60	2.15	0.13	0.05	0.11	0.08	0.08	0.08	0.07	0.06	0.05
	4.6		24/05/2011	47.60	2.15	0.15	0.07	0.14	0.13	0.14	0.12	0.10	0.09	0.07
HDPE, 3% PVDF	3.0		07/10/2010	15.67	2.53	0.10	0.07	0.09	0.09	0.09	0.09	0.09	0.08	0.07
HDPE, 5% PVDF, 10% MAH	3.0		05/10/2010	21.50	2.25	0.11	0.07	0.10	0.10	0.10	0.10	0.09	0.08	0.07
HDPE, 11% PVDF, 20% MAH	3.0		18/10/2010	21.33	2.57	0.11	0.06	0.09	0.09	0.11	0.10	0.09	0.09	0.07
80% PP, 10% HDPE, 10% EVA	3.0		20/10/2010	32.50	3.04	0.16	0.09	0.15	0.13	0.14	0.14	0.13	0.11	0.11
100% HDPE	3.0		21/10/2010	26.00	3.10	0.12	0.05	0.10	0.10	0.11	0.10	0.08	0.06	0.05

Table B.3 – Post-crack response of specimens cracked without stiffening bars

Fibre Type	Fibre Dosgae kg/m^3	Casting Method	Date Poured	No. Of Fibers	*Peak* (MPa)	*fmax* (MPa)	*fmin* (MPa)	*f0.5* (MPa)	*f1.0* (MPa)	*f2.0* (MPa)	*f4.0* (MPa)	*f6.0* (MPa)	*f8.0* (MPa)	*f10.0* (MPa)
Tuf-Strand SF	1.8	mix truck	23/06/2010	13.0	2.15	0.11	0.03	0.10	0.07	0.05	0.54	0.04	0.04	0.03
	2.4		29/06/2010	39.0	1.71	-0.09	-0.15	-0.14	-0.14	-0.15	-0.14	-0.12	-0.11	-0.09
	3.0		07/07/2010	49.0	2.23	0.23	0.15	0.19	0.20	0.22	0.22	0.20	0.17	0.15
	4.6		23/08/2010	59.0	1.96	0.20	0.13	0.19	0.18	0.19	0.20	0.18	0.15	0.13
	6.9		26/08/2010	75.0	2.27	0.25	0.12	0.22	0.22	0.24	0.22	0.18	0.15	0.12
	1.8	drum mixer	08/06/2011	31.3	2.47	0.11	0.04	0.10	0.10	0.10	0.08	0.06	0.05	0.04
	3.0		31/05/2011	72.0	3.05	0.23	0.08	0.21	0.16	0.19	1.86	0.13	0.09	0.08
	4.6		25/05/2011	111.0	2.19	0.41	0.13	0.29	0.31	0.33	3.43	0.24	0.16	0.13
HDPE, 10% EVA (38 mm)	1.8		06/06/2011	38.5	1.64	0.15	0.09	-	0.14	0.15	0.14	0.12	0.10	0.09
	3.0		02/06/2011	50.0	2.65	0.19	0.08	0.18	0.17	0.16	1.55	0.11	0.09	0.08
	4.6		26/05/2011	71.0	1.84	0.16	0.06	0.11	0.13	0.14	1.46	0.10	0.08	0.13
HDPE, 10% EVA (50 mm)	1.8		07/06/2011	19.0	2.95	0.14	0.02	0.09	0.08	0.09	1.00	0.08	0.07	0.03
	3.0		30/05/2011	48.0	0.90	0.15	0.08	-	0.12	0.14	0.14	0.12	0.10	0.08
	4.6		24/05/2011	42.0	3.12	0.15	0.09	0.12	0.14	0.14	0.14	0.12	0.10	0.09
HDPE, 3% PVDF	3.0		07/10/2010	13.0	1.99	0.12	0.06	0.12	0.10	0.09	0.08	0.07	0.07	0.07
HDPE, 5% PVDF, 10% MAH	3.0		05/10/2010	20.0	32.57	1.77	0.97	1.10	1.46	1.65	1.56	1.45	1.33	1.19
HDPE, 11% PVDF, 20% MAH	3.0		18/10/2010	17.0	4.16	-	-	-	-	-	-	-	-	-
80% PP, 10% HDPE, 10% EVA	3.0		20/10/2010	43.0	3.60	3.60	0.13	1.20	0.17	0.21	2.38	0.19	0.17	0.14
100% HDPE	3.0		21/10/2010	27.0	3.80	-	-	-	-	-	-	-	-	-

Table B.4 – Per fibre post-crack response of all specimens

Fibre Type	Fibre Dosgae kg/m^3	Casting Method	Date Poured	*fmax* (MPa)	*fmin* (MPa)	*f0.5* (MPa)	*f1.0* (MPa)	*f2.0* (MPa)	*f4.0* (MPa)	*f6.0* (MPa)	*f8.0* (MPa)	*f10.0* (MPa)
Tuf-Strand SF	1.8	mix truck	23/06/2010	0.0064	0.0028	0.0058	0.0041	0.0038	0.0035	0.0033	0.0030	0.0030
	2.4		29/06/2010	0.0042	0.0017	0.0036	0.0032	0.0034	0.0032	0.0029	0.0025	0.0017
	3.0		07/07/2010	0.0047	0.0022	0.0044	0.0043	0.0047	0.0045	0.0030	0.0026	0.0022
	4.6		23/08/2010	0.0040	0.0023	0.0037	0.0035	0.0040	0.0038	0.0033	0.0028	0.0023
	6.9		26/08/2010	0.0038	0.0017	0.0036	0.0033	0.0034	0.0032	0.0026	0.0021	0.0017
	1.8	drum mixer	08/06/2011	0.0038	0.0015	0.0032	0.0031	0.0037	0.0033	0.0025	0.0019	0.0015
	3.0		31/05/2011	0.0038	0.0014	0.0036	0.0033	0.0038	0.0031	0.0024	0.0018	0.0014
	4.6		25/05/2011	0.0033	0.0013	0.0028	0.0030	0.0032	0.0030	0.0022	0.0017	0.0013
HDPE, 10% EVA (38 mm)	1.8		06/06/2011	0.0036	0.0019	#N/A	0.0033	0.0036	0.0033	0.0027	0.0022	0.0019
	3.0		02/06/2011	0.0026	0.0013	0.0025	0.0025	0.0025	0.0022	0.0019	0.0016	0.0013
	4.6		26/05/2011	0.0025	0.0011	0.0022	0.0022	0.0024	0.0021	0.0017	0.0014	0.0011
HDPE, 10% EVA (50 mm)	1.8		07/06/2011	0.0047	0.0027	0.0045	0.0038	0.0042	0.0040	0.0037	0.0033	0.0027
	3.0		30/05/2011	0.0034	0.0019	#N/A	0.0029	0.0031	0.0031	0.0026	0.0023	0.0019
	4.6		24/05/2011	0.0030	0.0016	0.0029	0.0029	0.0030	0.0026	0.0023	0.0020	0.0016
HDPE, 3% PVDF	3.0		07/10/2010	0.0066	0.0048	0.0062	0.0059	0.0062	0.0060	0.0057	0.0054	0.0048
HDPE, 5% PVDF, 10% MAH	3.0		05/10/2010	0.0050	0.0034	0.0047	0.0047	0.0050	0.0047	0.0044	0.0038	0.0036
HDPE, 11% PVDF, 20% MAH	3.0		18/10/2010	0.0050	0.0028	0.0043	0.0044	0.0049	0.0047	0.0044	0.0040	0.0034
80% PP, 10% HDPE, 10% EVA	3.0		20/10/2010	0.0047	0.0031	#N/A	0.0040	0.0045	0.0045	0.0041	0.0036	0.0033
100% HDPE	3.0		21/10/2010	0.0045	0.0020	0.0039	0.0039	0.0044	0.0039	0.0030	0.0025	0.0020

Table B.5 – Per fibre post-crack response of specimens cracked with stiffening bars

Fibre Type	Fibre Dosgae kg/m^3	Casting Method	Date Poured	*fmax* (MPa)	*fmin* (MPa)	*f0.5* (MPa)	*f1.0* (MPa)	*f2.0* (MPa)	*f4.0* (MPa)	*f6.0* (MPa)	*f8.0* (MPa)	*f10.0* (MPa)
Tuf-Strand SF	1.8	mix truck	23/06/2010	0.0072	0.0029	0.0060	0.0042	0.0040	0.0037	0.0035	0.0032	0.0032
	2.4		29/06/2010	0.0044	0.0015	0.0036	0.0031	0.0032	0.0031	0.0028	0.0024	0.0015
	3.0		07/07/2010	0.0050	0.0017	0.0042	0.0039	0.0044	0.0041	0.0023	0.0020	0.0017
	4.6		23/08/2010	0.0042	0.0023	0.0038	0.0036	0.0042	0.0040	0.0034	0.0028	0.0023
	6.9		26/08/2010	0.0038	0.0017	0.0036	0.0034	0.0035	0.0032	0.0026	0.0022	0.0017
	1.8	drum mixer	08/06/2011	0.0036	0.0015	0.0031	0.0030	0.0035	0.0032	0.0024	0.0018	0.0015
	3.0		31/05/2011	0.0044	0.0016	0.0040	0.0038	0.0043	0.0035	0.0026	0.0021	0.0016
	4.6		25/05/2011	0.0035	0.0014	0.0029	0.0032	0.0034	0.0032	0.0024	0.0019	0.1220
HDPE, 10% EVA (38 mm)	1.8		06/06/2011	0.0028	0.0014	0.0026	0.0025	0.0026	0.0024	0.0019	0.0016	0.0014
	3.0		02/06/2011	0.0024	0.0002	0.0020	0.0021	0.0023	0.0021	0.0018	0.0015	0.0012
	4.6		26/05/2011	0.0025	0.0011	0.0023	0.0022	0.0025	0.0021	0.0017	0.0014	0.0011
HDPE, 10% EVA (50 mm)	1.8		07/06/2011	0.0051	0.0029	0.0045	0.0038	0.0041	0.0039	0.0036	0.0032	0.0029
	3.0		30/05/2011	0.0027	0.0011	0.0022	0.0017	0.0018	0.0017	0.0014	0.0014	0.0011
	4.6		24/05/2011	0.0032	0.0016	0.0029	0.0028	0.0029	0.0025	0.0022	0.0019	0.0016
HDPE, 3% PVDF	3.0		07/10/2010	0.0066	0.0046	0.0059	0.0057	0.0060	0.0057	0.0055	0.0052	0.0046
HDPE, 5% PVDF, 10% MAH	3.0		05/10/2010	0.0049	0.0033	0.0045	0.0046	0.0048	0.0046	0.0043	0.0037	0.0035
HDPE, 11% PVDF, 20% MAH	3.0		18/10/2010	0.0050	0.0028	0.0043	0.0044	0.0049	0.0047	0.0044	0.0040	0.0034
80% PP, 10% HDPE, 10% EVA	3.0		20/10/2010	0.0049	0.0028	0.0045	0.0040	0.0043	0.0044	0.0040	0.0034	0.0034
100% HDPE	3.0		21/10/2010	0.0045	0.0020	0.0039	0.0039	0.0044	0.0039	0.0030	0.0025	0.0020

Table B.6 – Per fibre post-crack response of specimens cracked without stiffening bars

Fibre Type	Fibre Dosgae kg/m^3	Casting Method	Date Poured	*fmax* (MPa)	*fmin* (MPa)	*f0.5* (MPa)	*f1.0* (MPa)	*f2.0* (MPa)	*f4.0* (MPa)	*f6.0* (MPa)	*f8.0* (MPa)	*f10.0* (MPa)
Tuf-Strand SF	1.8	mix truck	23/06/2010	0.0086	0.0024	0.0073	0.0053	0.0038	0.0412	0.0030	0.0027	0.0026
	2.4		29/06/2010	0.0024	0.0039	0.0036	0.0036	0.0039	0.0035	0.0032	0.0029	0.0024
	3.0		07/07/2010	0.0047	0.0030	0.0038	0.0042	0.0045	0.0044	0.0040	0.0035	0.0030
	4.6		23/08/2010	0.0034	0.0022	0.0033	0.0031	0.0033	0.0034	0.0030	0.0026	0.0022
	6.9		26/08/2010	0.0033	0.0017	0.0030	0.0029	0.0032	0.0029	0.0024	0.0019	0.0017
	1.8	drum mixer	08/06/2011	0.0036	0.0012	0.0033	0.0032	0.0031	0.0025	0.0019	0.0015	0.0012
	3.0		31/05/2011	0.0032	0.0011	0.0029	0.0023	0.0026	0.0259	0.0018	0.0013	0.0011
	4.6		25/05/2011	0.0037	0.0012	0.0026	0.0028	0.0030	0.0309	0.0021	0.0014	0.0012
HDPE, 10% EVA (38 mm)	1.8		06/06/2011	0.0039	0.0023	-	0.0036	0.0039	0.0036	0.0030	0.0025	0.0023
	3.0		02/06/2011	0.0037	0.0016	0.0036	0.0034	0.0031	0.0310	0.0023	0.0018	0.0016
	4.6		26/05/2011	0.0023	0.0008	0.0015	0.0018	0.0019	0.0205	0.0014	0.0011	0.0019
HDPE, 10% EVA (50 mm)	1.8		07/06/2011	0.0072	0.0012	0.0047	0.0044	0.0050	0.0525	0.0041	0.0038	0.0015
	3.0		30/05/2011	0.0032	0.0017	-	0.0026	0.0030	0.0029	0.0024	0.0021	0.0017
	4.6		24/05/2011	0.0035	0.0021	0.0021	0.0021	0.0021	0.0021	0.0021	0.0021	0.2381
HDPE, 3% PVDF	3.0		07/10/2010	0.0089	0.0047	0.0089	0.0075	0.0068	0.0060	0.0054	0.0056	0.0051
HDPE, 5% PVDF, 10% MAH	3.0		05/10/2010	0.0887	0.0483	0.0551	0.0731	0.0823	0.0781	0.0727	0.0663	0.0595
HDPE, 11% PVDF, 20% MAH	3.0		18/10/2010	-	-	-	-	-	-	-	-	-
80% PP, 10% HDPE, 10% EVA	3.0		20/10/2010	0.0838	0.0030	0.0279	0.0040	0.0049	0.0555	0.0044	0.0039	0.0031
100% HDPE	3.0		21/10/2010	-	-	-	-	-	-	-	-	-

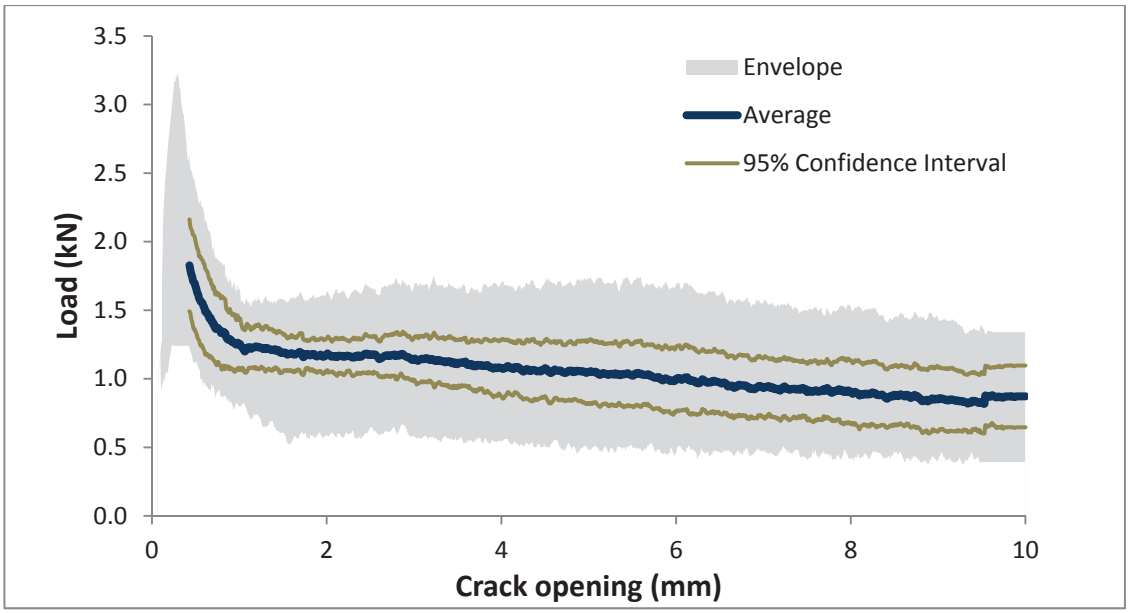

Figure B.1 - Post-crack response: Tuf-Strand SF (mix truck), 1.8 kg/m^3, all specimens.

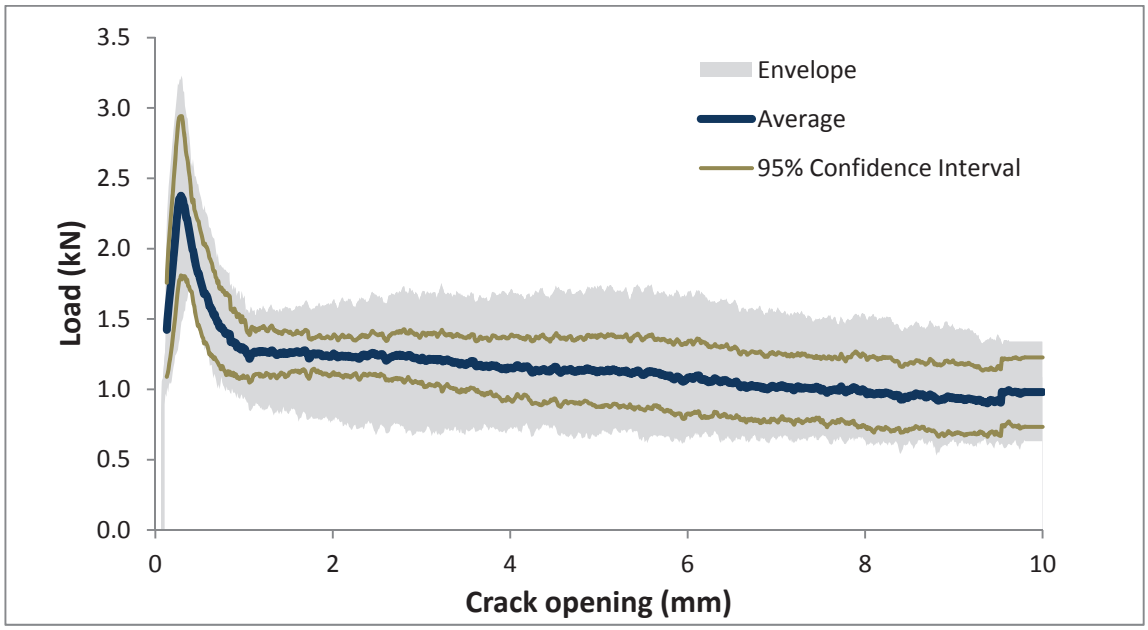

Figure B.2 - Post-crack response: Tuf-Strand SF (mix truck), 1.8 kg/m^3, cracked with steel stiffening bars.

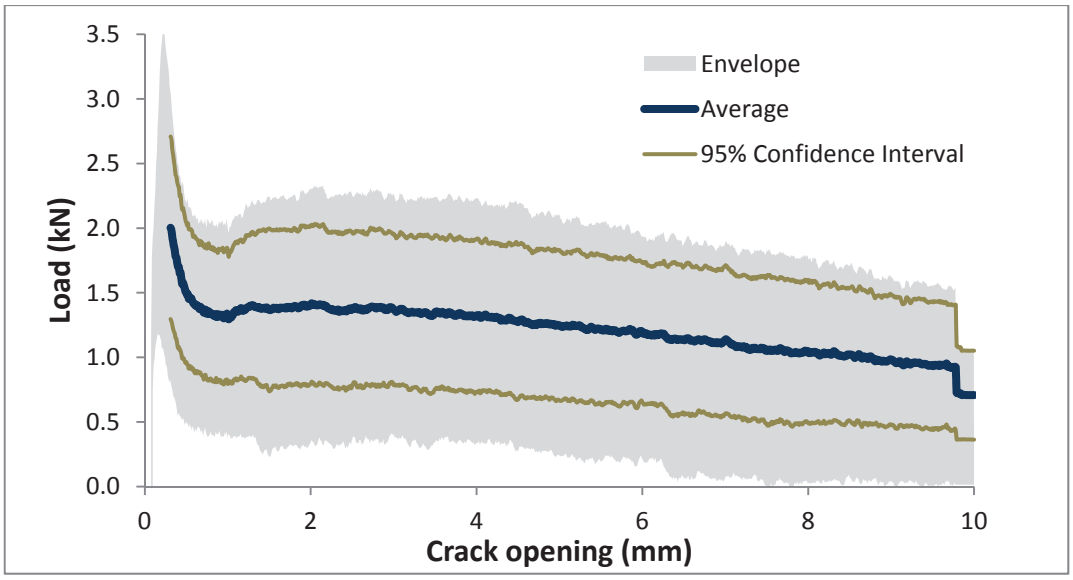

Figure B.3 - Post-crack response: Tuf-Strand SF (mix truck), 2.4 kg/m^3, all specimens.

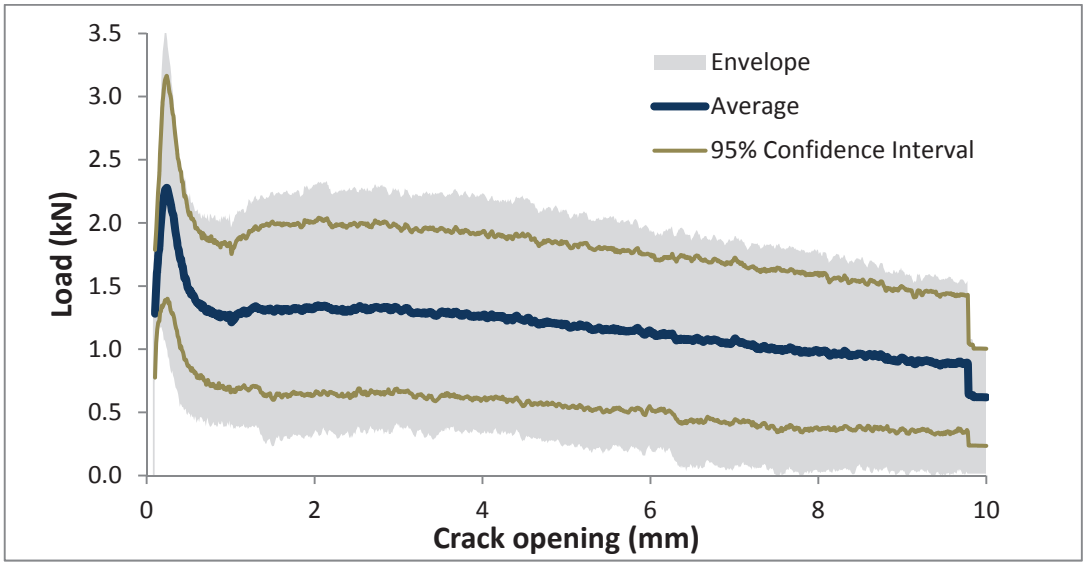

Figure B.4 - Post-crack response: Tuf-Strand SF (mix truck), 2.4 kg/m^3, specimens cracked with steel stiffening bars.

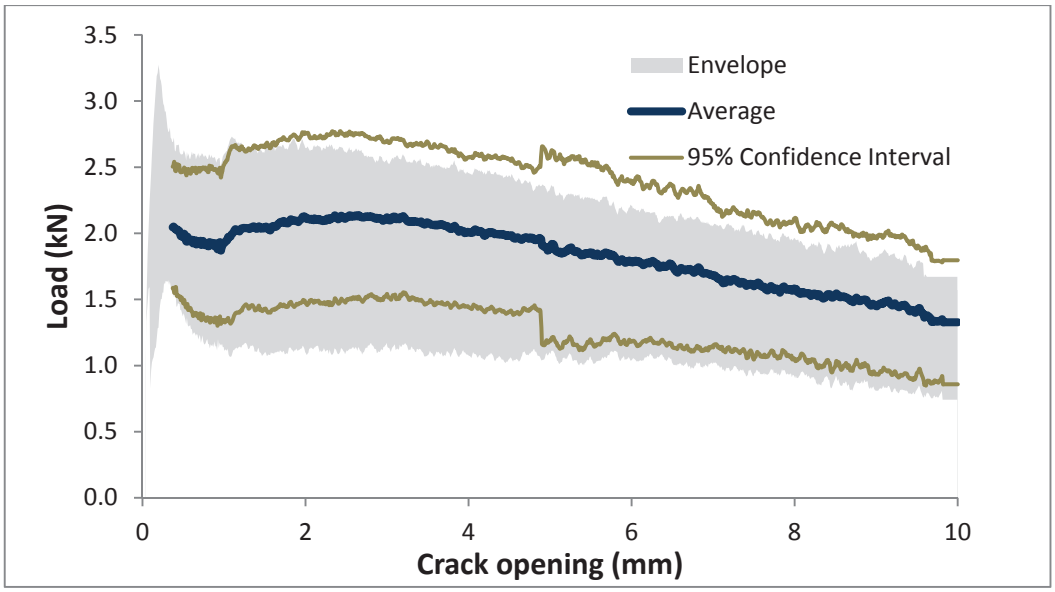

Figure B.5 - Post-crack response: Tuf-Strand SF (mix truck), 3.0 kg/m^3, all specimens.

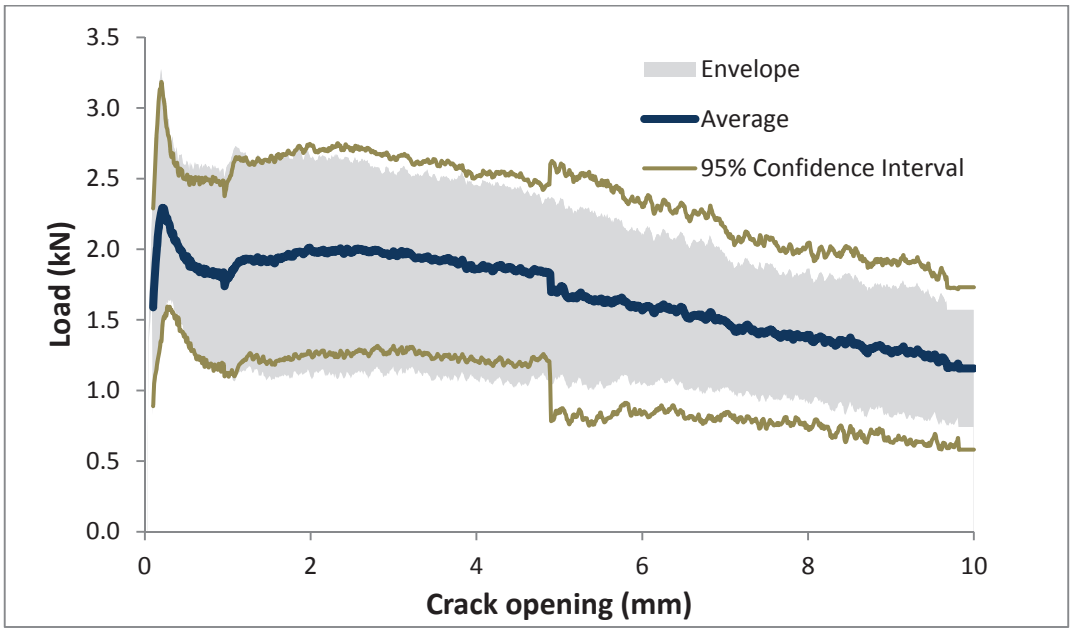

Figure B.6 - Post-crack response: Tuf-Strand SF (mix truck), 3.0 kg/m^3, specimens cracked with steel stiffening bars.

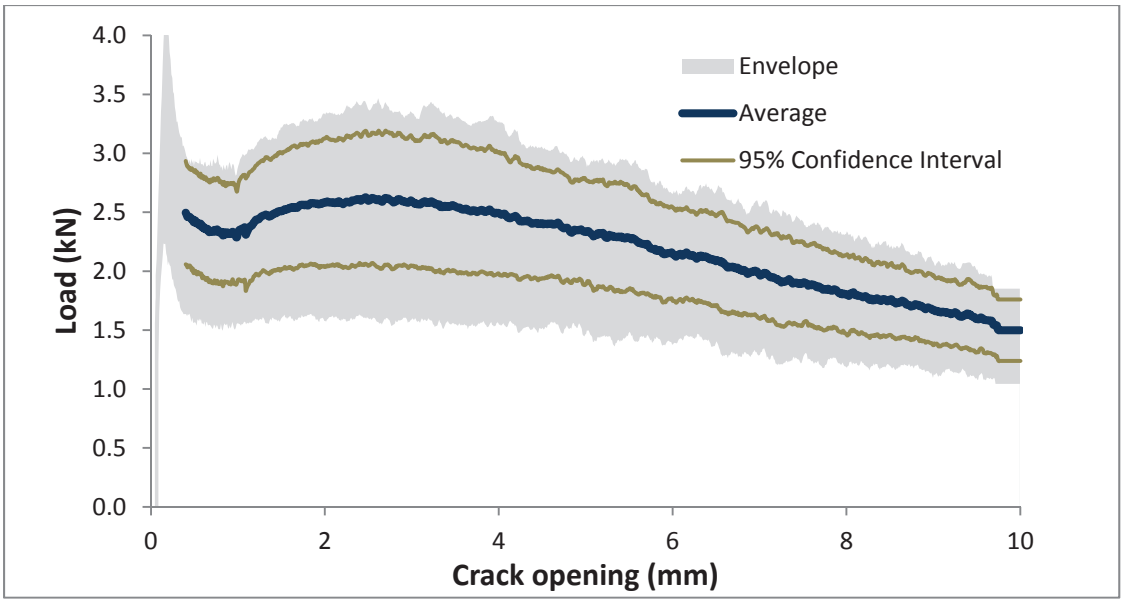

Figure B.7 - Post-crack response: Tuf-Strand SF (mix truck), 4.6 kg/m^3, all specimens.

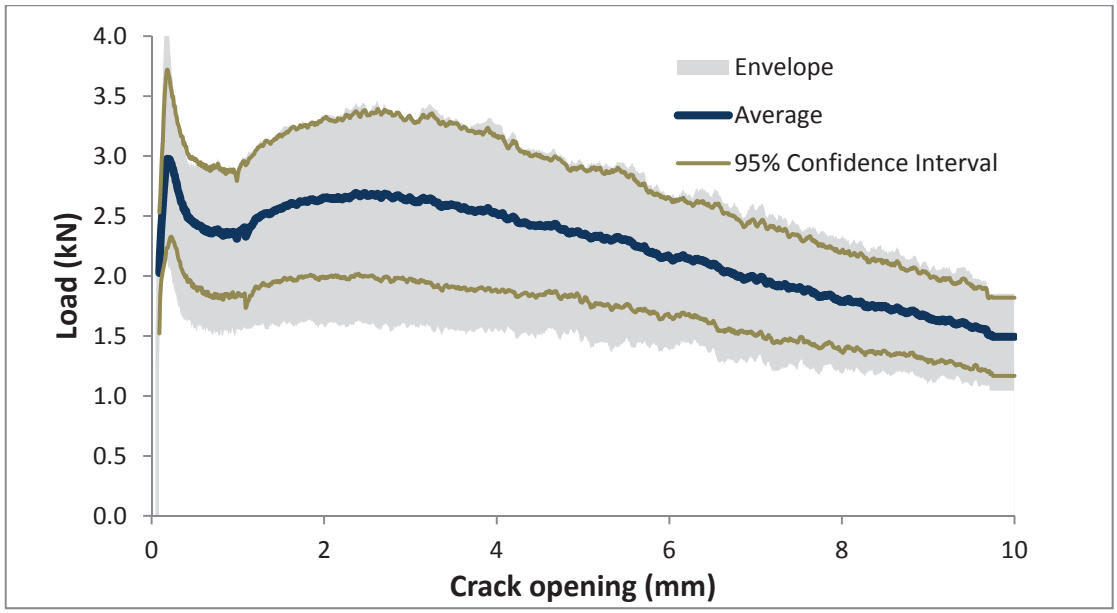

Figure B.8 - Post-crack response: Tuf-Strand SF (mix truck), 4.6 kg/m^3, specimens cracked with steel stiffening bars.

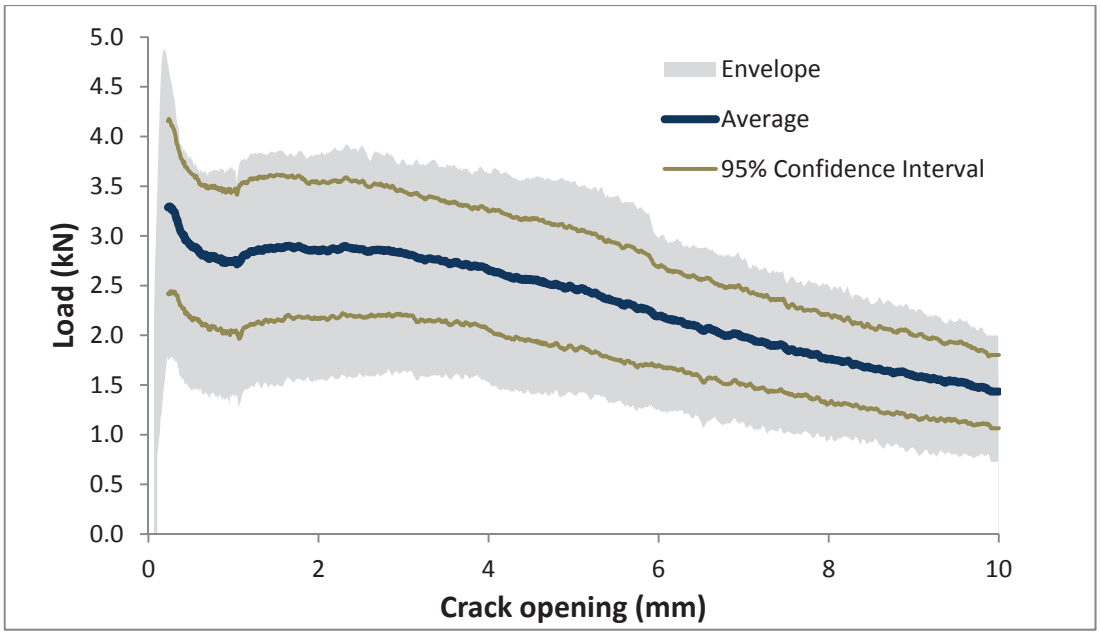

Figure B.9 - Post-crack response: Tuf-Strand SF (mix truck), 6.9 kg/m^3, all specimens

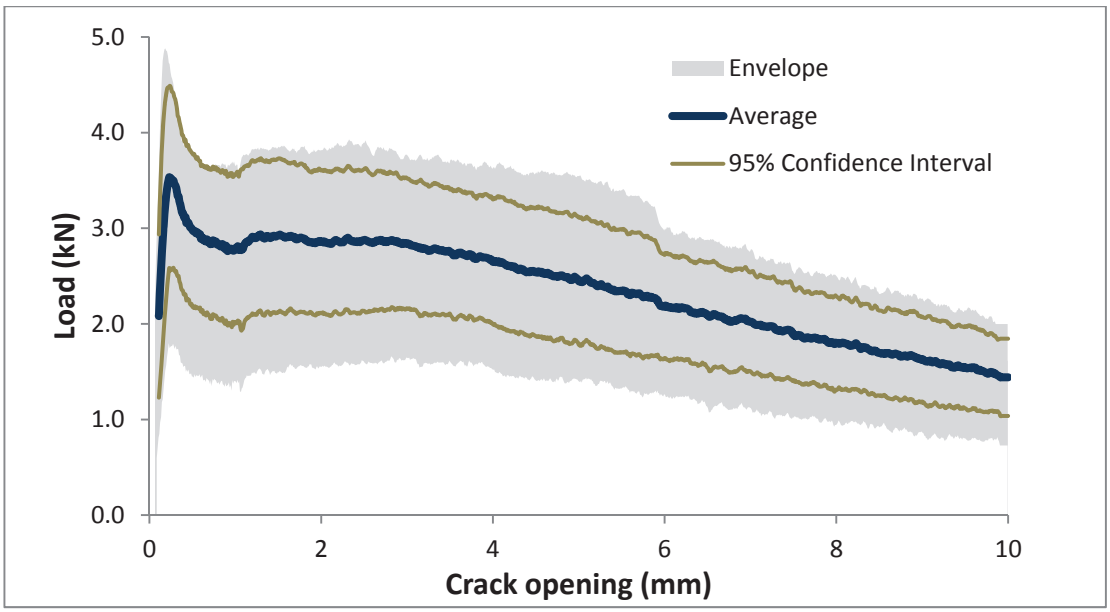

Figure B.10 - Post-crack response: Tuf-Strand SF (mix truck), 6.9 kg/m^3, specimens cracked with steel stiffening bars.

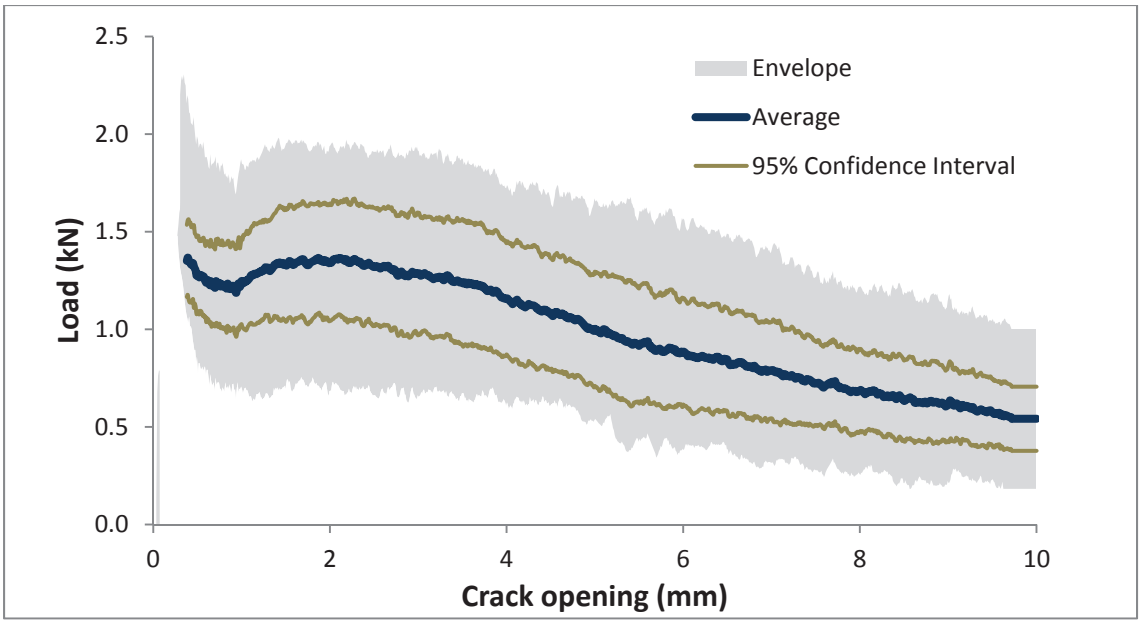

Figure B.11 - Post-crack response: Tuf-Strand SF (drum mixer), 1.8 kg/m^3, all specimens.

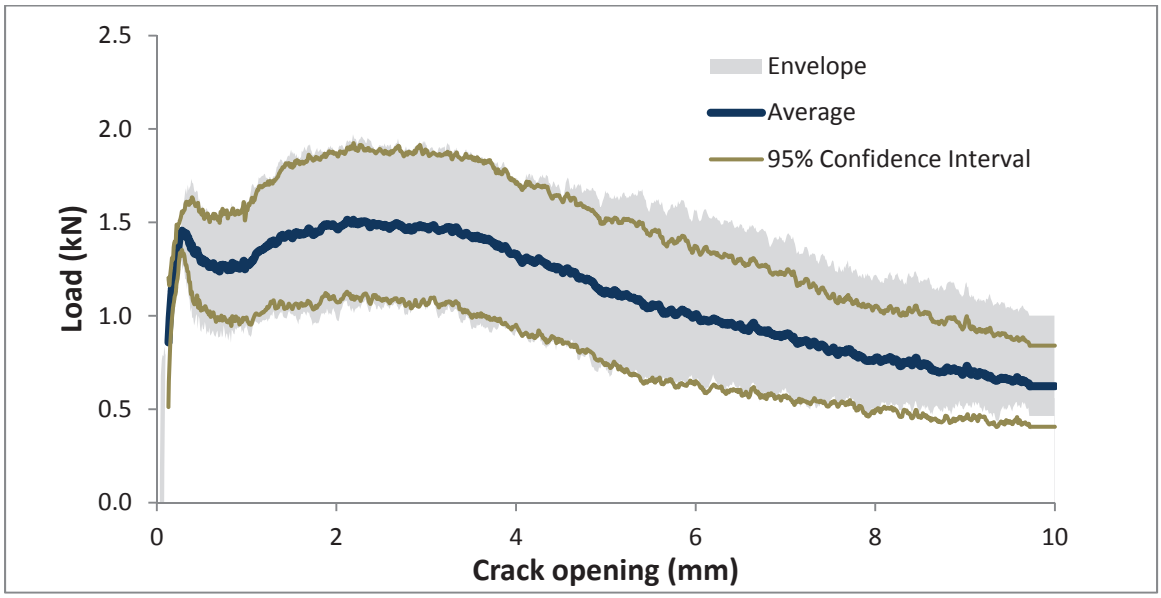

Figure B.12 - Post-crack response: Tuf-Strand SF (drum mixer), 1.8 kg/m^3, specimens cracked with steel stiffening bars.

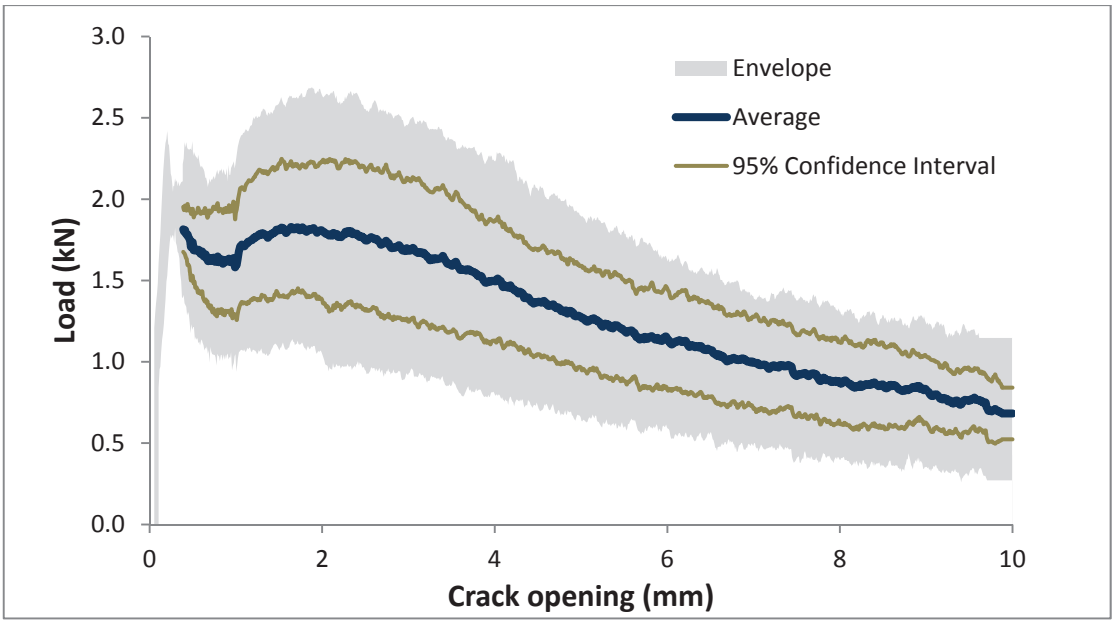

Figure B.13 - Post-crack response: Tuf-Strand SF (drum mixer), 3.0 kg/m^3, all specimens.

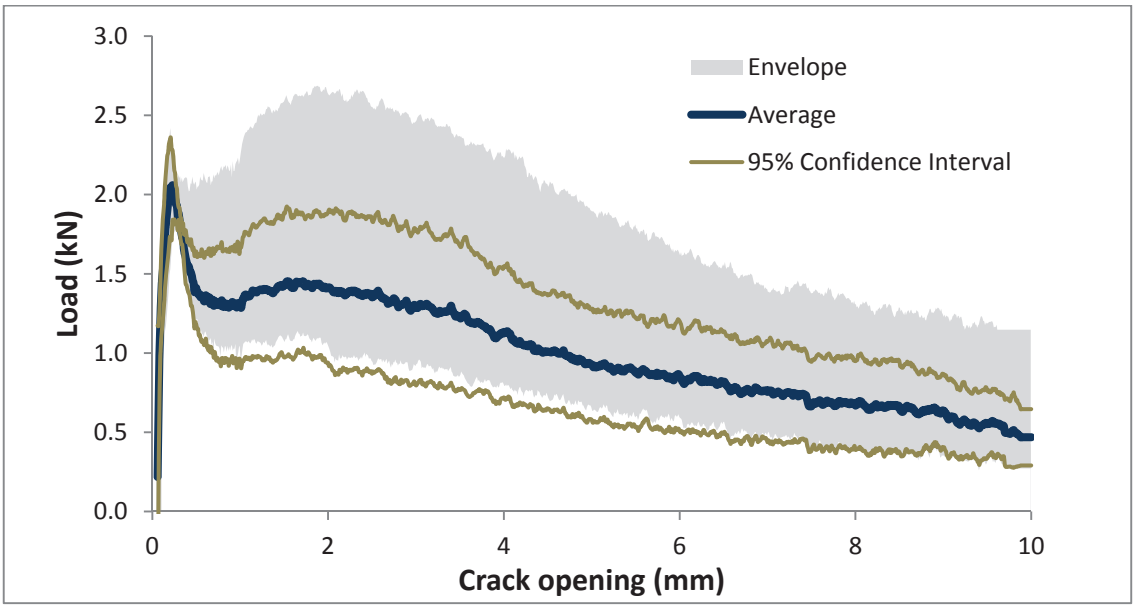

Figure B.14 - Post-crack response:Tuf-Strand SF (drum mixer), 3.0 kg/m^3, specimens cracked with steel stiffening bars.

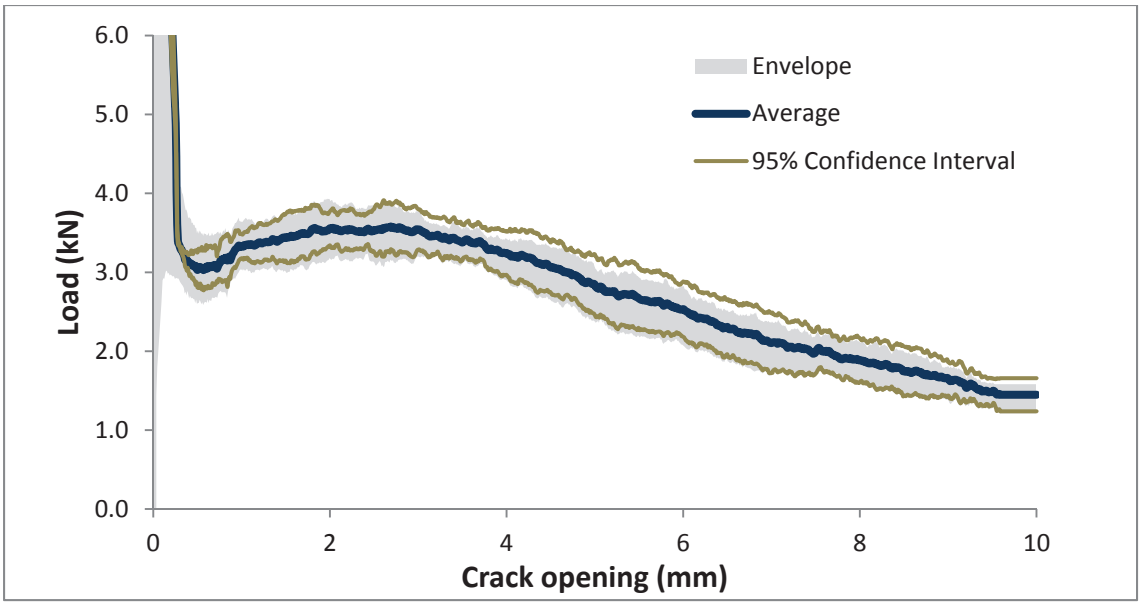

Figure B.15 - Post-crack response: Tuf-Strand SF (drum mixer), 4.6 kg/m^3, all specimens.

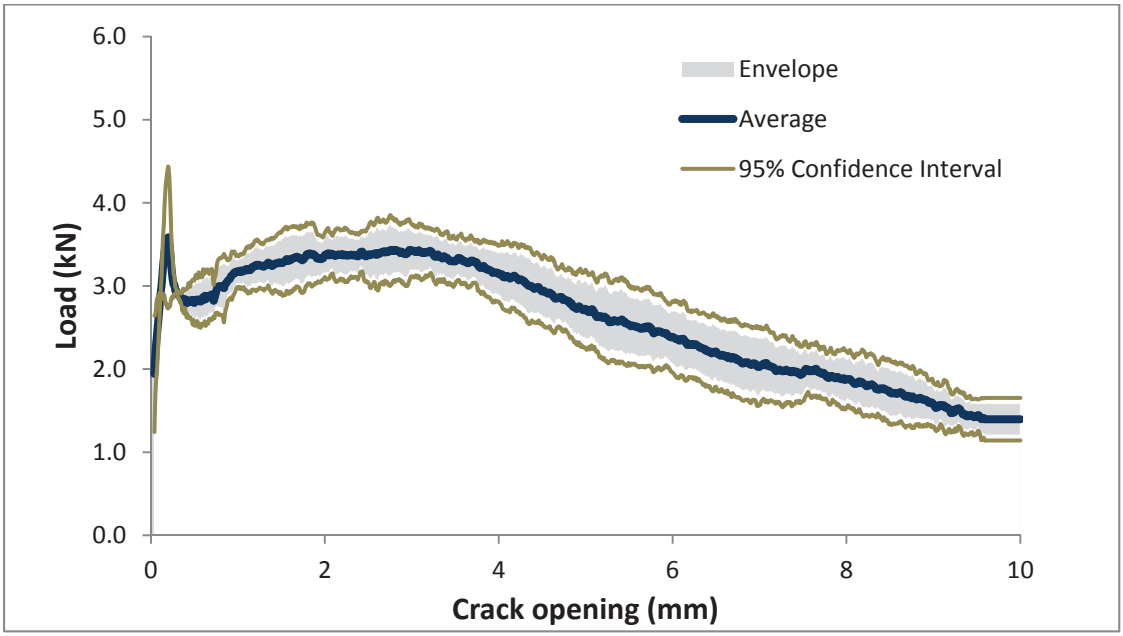

Figure B.16 - Post-crack response: Tuf-Strand SF (drum mixer), 4.6 kg/m^3, specimens cracked with steel stiffening bars.

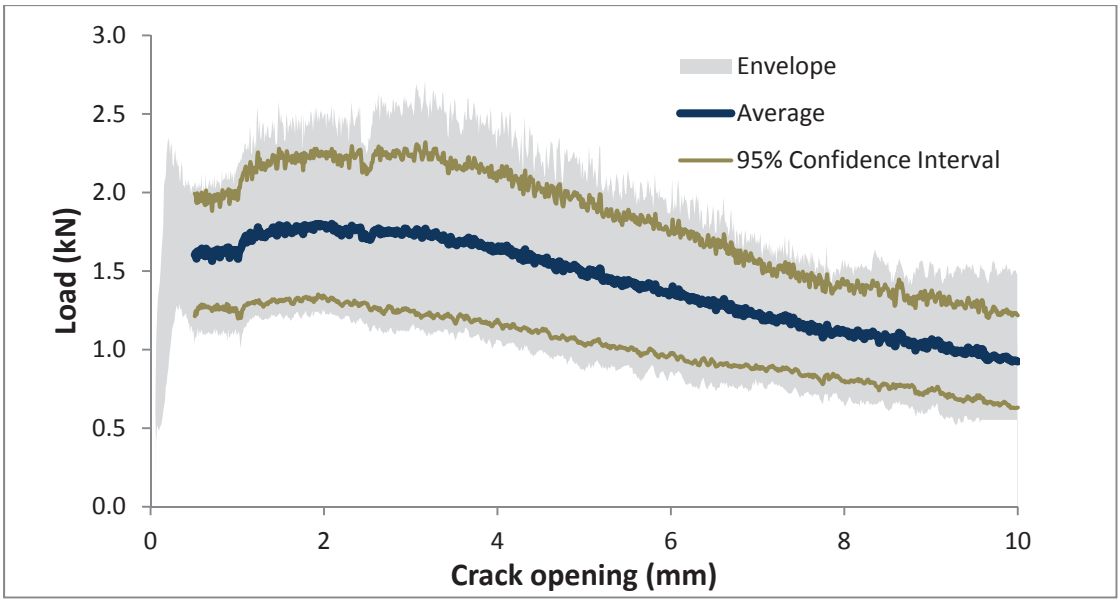

Figure B.17 - Post-crack response: HDPE and 10% EVA, 1.8 kg/m^3, 38 mm length, all specimens.

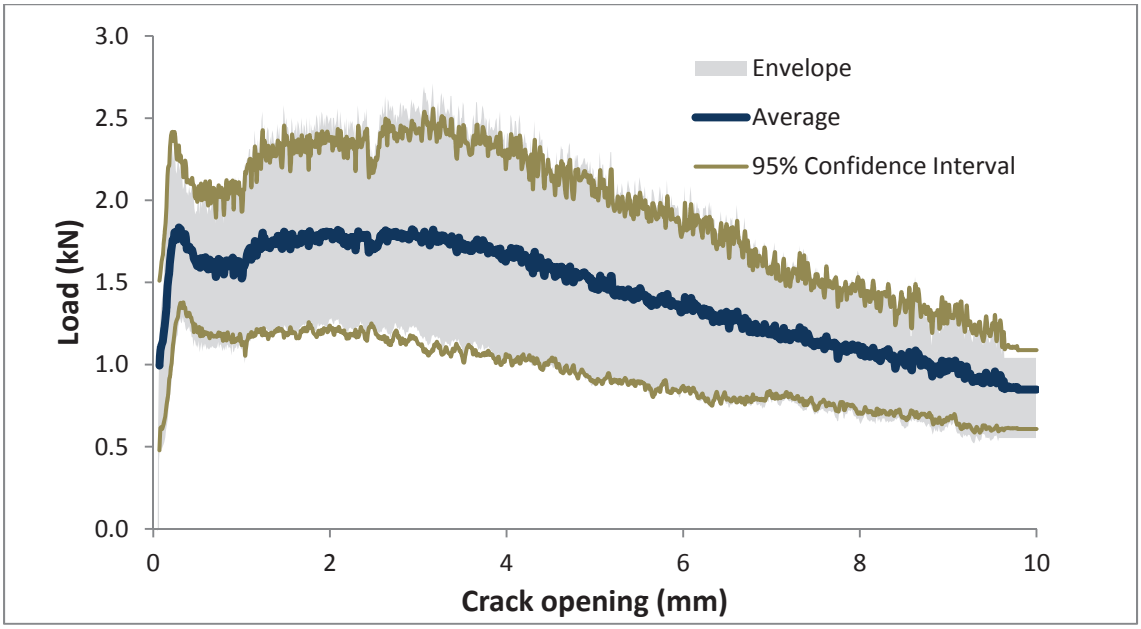

Figure B.18 - Post-crack response: HDPE and 10% EVA, 1.8 kg/m^3, 38 mm length, specimens cracked with steel stiffening bars.

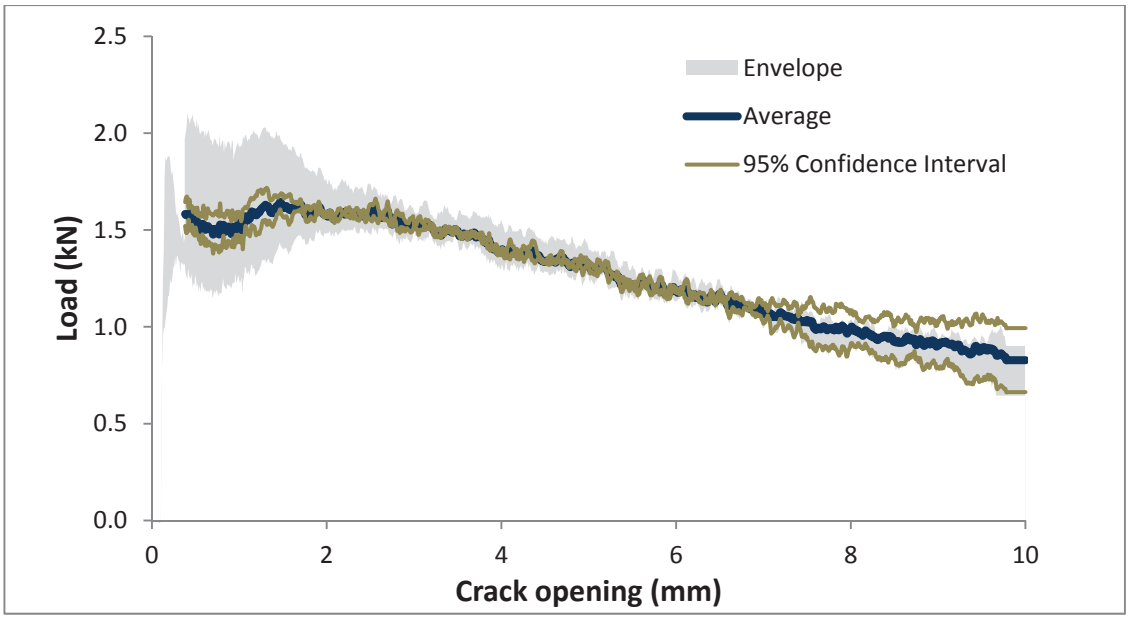

Figure B.19 - Post-crack response: HDPE and 10% EVA, 3.0 kg/m^3, 38 mm length, all specimens.

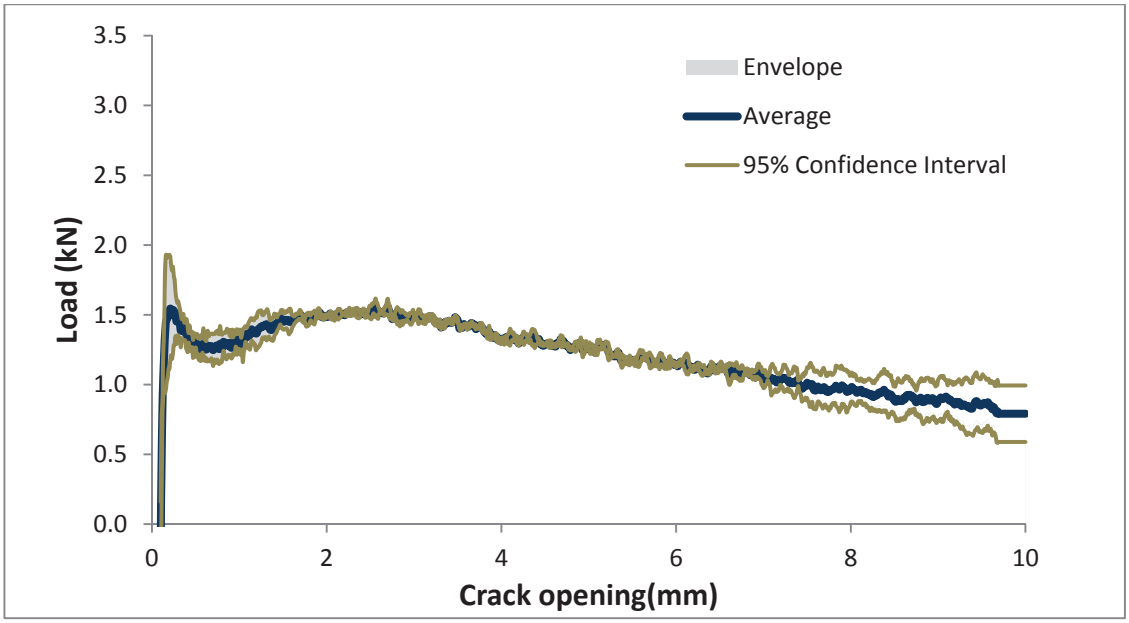

Figure B.20 - Post-crack response: HDPE and 10% EVA, 3.0 kg/m^3, 38 mm length, specimens cracked with steel stiffening bars.

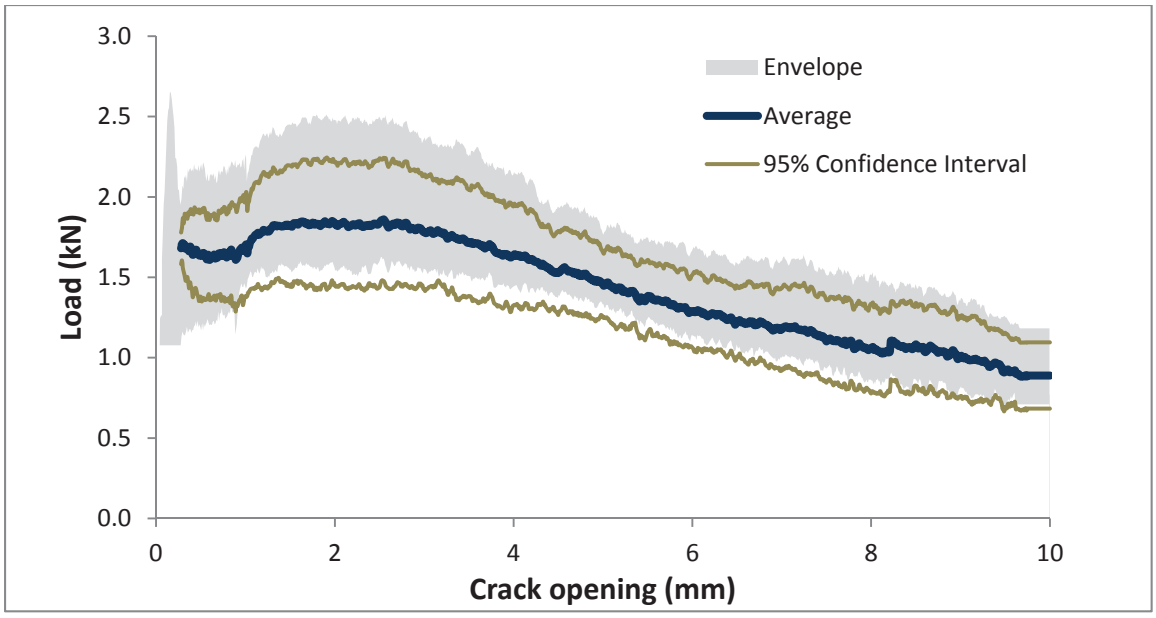

Figure B.21 - Post-crack response: HDPE and 10% EVA, 4.6 kg/m^3, 38 mm length, all specimens.

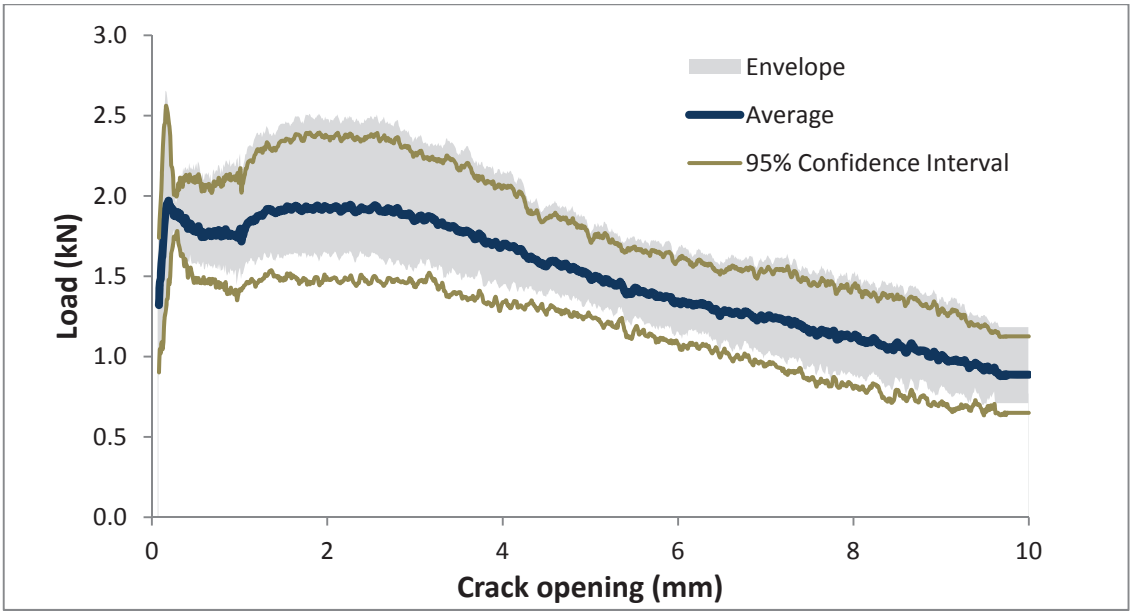

Figure B.22 - Post-crack response: HDPE and 10% EVA, 4.6 kg/m^3, 38 mm length, specimens cracked with steel stiffening bars.

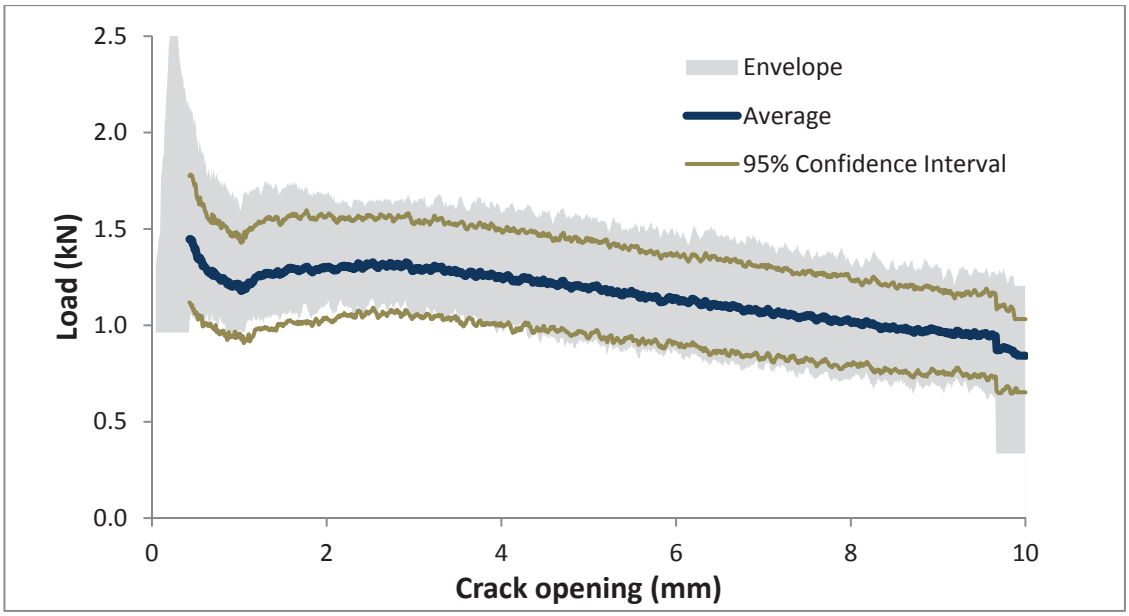

Figure B.23 - Post-crack response: HDPE and 10% EVA, 1.8 kg/m^3, 50 mm length, all specimens.

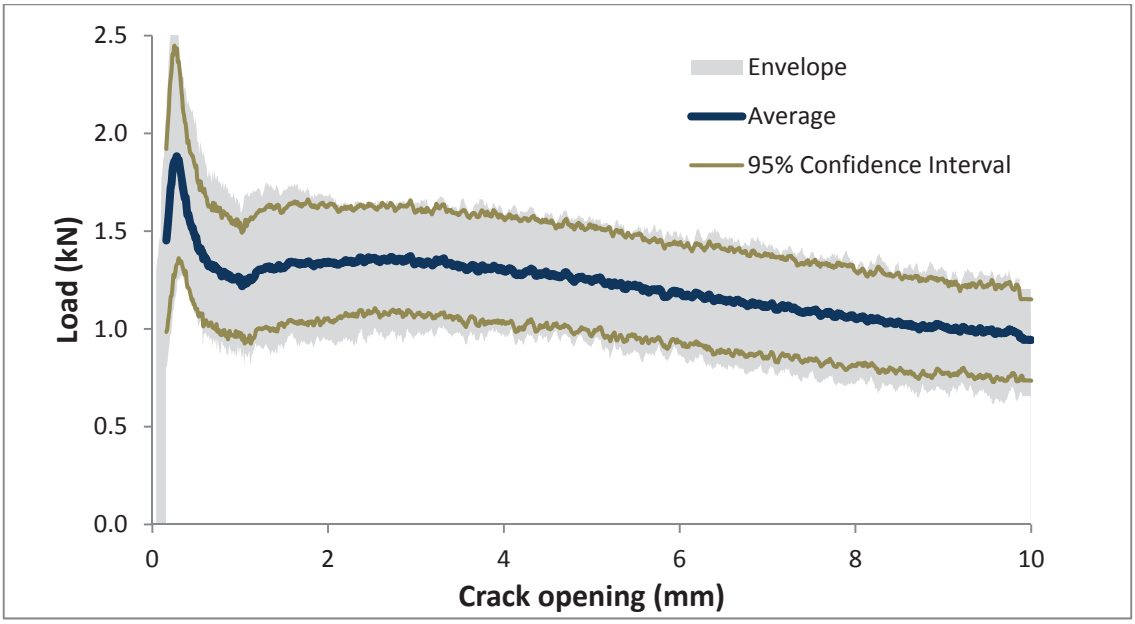

Figure B.24 - Post-crack response: HDPE and 10% EVA, 1.8 kg/m^3, 50 mm length, specimens cracked with steel stiffening bars.

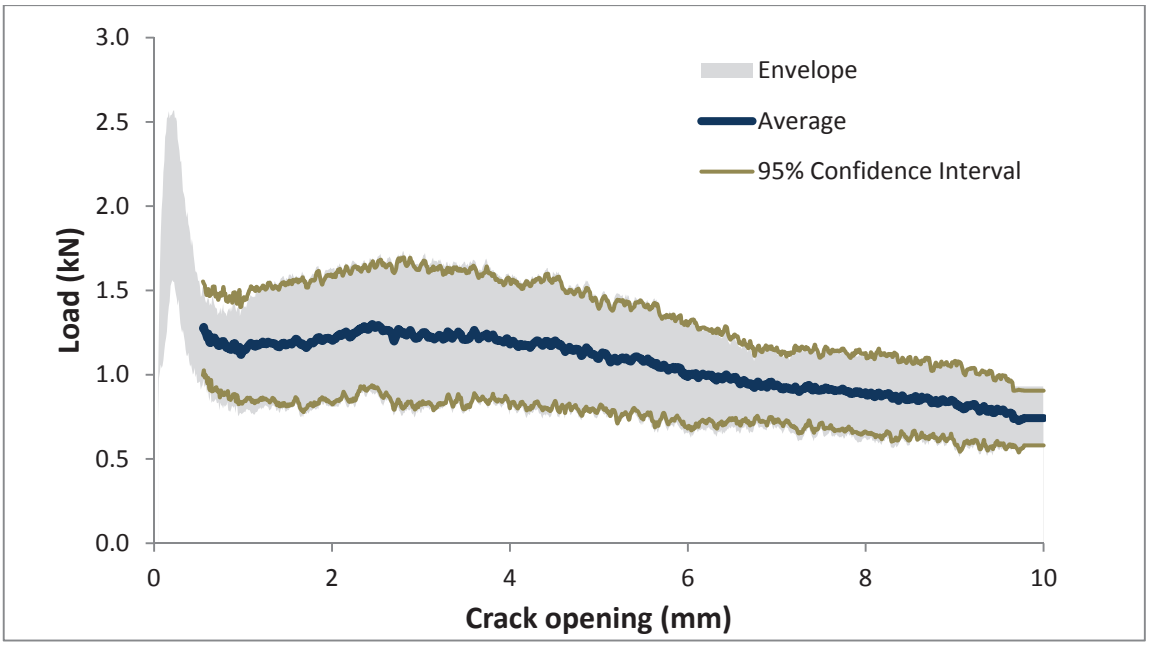

Figure B.25 - Post-crack response: HDPE and 10% EVA, 3.0 kg/m^3, 50 mm length, all specimens.

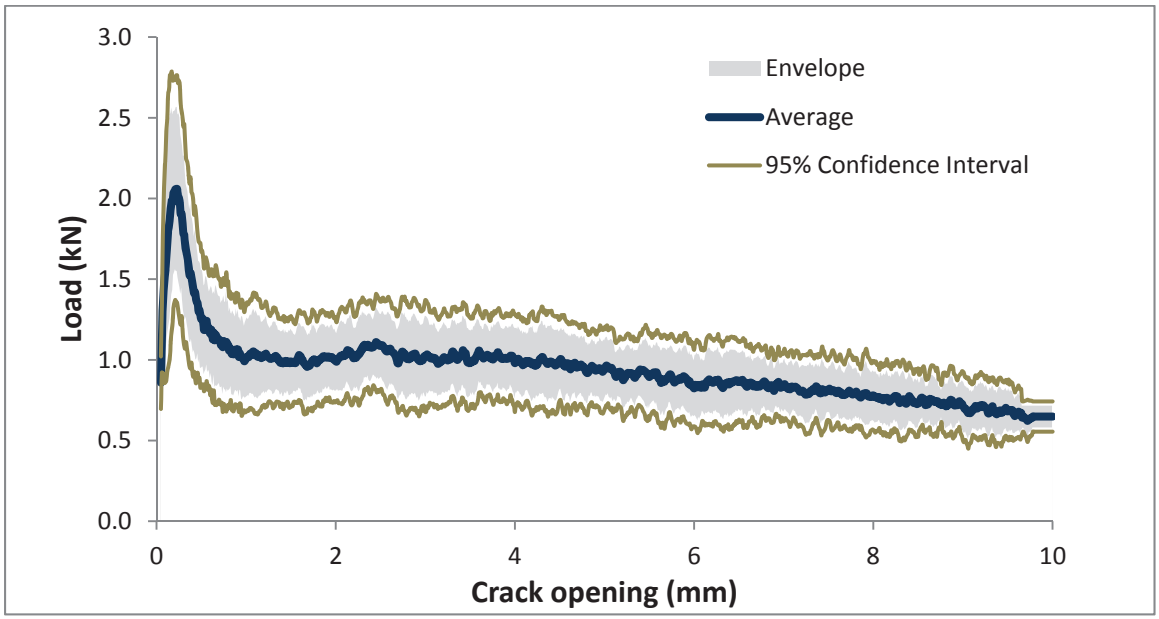

Figure B.26 - Post-crack response: HDPE and 10% EVA, 3.0 kg/m^3, 50 mm length, specimens cracked with steel stiffening bars.

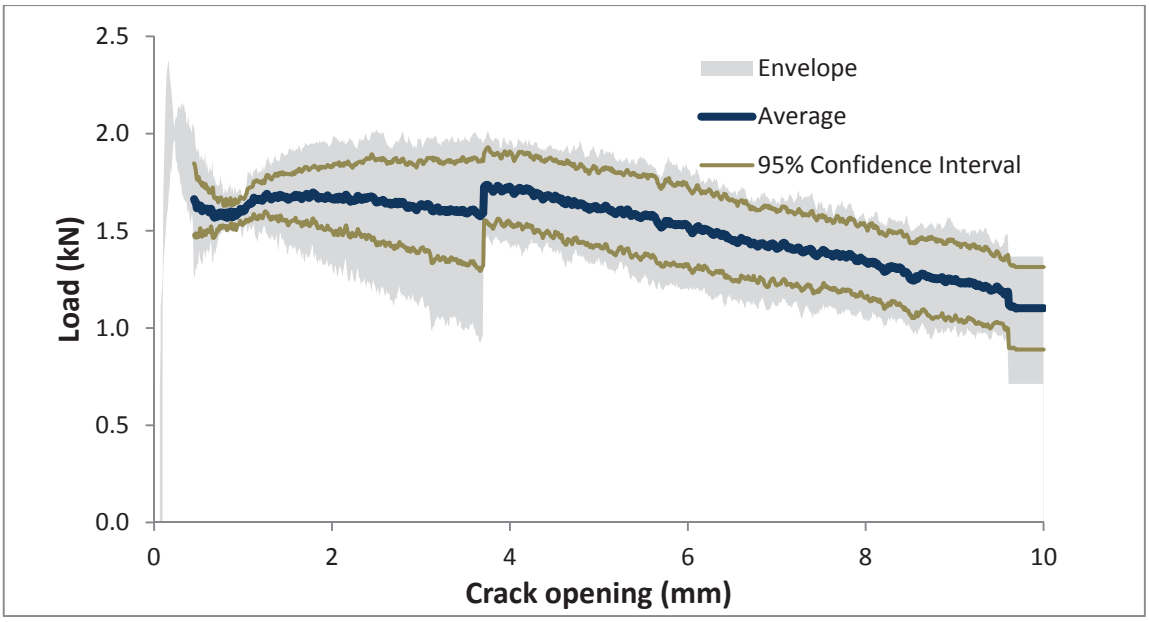

Figure B.27 - Post-crack response: HDPE and 10% EVA, 4.6 kg/m^3, 50 mm length, all specimens.

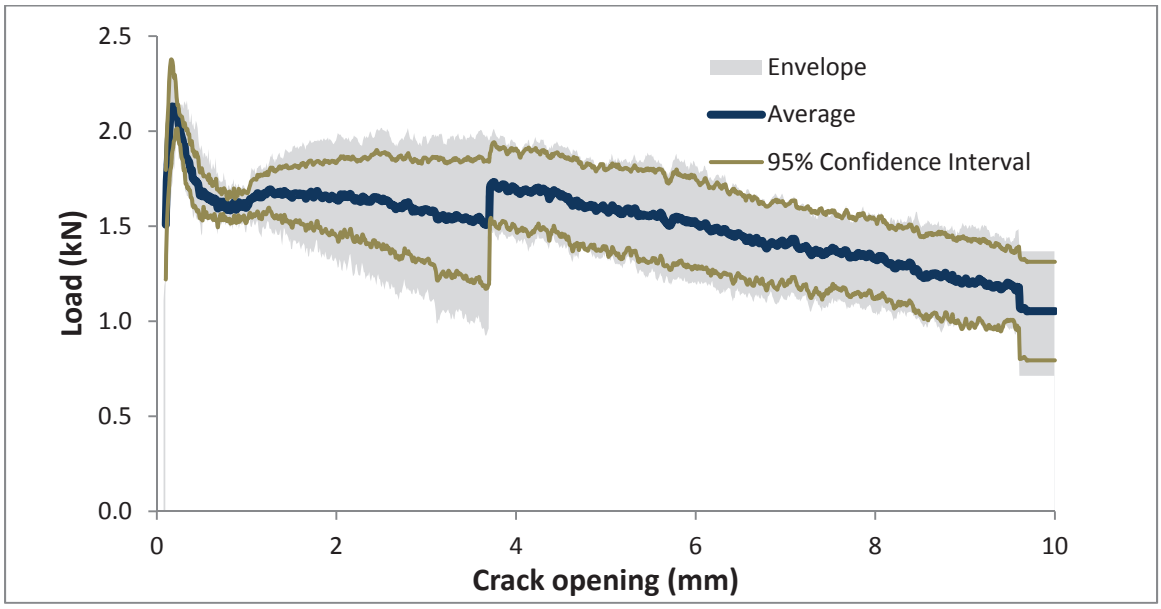

Figure B.28 - Post-crack response: HDPE and 10% EVA, 4.6 kg/m^3, 50 mm length, specimens cracked with steel stiffening bars.

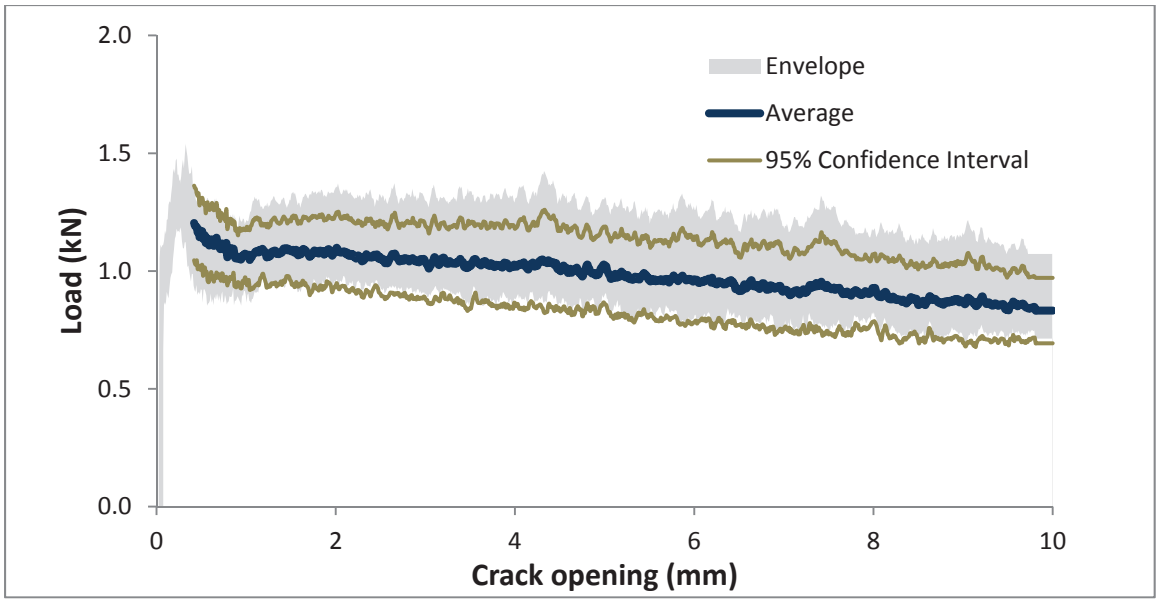

Figure B.29 - Post-crack response: HDPE and 3% PVDF, 3.0 kg/m^3, all specimens.

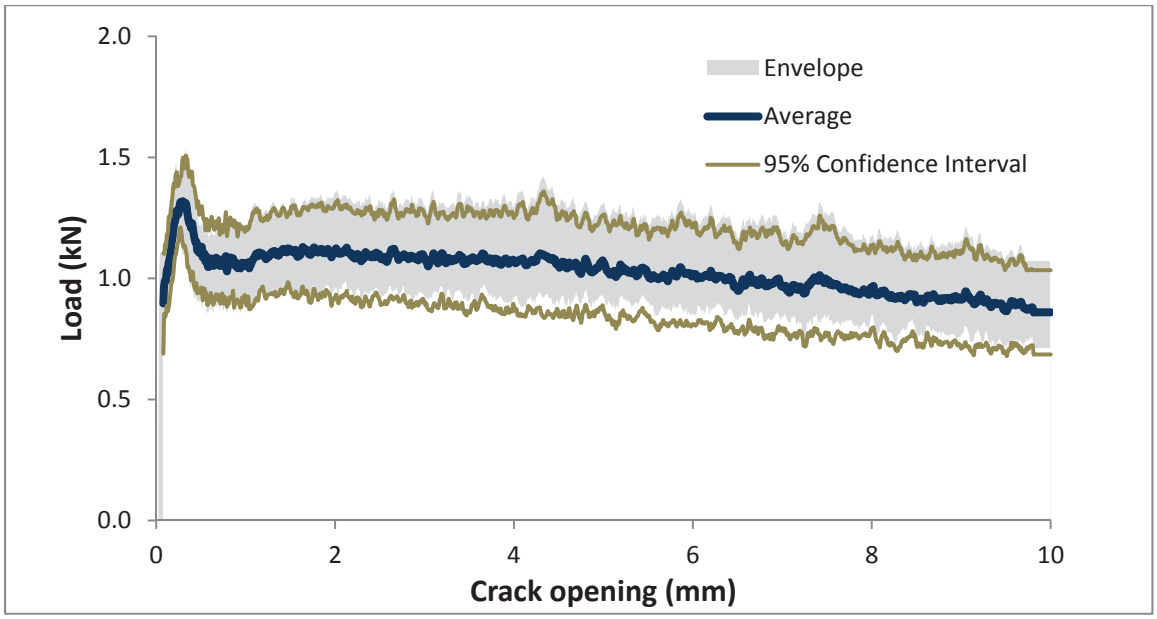

Figure B.30 - Post-crack response: HDPE and 3% PVDF, 3.0 kg/m^3, specimens cracked with steel stiffening bars.

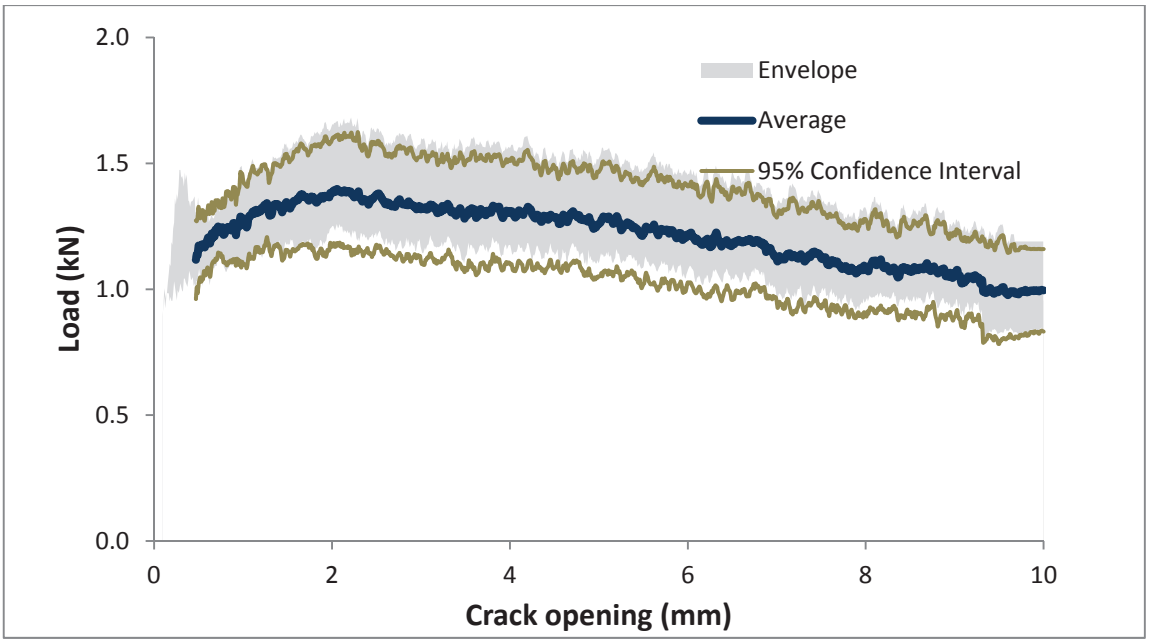

Figure B.31 - Post-crack response: HDPE, 5% PVDF, and 10% MAH, 3.0 kg/m^3, all specimens.

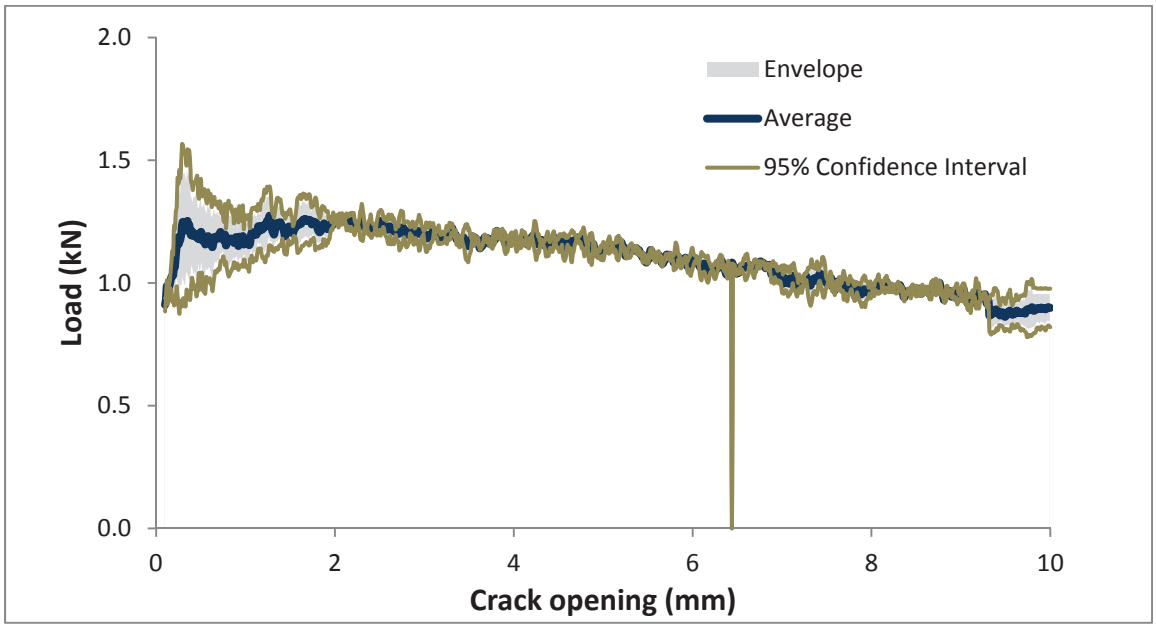

Figure B.32 - Post-crack response: HDPE, 5% PVDF, and 10% MAH, 3.0 kg/m^3, specimens cracked with steel stiffening bars.

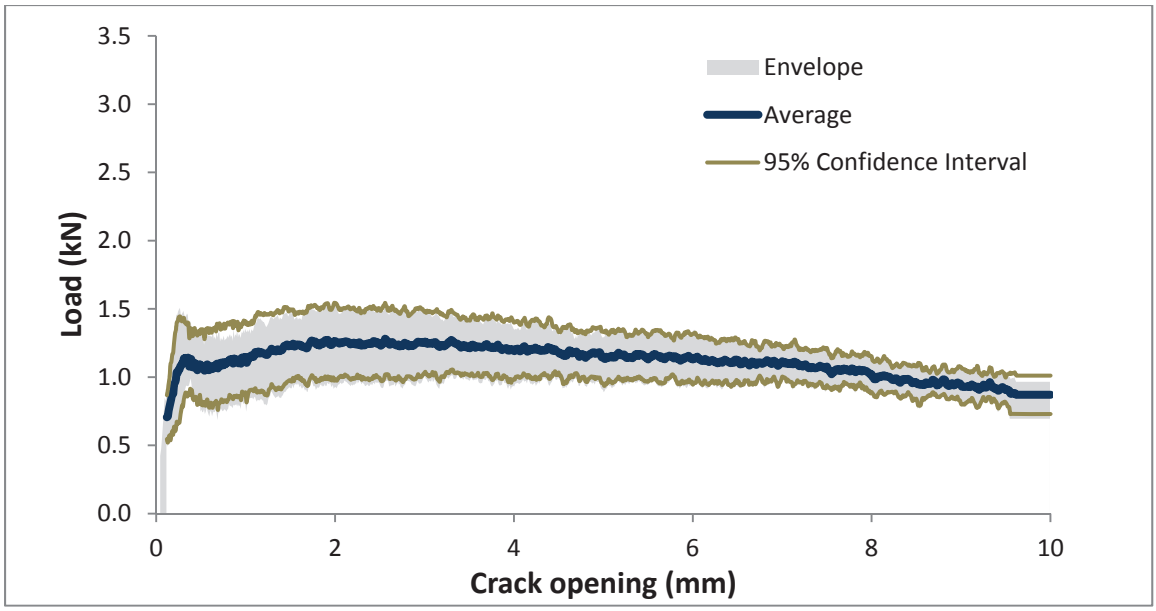

Figure B.33 - Post-crack response: HDPE, 11% PVDF, and 20% MAH, 3.0 kg/m^3, all specimens.

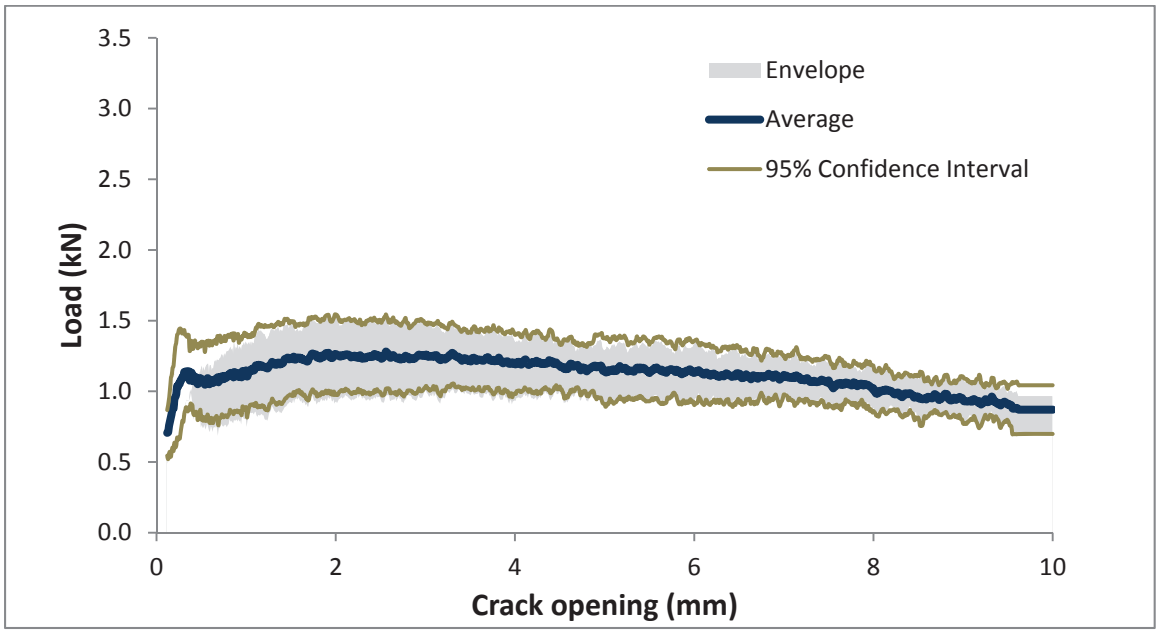

Figure B.34 - Post-crack response: HDPE, 11% PVDF, and 20% MAH, 3.0 kg/m^3, specimens cracked with steel stiffening bars.

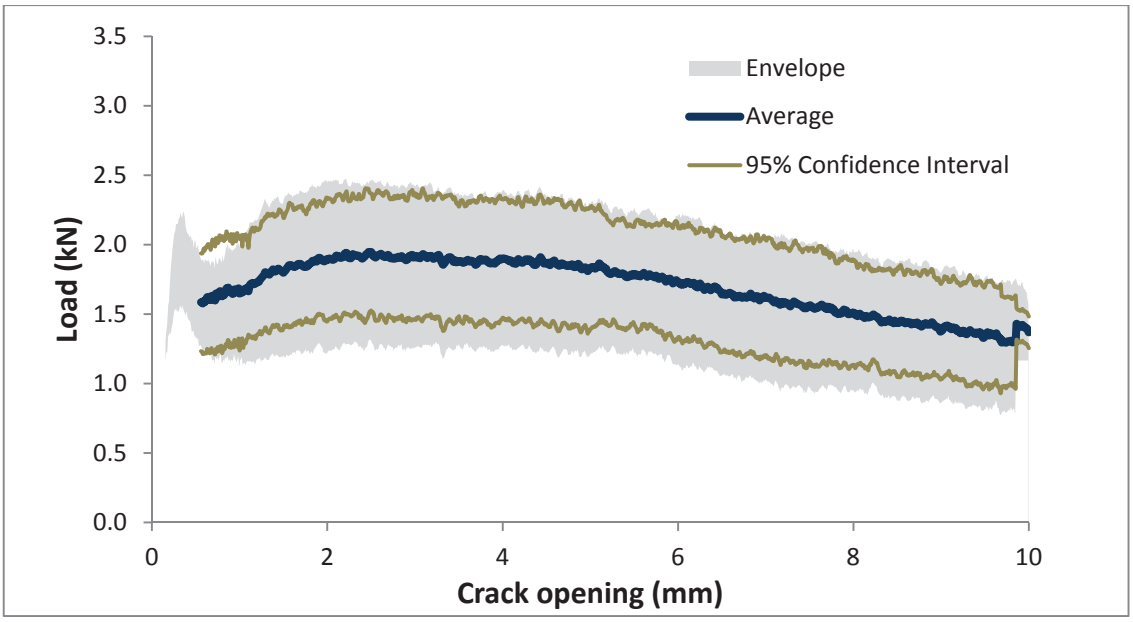

Figure B.35 - Post-crack response: 80% PP, 10% PE, and 10% EVA, 3.0 kg/m^3, all specimens.

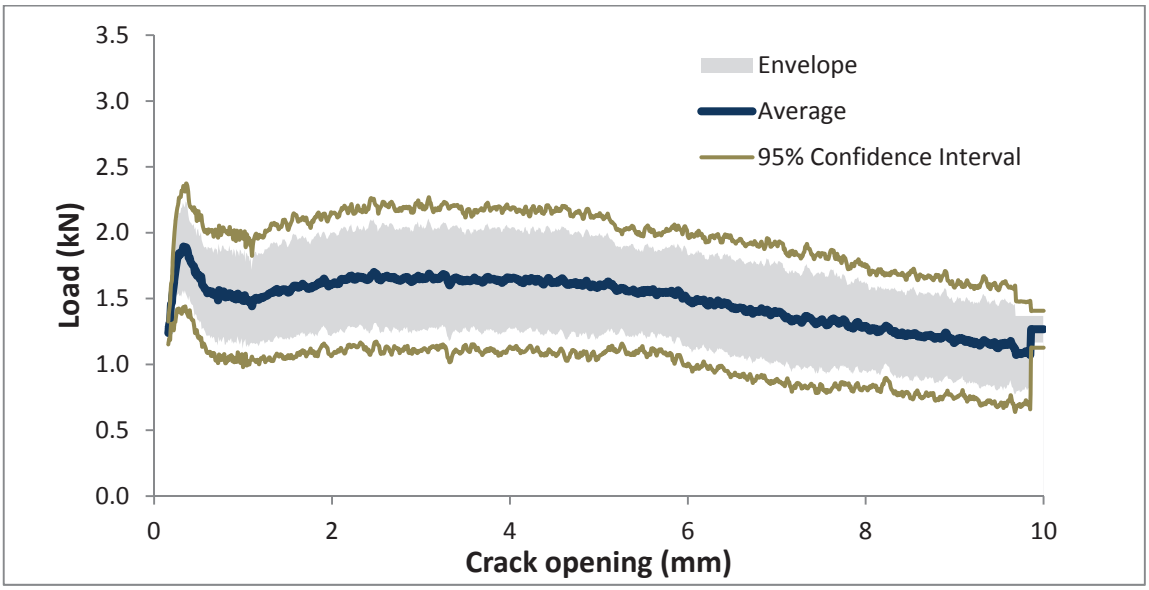

Figure B.36 - Post-crack response: 80% PP, 10% PE, and 10% EVA, 3.0 kg/m^3, specimens cracked with steel stiffening bars.

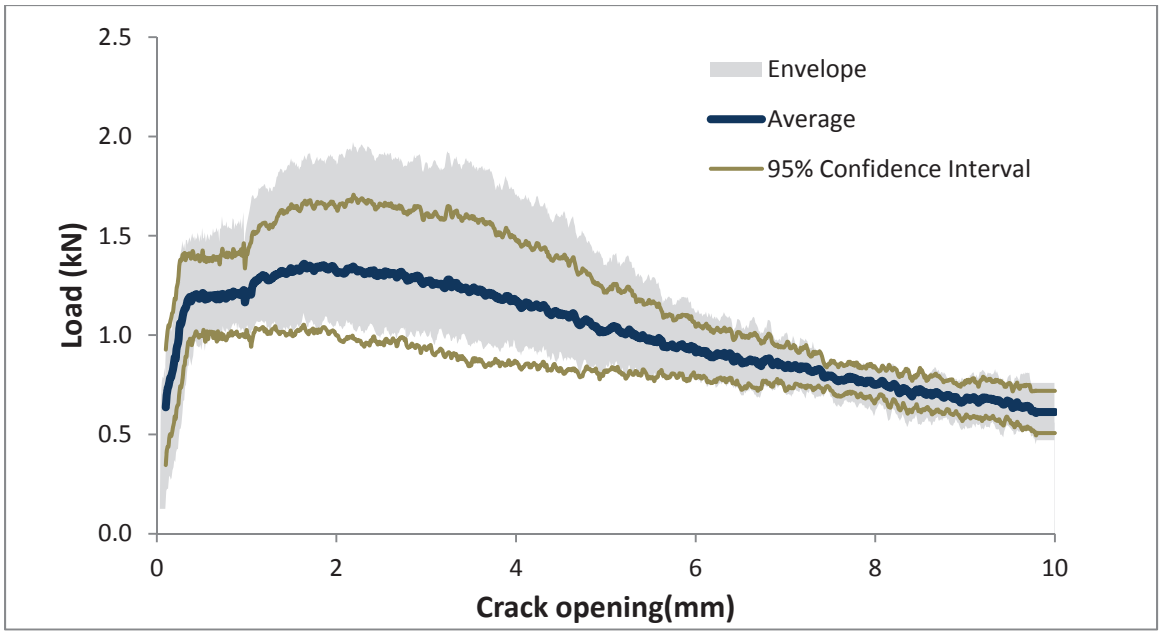

Figure B.37 - Post-crack response: 100% HDPE, 3.0 kg/m^3, all specimens.

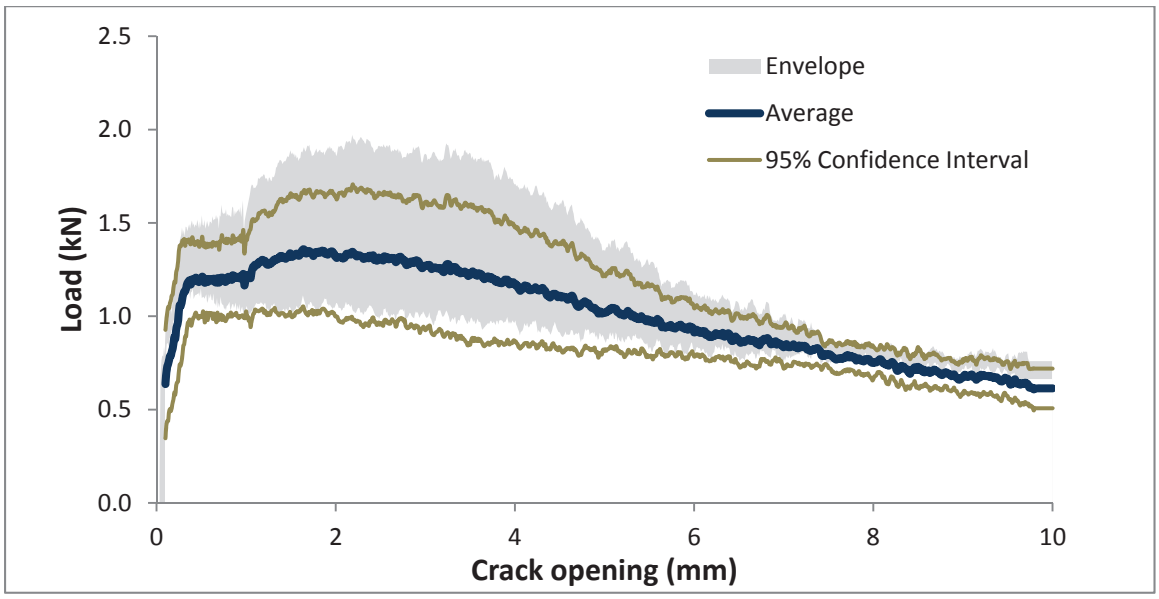

Figure B.38 - Post-crack response: 100% HDPE, 3.0 kg/m^3, specimens cracked with steel stiffening bars.

APPENDIX C – ADDITIONAL PLOTS FOR PER FIBRE UTT POST-CRACK RESPONSE

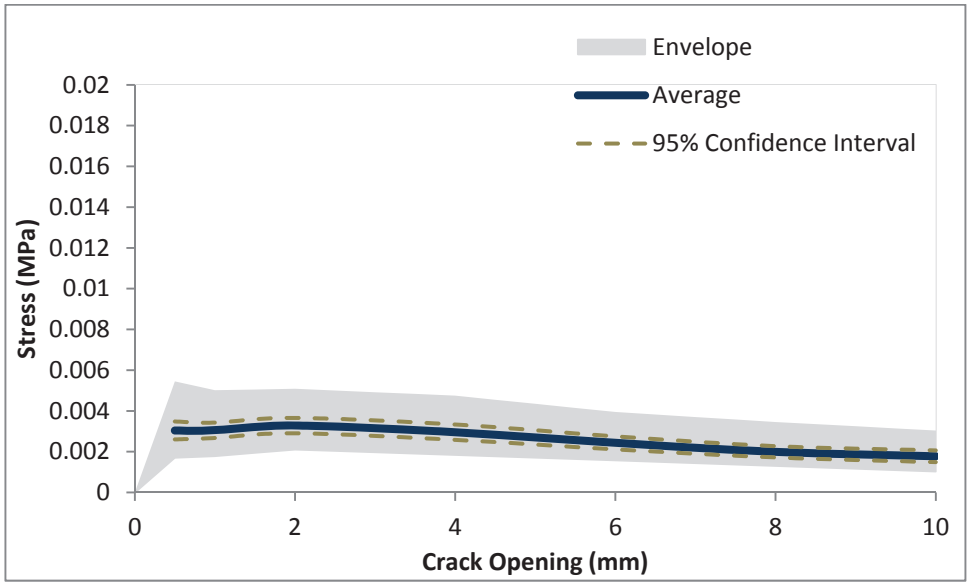

Figure C.1 – Per fibre σ(w) curve: HDPE and 10% EVA, 38 mm length

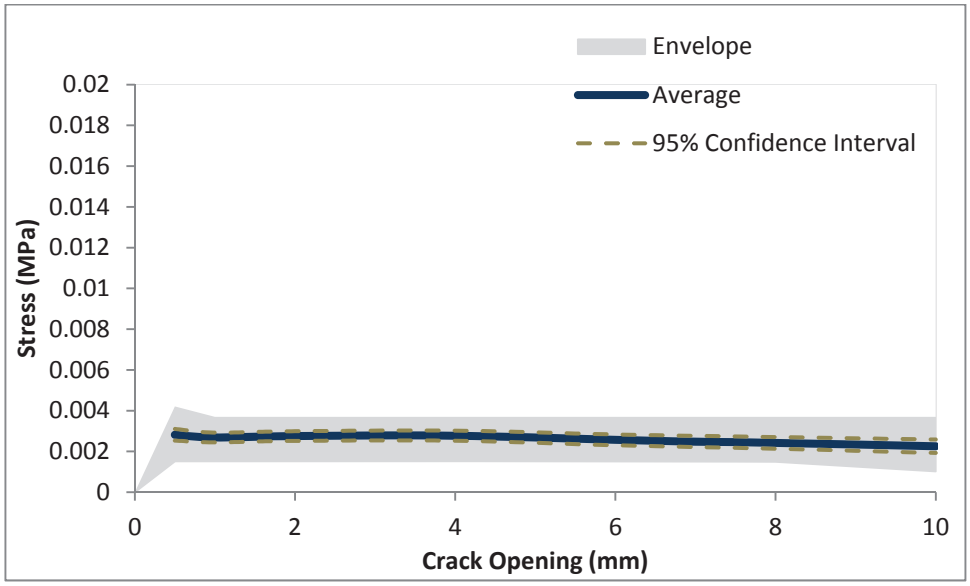

Figure C.2 – Per fibre σ(w) curve: HDPE and 10% EVA, 50 mm length

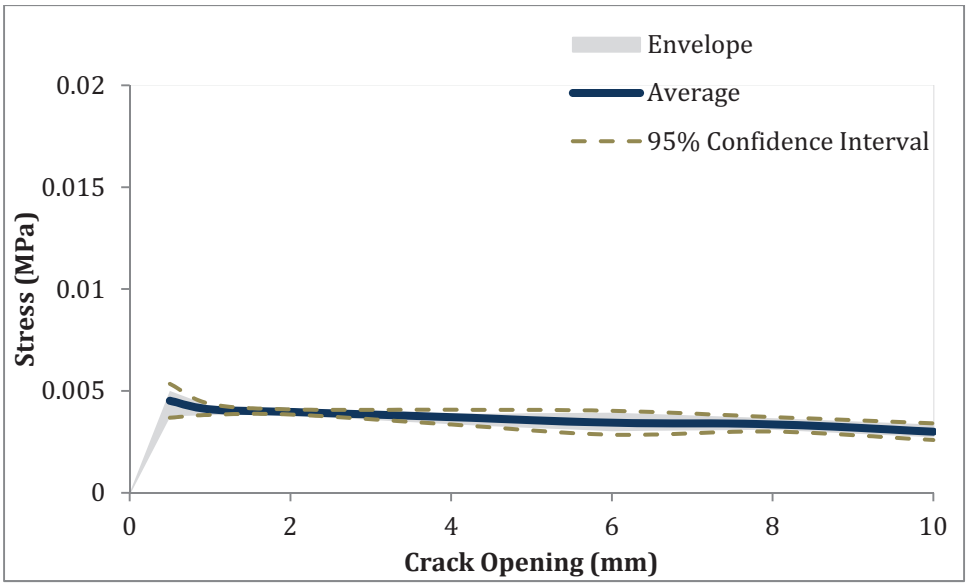

Figure C.3 – Per fibre σ(w) curve: HDPE and 3% PVDF

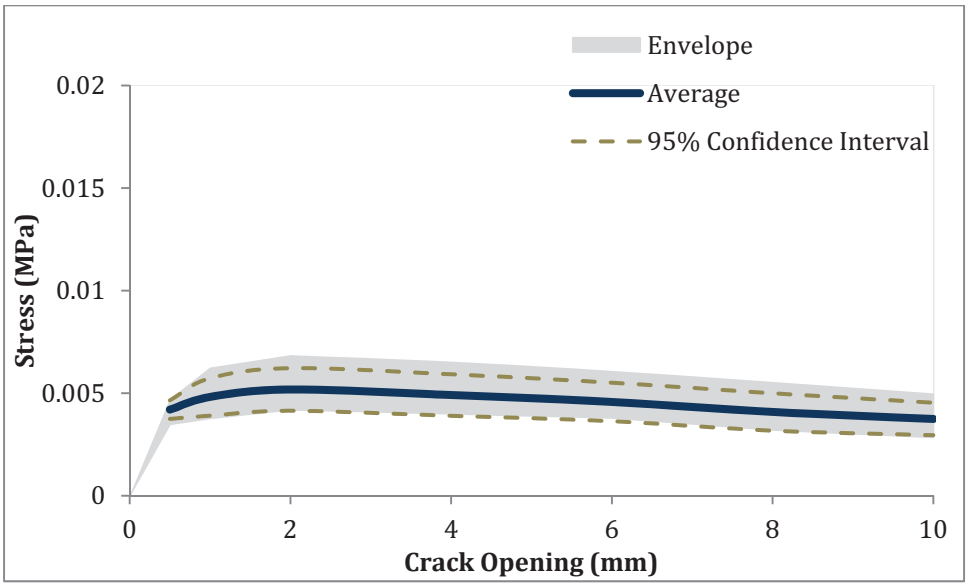

Figure C.4 – Per fibre σ(w) curve: HDPE, 5% PVDF, and 10% MAH

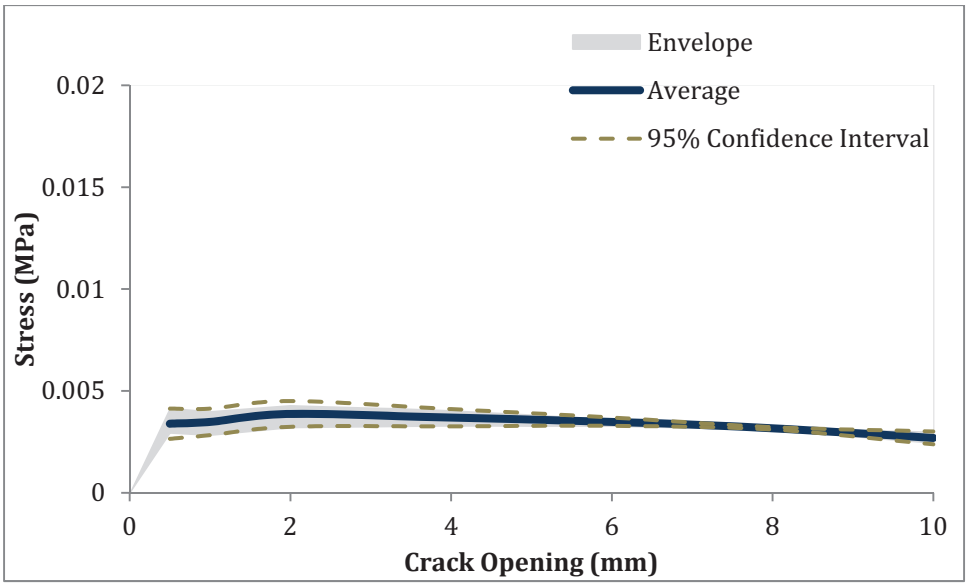

Figure C.5 – Per fibre σ(w) curve: HDPE, 11% PVDF, and 20% MAH

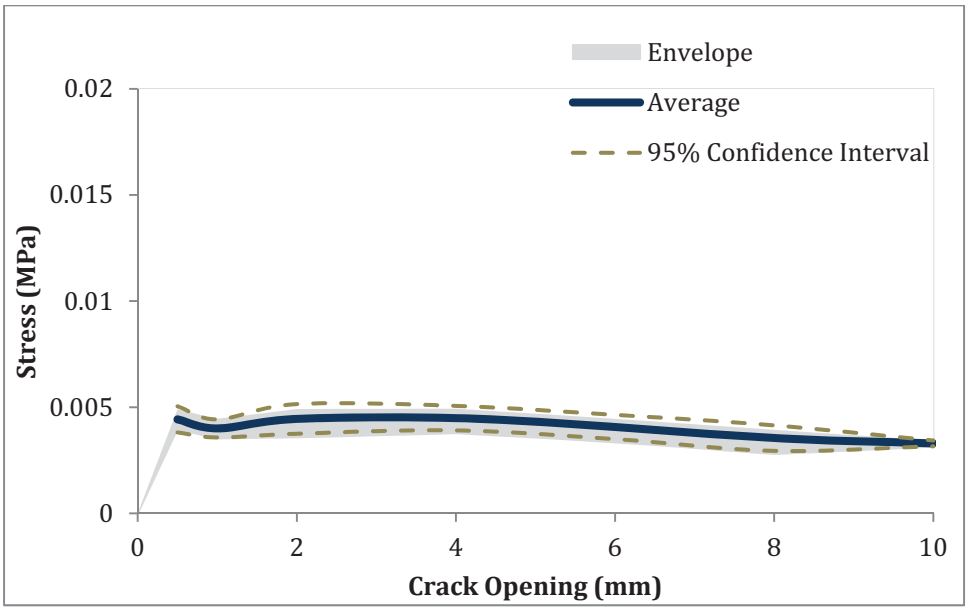

Figure C.6 – Per fibre σ(w) curve: 80% PP, 10% PE, and 10% EVA

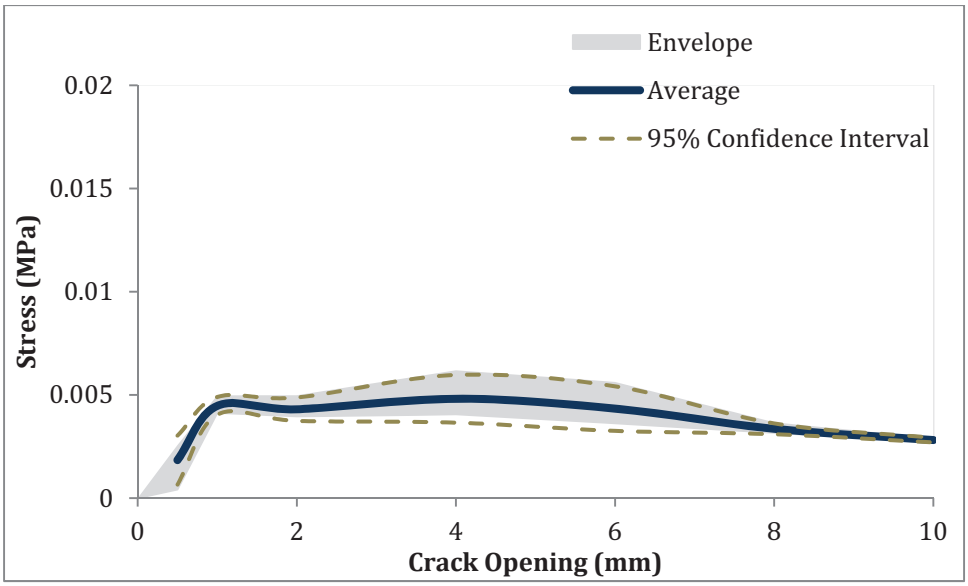

Figure C.7 – Per fibre σ(w) curve: 100% HDPE

APPENDIX D – ADDITIONAL PLOTS FOR COMPARISON OF PER FIBRE UTT POST-CRACK RESPONSE AND PULLOUT TESTING

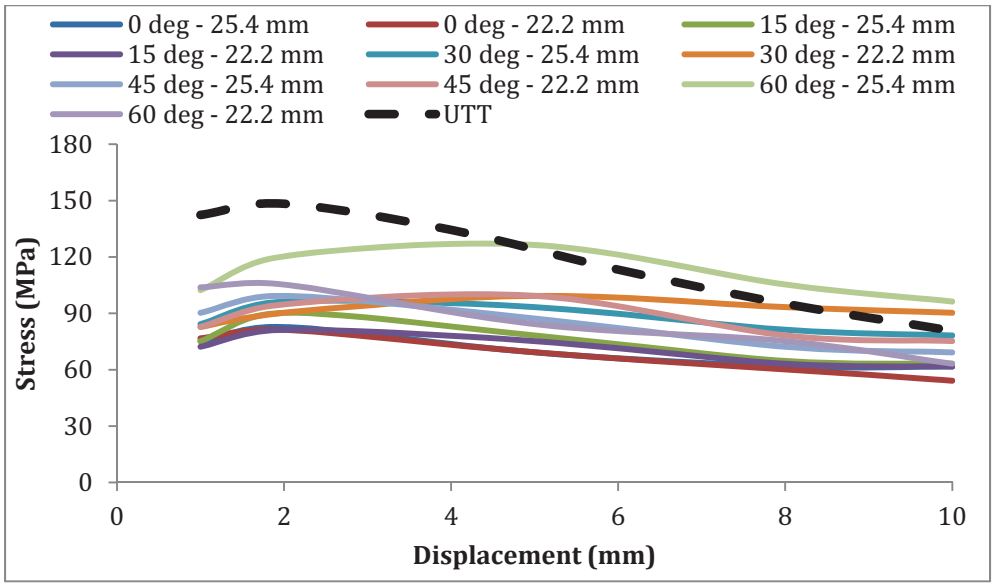

Figure D.1 - Per fibre σ(w) and pullout curves: Tuf-Strand SF

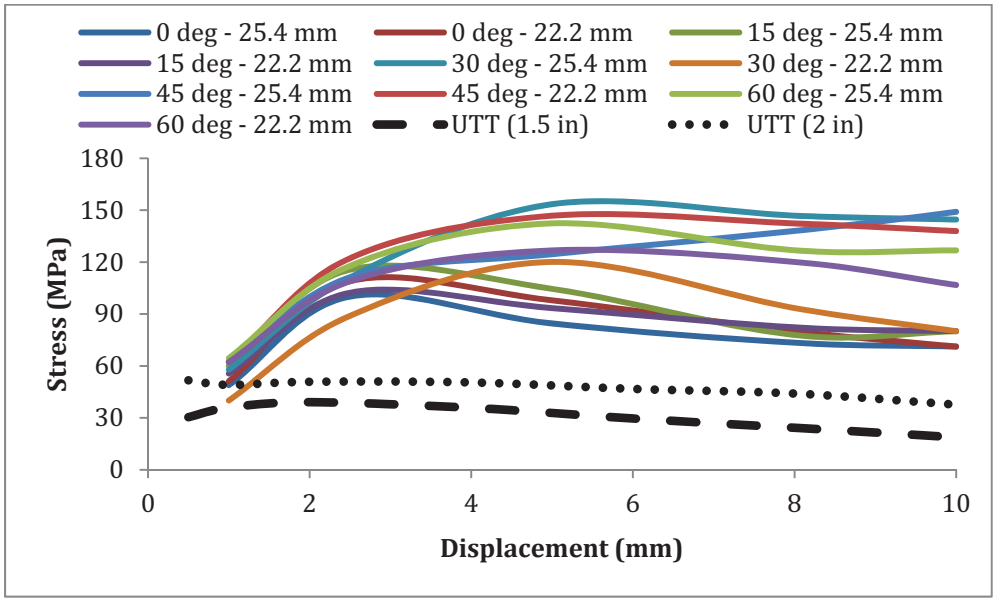

Figure D.2 - Per fibre σ(w) and pullout curves: HDPE and 10% EVA

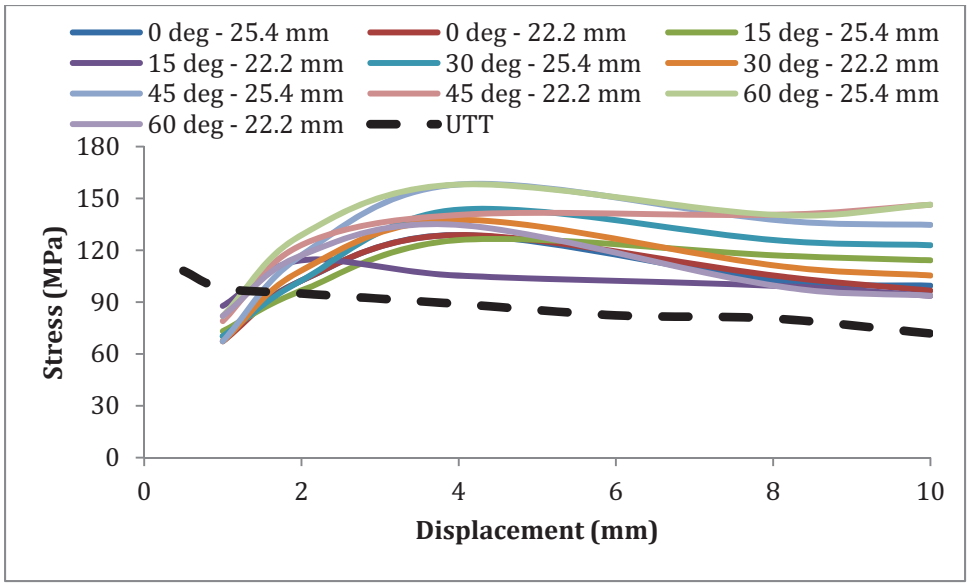

Figure D.3 - Per fibre σ(w) and pullout curves: HDPE, 3% PVDF

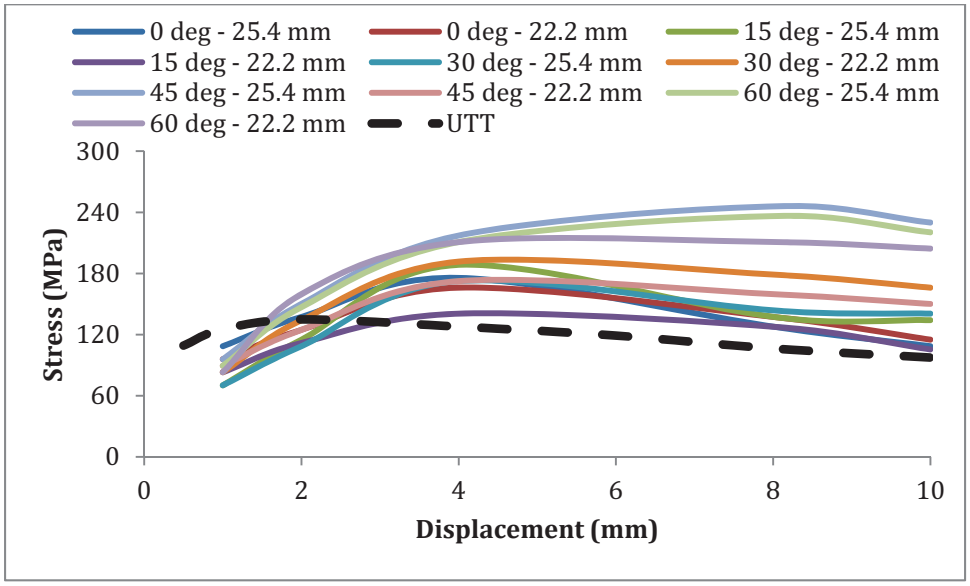

Figure D.4 - Per fibre σ(w) and pullout curves: HDPE, 5% PVDF, and 10% MAH

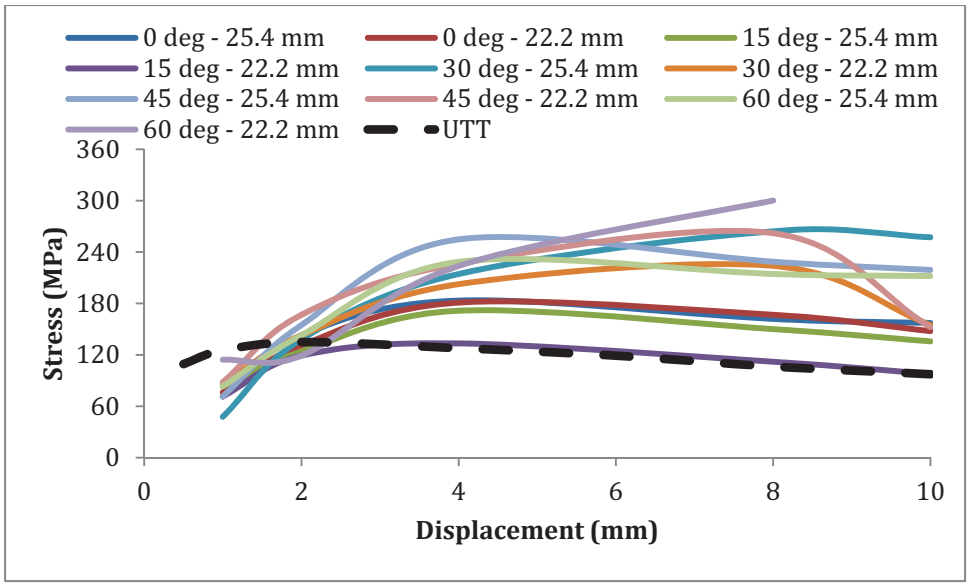

Figure D.5 - Per fibre σ(w) and pullout curves: HDPE, 11% PVDF, and 20% MAH

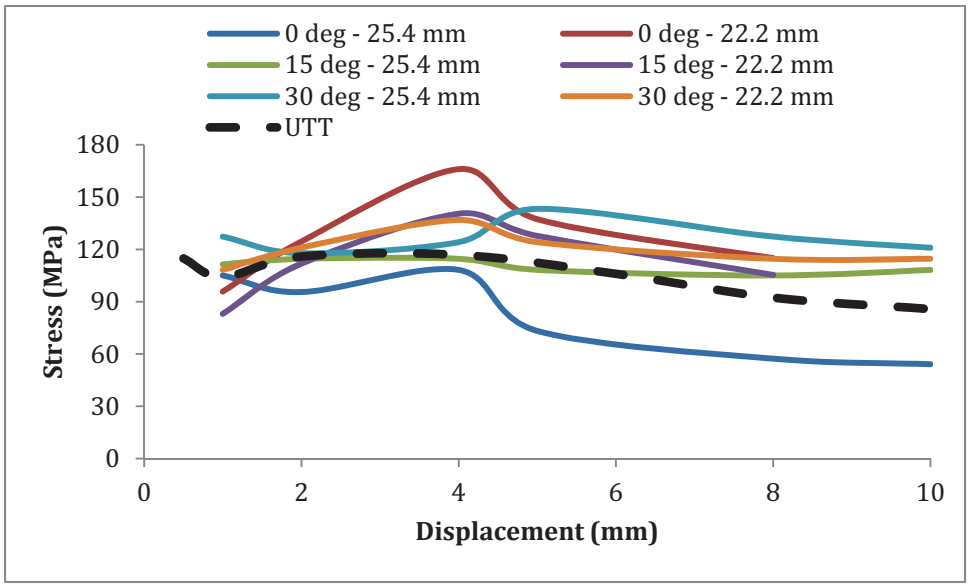

Figure D.6 - Per fibre σ(w) and pullout curves: 80% PP, 10% PE, and 10% EVA

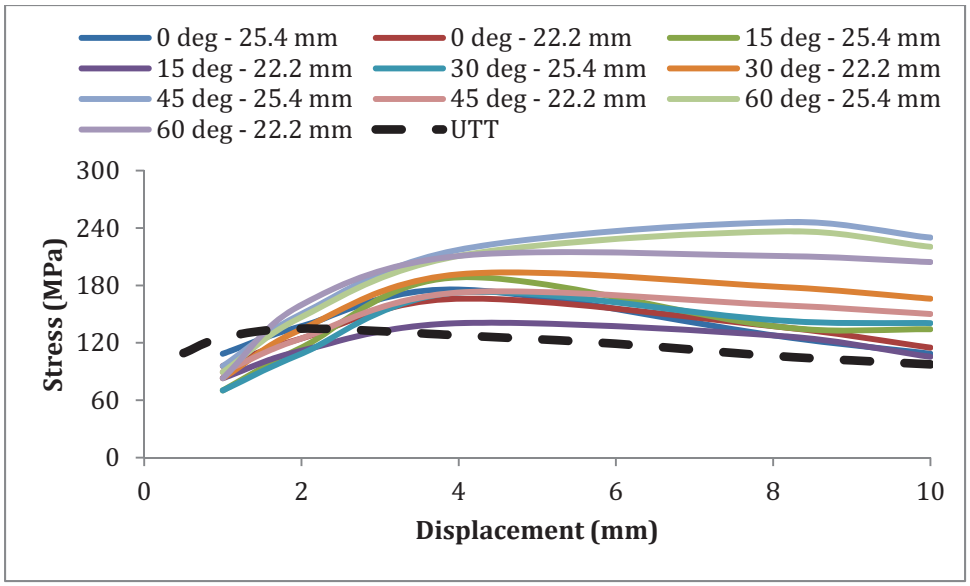

Figure D.7 - Per fibre σ(w) and pullout curves: 100% HDPE

APPENDIX E – ADDITIONAL CHARTS FOR SPECIMEN FIBRE COUNTS AND CROSS SECTION DIMENSIONS – UTT AND ASTM C1609 SPECIMENS

Table E.1 – UTT fibre counts and cross-section dimensions (1 of 5)

Fibre Type *Dosage*	Specimen Number	Fibre Count	Diameter (Average of 3)	Notch Depth (Average of 3)
Tuf-Strand SF (Mix Truck) *1.8 kg/m³*	1	29	152.9	15.89
	2	23	153.3	15.29
	3	22	153.3	15.60
	4	35	153.2	15.78
	5	14	153.0	15.41
	6	13	153.1	15.66
	7	27	153.0	15.41
Tuf-Strand SF (Mix Truck) *2.4 kg/m³*	17	43	153.2	16.69
	18	39	153.0	16.13
	21	26	153.1	16.58
	22	39	152.7	16.09
	23	30	153.2	15.83
Tuf-Strand SF (Mix Truck) *3.0 kg/m³*	33	50	153.3	14.22
	34	20	152.7	14.95
	35	45	153.3	15.68
	36	49	153.1	16.83
Tuf-Strand SF (Mix Truck) *4.6 kg/m³*	41	57	153.3	14.22
	42	43	152.7	14.95
	45	55	153.3	15.68
	46	58	153.4	14.59
	48	59	153.1	14.84
Tuf-Strand SF (Mix Truck) *6.9 kg/m³*	50	73	153.3	14.22
	57	82	153.3	15.68
	58	75	153.2	15.90
	59	62	153.4	14.59
	60	62	153.3	15.32

Table E.1 – UTT fibre counts and cross-section dimensions (2 of 5)

Fibre Type *Dosage*	Specimen Number	Fibre Count	Diameter (Average of 3)	Notch Depth (Average of 3)
Tuf-Strand SF (Drum Mixer) *1.8 kg/m³*	173	43	153.3	14.22
	174	26	152.7	14.95
	175	20	153.1	14.96
	176	35	153.0	14.35
	177	24	153.3	15.68
	178	51	153.4	14.59
	179	30	153.1	15.32
	180	39	153.1	15.26
Tuf-Strand SF (Drum Mixer) *3.0 kg/m³*	141	74	153.4	14.93
	143	32	152.8	13.61
	144	72	153.3	14.37
	145	52	153.4	15.11
	146	27	152.8	15.76
	147	30	152.9	14.52
Tuf-Strand SF (Drum Mixer) *4.6 kg/m³*	118	82	152.7	14.95
	119	97	153.3	15.68
	120	111	153.1	14.96
	122	82	153.4	14.59
	123	78	153.3	15.32
	124	56	153.0	14.35
HDPE, 10% EVA (38 mm) (Drum Mixer) *1.8 kg/m³*	157	46	152.8	13.62
	158	50	153.1	15.16
	159	47	152.9	15.89
	160	34	153.3	14.92
	161	28	153.1	15.55
	162	43	153.5	16.15
	163	34	153.5	16.15
	164	43	153.1	15.16

Table E.1 – UTT fibre counts and cross-section dimensions (3 of 5)

Fibre Type *Dosage*	Specimen Number	Fibre Count	Diameter (Average of 3)	Notch Depth (Average of 3)
HDPE, 10% EVA (38 mm) (Drum Mixer) *3.0 kg/m³*	149	40	153.3	14.22
	153	60	152.7	14.95
	154	52	153.3	15.68
	156	49	153.3	14.86
HDPE, 10% EVA (38 mm) (Drum Mixer) *4.6 kg/m³*	125	54	153.1	15.59
	126	85	153.3	14.39
	128	52	152.8	14.97
	129	66	153.3	14.85
	130	68	153.2	15.17
	131	80	153.1	14.58
	132	117	153.1	15.59
HDPE, 10% EVA (2.0") (Drum Mixer) *1.8 kg/m³*	165	26	152.9	15.89
	166	20	153.4	15.42
	167	25	153.3	15.60
	168	19	153.1	15.66
	169	28	153.2	15.78
	171	30	153.0	15.41
	172	37	153.0	15.11
HDPE, 10% EVA (2.0") (Drum Mixer) *3.0 kg/m³*	133	31	153.3	14.22
	135	31	153.3	14.22
	136	50	153.4	14.64
	137	26	152.7	14.95
	138	29	153.3	15.68
	139	33	153.4	14.59
	140	33	152.9	13.48

Table E.1 – UTT fibre counts and cross-section dimensions (4 of 5)

Fibre Type *Dosage*	Specimen Number	Fibre Count	Diameter (Average of 3)	Notch Depth (Average of 3)
HDPE, 10% EVA (2.0") (Drum Mixer) *4.6 kg/m³*	110	54	153.3	14.22
	111	57	153.3	14.22
	112	48	152.8	15.65
	113	51	153.3	14.22
	114	59	152.7	14.95
	115	55	153.3	15.68
	116	50	153.4	14.59
HDPE, 3% PVDF *3.0 kg/m³*	73	21	153.3	14.22
	74	20	152.7	14.95
	75	23	152.8	16.05
	76	19	153.3	15.68
	77	22	153.4	14.59
	78	18	153.0	14.35
HDPE, 5% PVDF, 10% MAH *3.0 kg/m³*	68	23	153.3	14.22
	70	23	153.4	14.95
	71	25	153.3	15.41
	72	20	153.1	14.96
HDPE, 11% PVDF, 20% MAH *3.0 kg/m³*	85	30	153.3	14.22
	88	27	152.7	14.95
	89	24	153.0	20.04
	90	27	153.3	15.68
80% PP, 10% HDPE, 10% EVA *3.0 kg/m³*	97	30	152.6	15.65
	98	35	153.4	15.42
	99	36	153.3	14.22
	100	43	153.1	15.66

Table E.1 – UTT fibre counts and cross-section dimensions (5 of 5)

Fibre Type *Dosage*	Specimen Number	Fibre Count	Diameter (Average of 3)	Notch Depth (Average of 3)
100% HDPE *3.0 kg/m^3*	103	26	152.8	15.97
	105	37	153.4	19.53
	106	22	153.3	15.68
	107	25	153.4	14.59
	108	36	153.2	16.74

Table E.2 – ASTM 1609 fibre counts and cross-section dimensions (1 of 3)

Fibre Type *Dosage*	Sample Number	Fibre Count	Height (mm)	Width (mm)
Tuf-Strand SF (Mix Truck) *1.8 kg/m^3*	B-1	64	154	153
	B-2	70	153	153
	B-3	75	153	153
	B-4	76	152	153
Tuf-Strand SF (Mix Truck) *2.4 kg/m^3*	B-1	72	152	152
	B-2	88	153	153
	B-3	87	156	152
	B-4	89	153	151
	B-5	120	154	152
Tuf-Strand SF (Mix Truck) *3.0 kg/m^3*	B-1	100	153	153
	B-2	102	153	152
	B-3	119	156	154
	B-4	108	154	153
	B-5	98	153	153
Tuf-Strand SF (Mix Truck) *4.6 kg/m^3*	B-1	93	153	154
	B-2	143	154	153
	B-3	102	153	153
	B-4	125	154	154
	B-5	135	154	154
Tuf-Strand SF (Mix Truck) *6.9 kg/m^3*	B-1	220	153	154
	B-2	225	153	153
	B-3	174	153	153
	B-4	200	154	154
	B-5	200	153	153
Tuf-Strand SF (Drum Mixer) *1.8 kg/m^3*	B-1	62	152	152
	B-2	82	154	152
	B-3	76	153	152
	B-4	69	154	151
	B-5	62	153	152

Table E.2 – ASTM 1609 fibre counts and cross-section dimensions (2 of 3)

Fibre Type *Dosage*	Sample Number	Fibre Count	Height (mm)	Width (mm)
Tuf-Strand SF (Drum Mixer) *3.0 kg/m³*	B-1	101	152	153
	B-2	66	152	152
	B-3	78	152	150
	B-4	73	153	150
	B-5	85	152	151
Tuf-Strand SF (Drum Mixer) *4.6 kg/m³*	B-1	122	151	151
	B-2	115	153	152
	B-3	98	153	151
	B-4	110	153	151
	B-5	122	153	153
HDPE, 10% EVA (38 mm) (Drum Mixer) *1.8 kg/m³*	B-1	62	153	152
	B-2	61	152	152
	B-3	75	151	152
	B-4	55	152	153
	B-5	66	152	152
HDPE, 10% EVA (38 mm) (Drum Mixer) *3.0 kg/m³*	B-1	78	152	153
	B-2	77	152	151
	B-3	84	153	152
	B-4	84	153	152
	B-5	80	152	151
HDPE, 10% EVA (38 mm) (Drum Mixer) *4.6 kg/m³*	B-1	185	153	149
	B-2	156	152	152
	B-3	98	152	150
	B-4	90	152	152
	B-5	121	152	147
HDPE, 10% EVA (2.0") (Drum Mixer) *1.8 kg/m³*	B-1	61	153	151
	B-2	40	152	153
	B-3	70	153	151
	B-4	63	153	152
	B-5	39	153	150

Table E.2 - ASTM 1609 fibre counts and cross-section dimensions (3 of 3)

Fibre Type *Dosage*	Sample Number	Fibre Count	Height (mm)	Width (mm)
HDPE, 10% EVA (2.0") (Drum Mixer) *3.0 kg/m^3*	B-1	93	153	151
	B-2	78	152	153
	B-3	85	153	151
	B-4	99	153	152
	B-5	86	153	150
HDPE, 10% EVA (2.0") (Drum Mixer) *4.6 kg/m^3*	B-1	130	152	153
	B-2	122	151	152
	B-3	104	153	153
	B-4	94	152	153
	B-5	90	154	154

APPENDIX F – ADDITIONAL PLOTS FOR COMPRISON OF STRESS-STRAIN RESPONSE

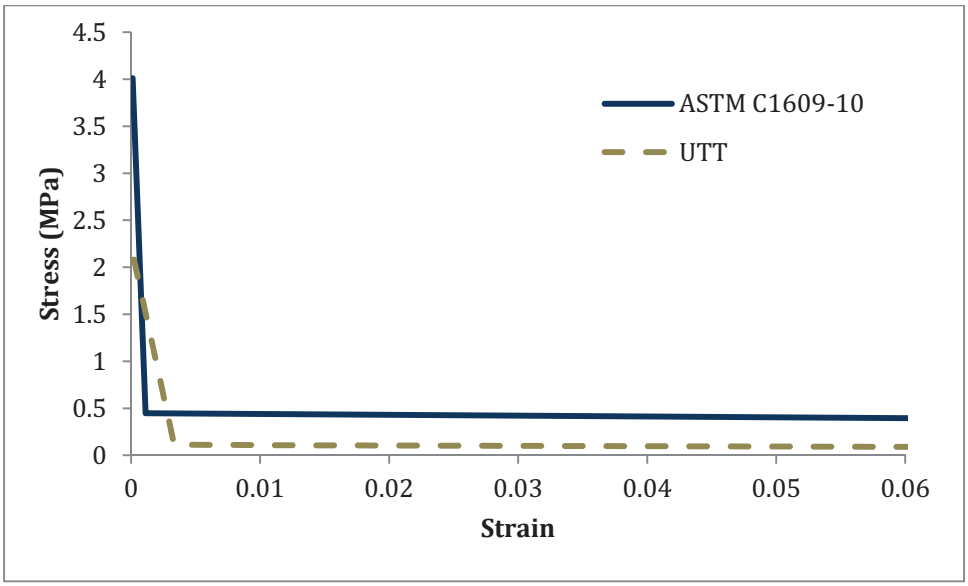

Figure F.1 – Comparison of σ–ε responses: Tuf-Strand SF (mix truck), 1.8 kg/m³.

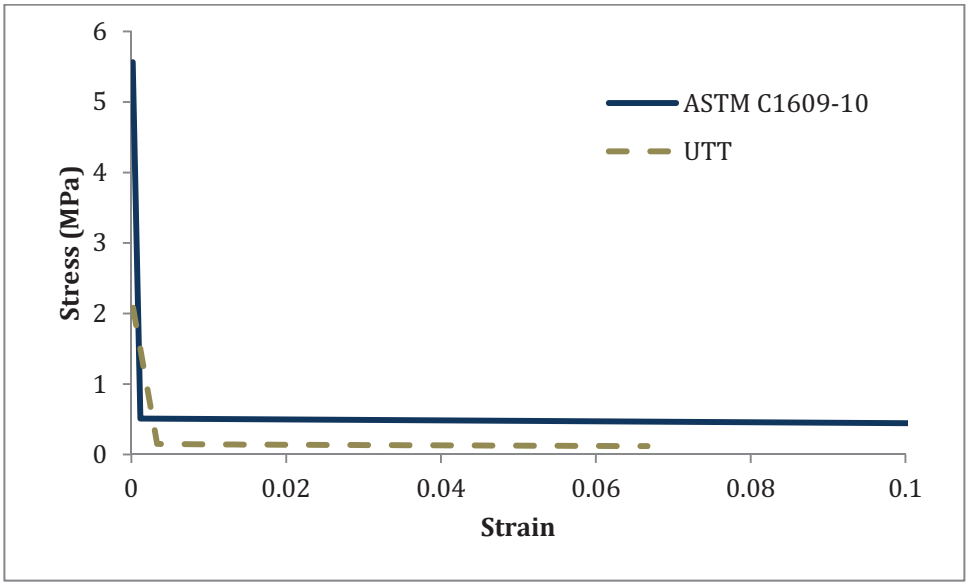

Figure F.2 – Comparison of σ–ε responses: Tuf-Strand SF (mix truck), 2.4 kg/m³.

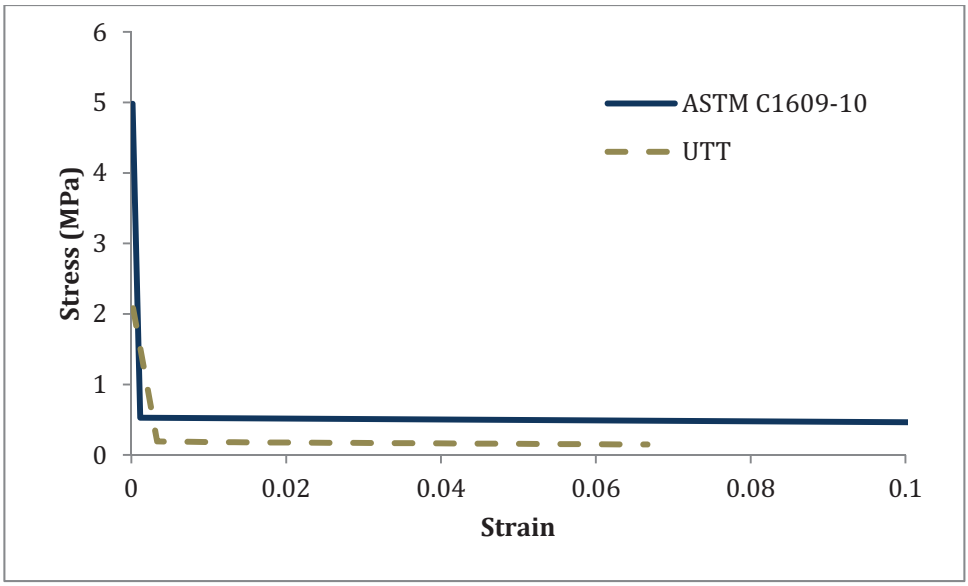

Figure F.3 – Comparison of σ–ε responses: Tuf-Strand SF (mix truck), 3.0 kg/m^3.

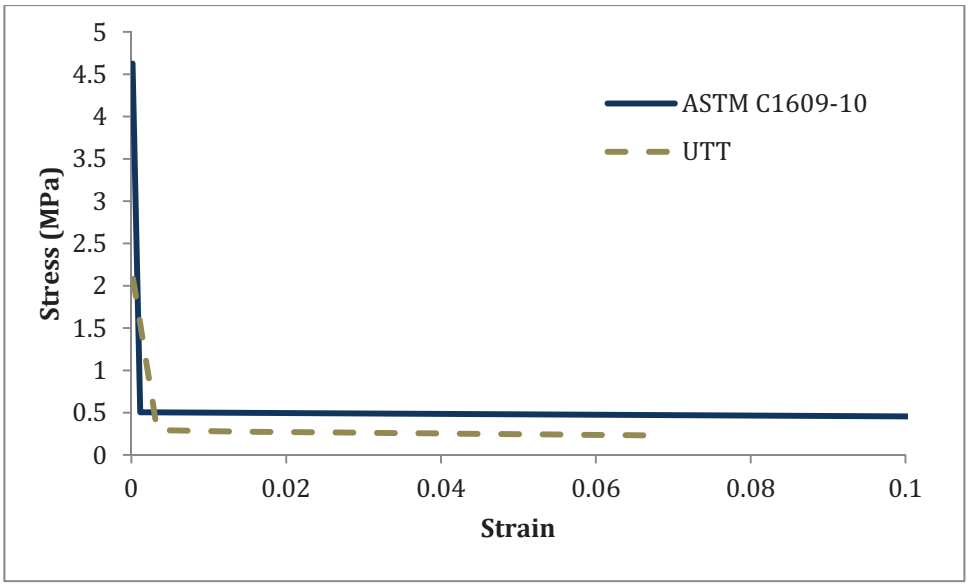

Figure F.4 – Comparison of σ–ε responses: Tuf-Strand SF (mix truck), 4.6 kg/m^3.

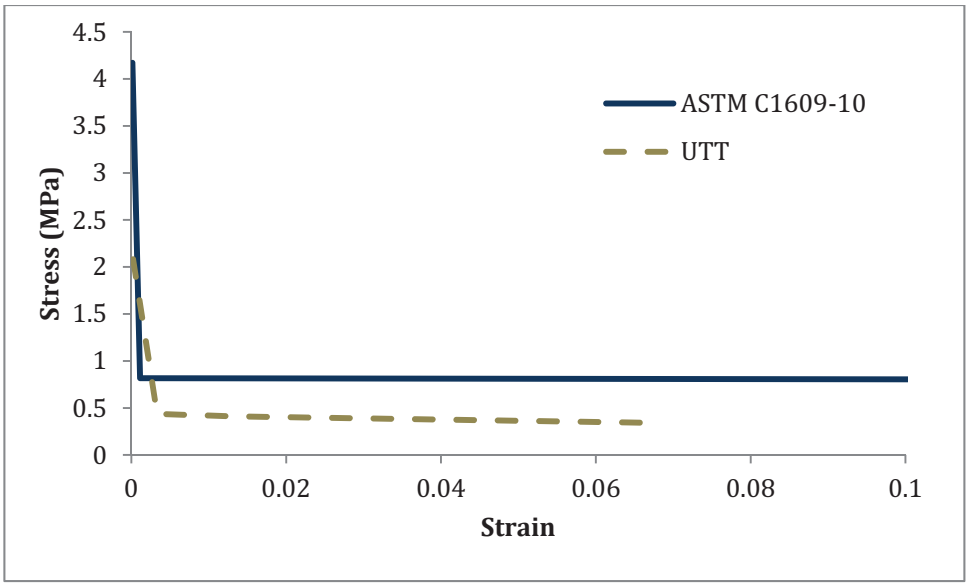

Figure F.5 – Comparison of σ–ε responses: Tuf-Strand SF (mix truck), 6.9 kg/m^3.

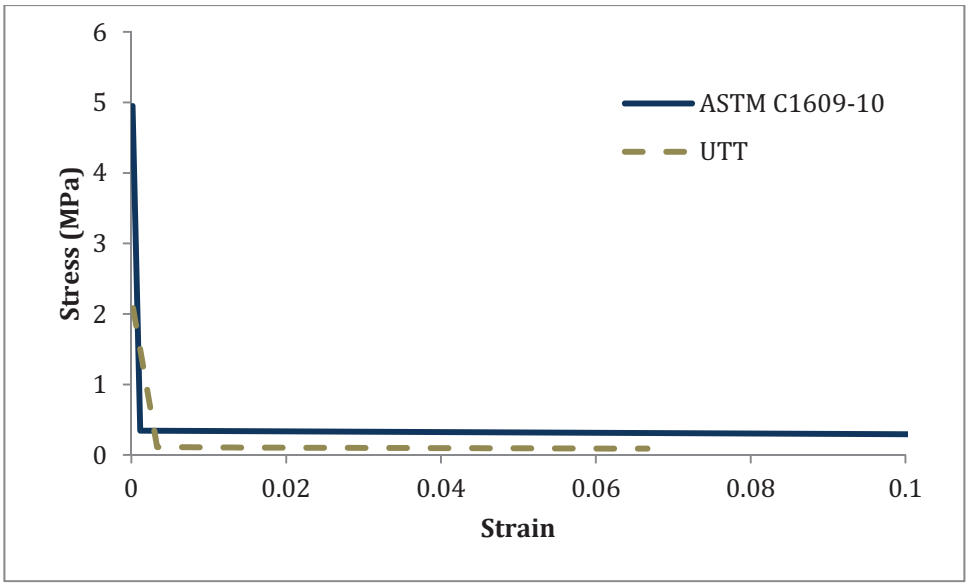

Figure F.6 – Comparison of σ–ε responses: Tuf-Strand SF (drum mixer), 1.8 kg/m^3.

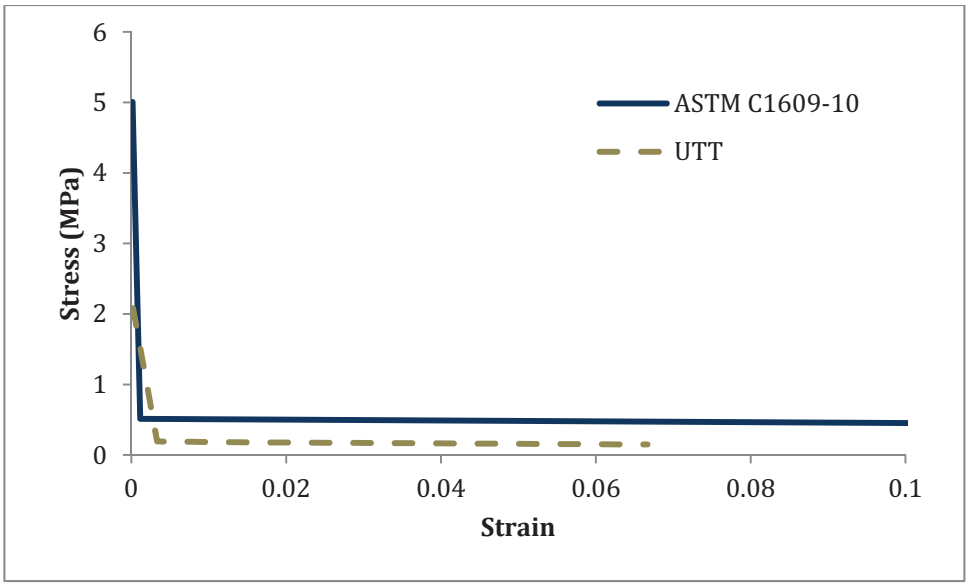

Figure F.7 – Comparison of σ–ε responses: Tuf-Strand SF (drum mixer), 3.0 kg/m^3.

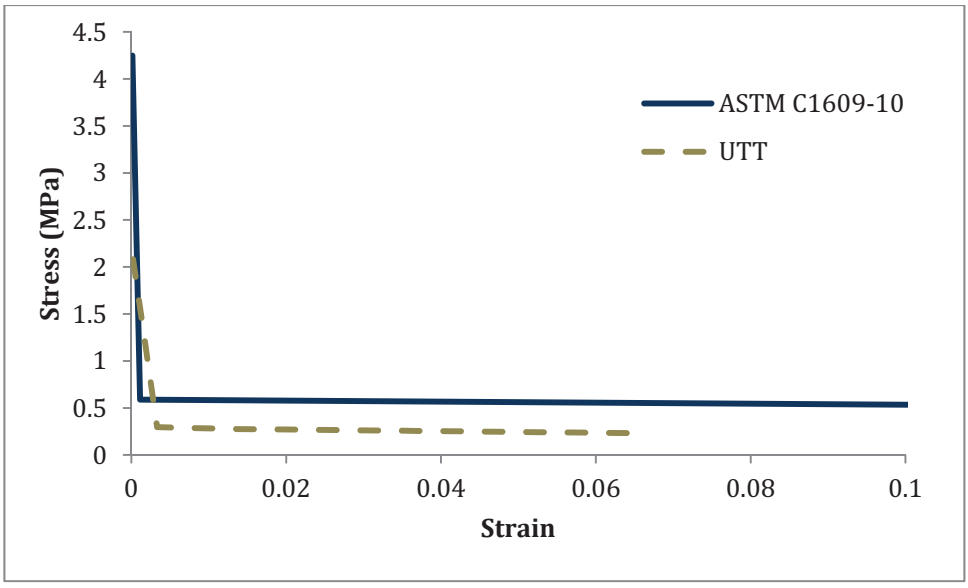

Figure F.8 – Comparison of σ–ε responses: Tuf-Strand SF (drum mixer), 4.6 kg/m^3.

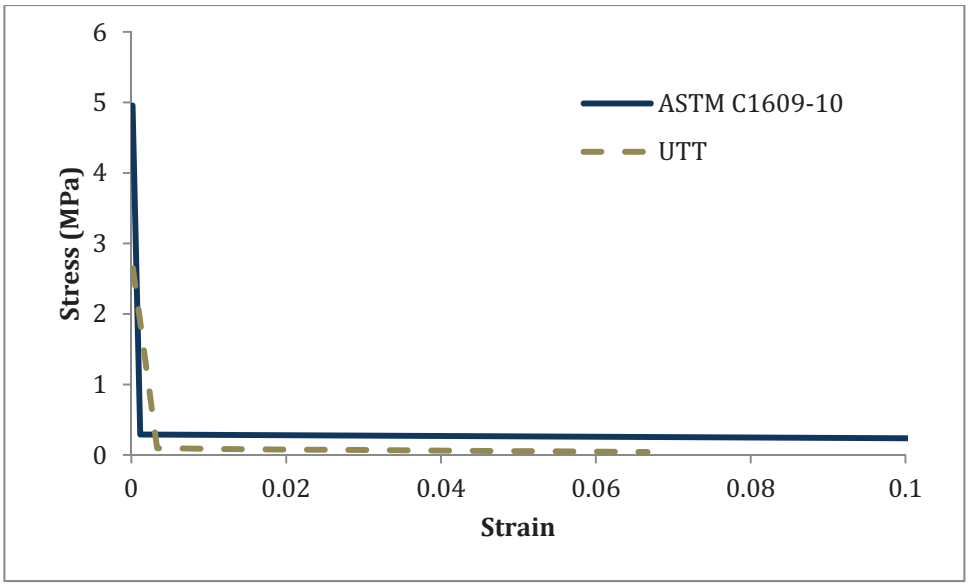

Figure F.9 – Comparison of σ–ε responses: HDPE and 10% EVA, 1.8 kg/m^3, 38 mm length.

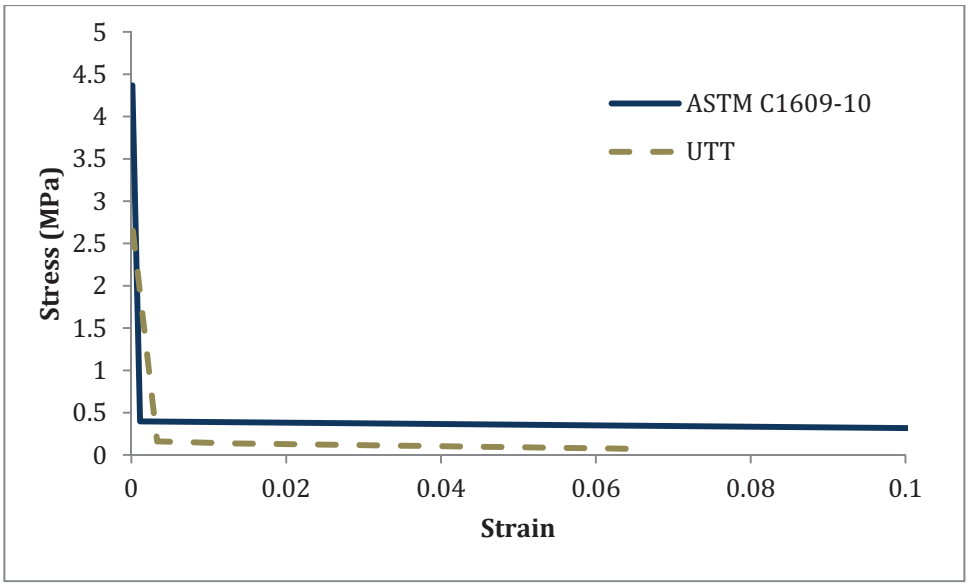

Figure F.10 – Comparison of σ–ε responses: HDPE and 10% EVA, 3.0 kg/m^3, 38 mm length.

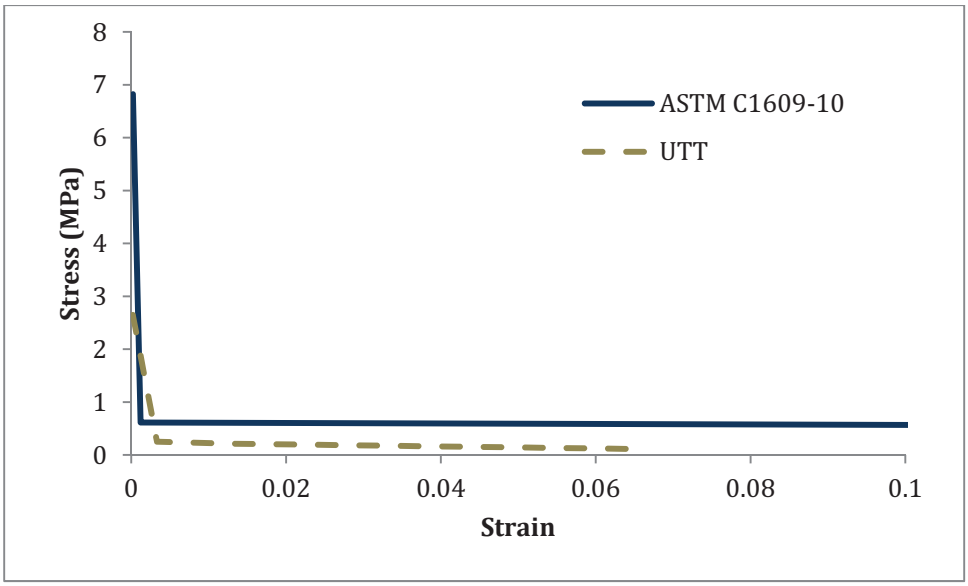

Figure F.11 – Comparison of σ–ε responses: HDPE and 10% EVA, 4.6 kg/m^3, 38 mm length.

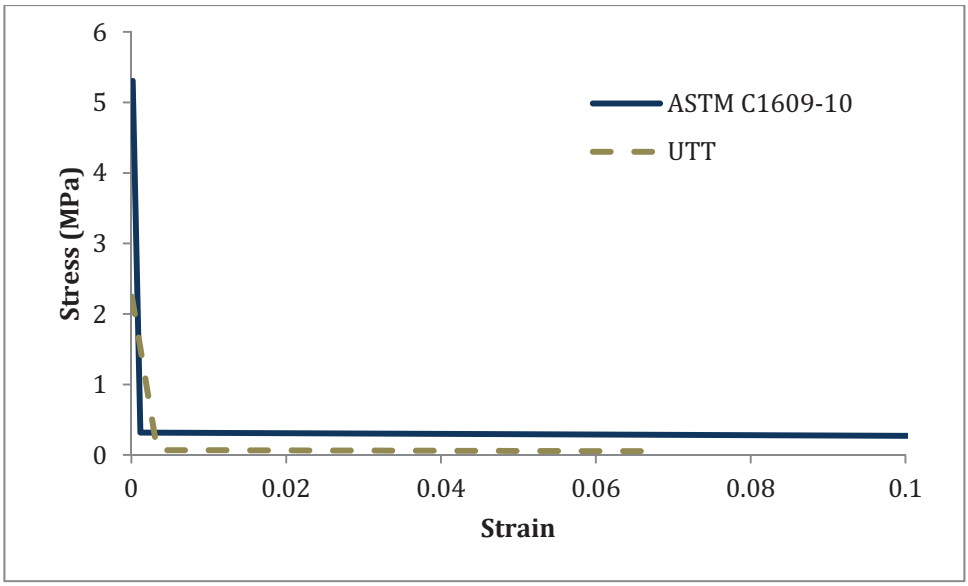

Figure F.12 – Comparison of σ–ε responses: HDPE and 10% EVA, 1.8 kg/m^3, 50 mm length.

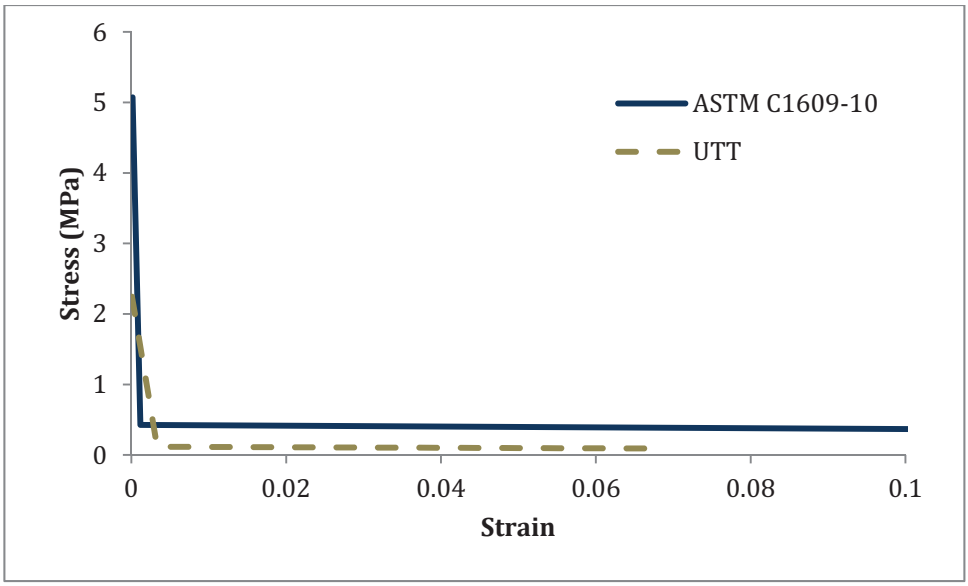

Figure F.13 – Comparison of σ–ε responses: HDPE and 10% EVA, 3.0 kg/m^3, 50 mm length.

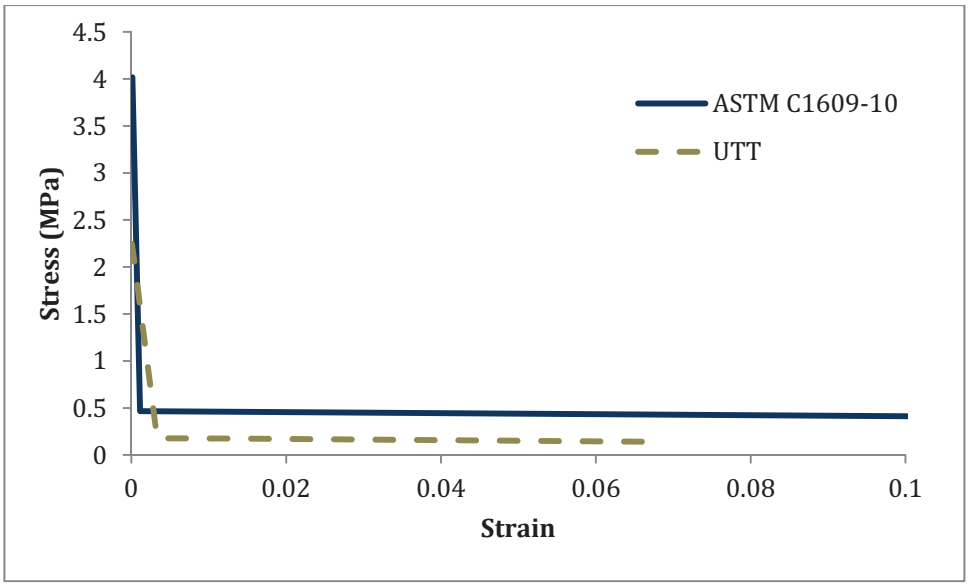

Figure F.14 – Comparison of σ–ε responses: HDPE and 10% EVA, 4.6 kg/m^3, 50 mm length.

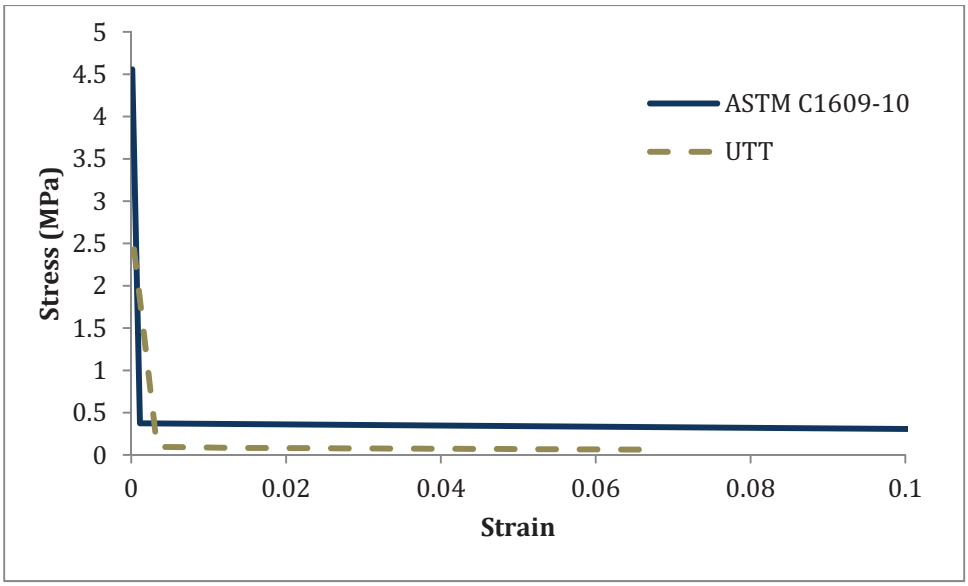

Figure F.15 – Comparison of σ–ε responses: HDPE and 3% PVDF, 3.0 kg/m³.

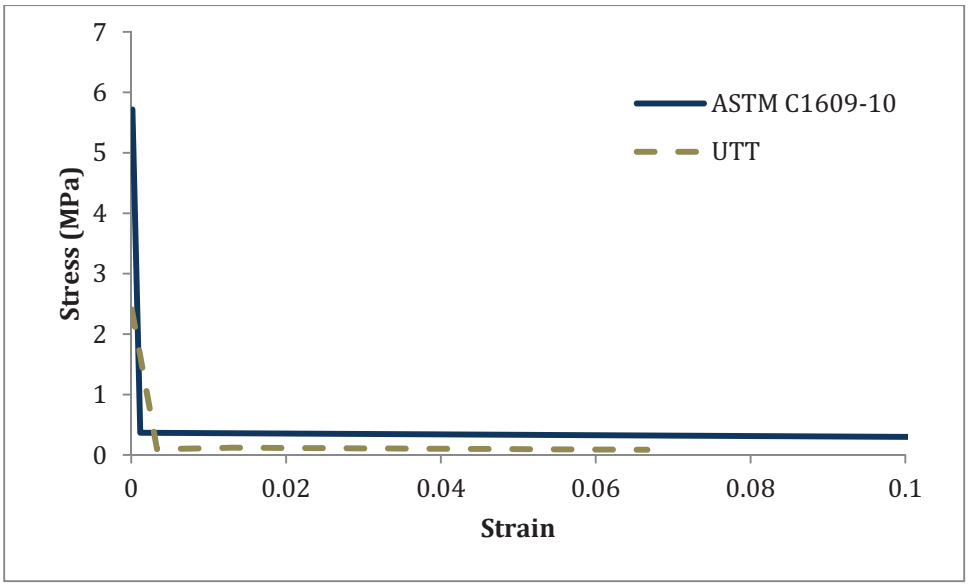

Figure F.16 – Comparison of σ–ε responses: HDPE, 5% PVDF, and 10% MAH, 3.0 kg/m³.

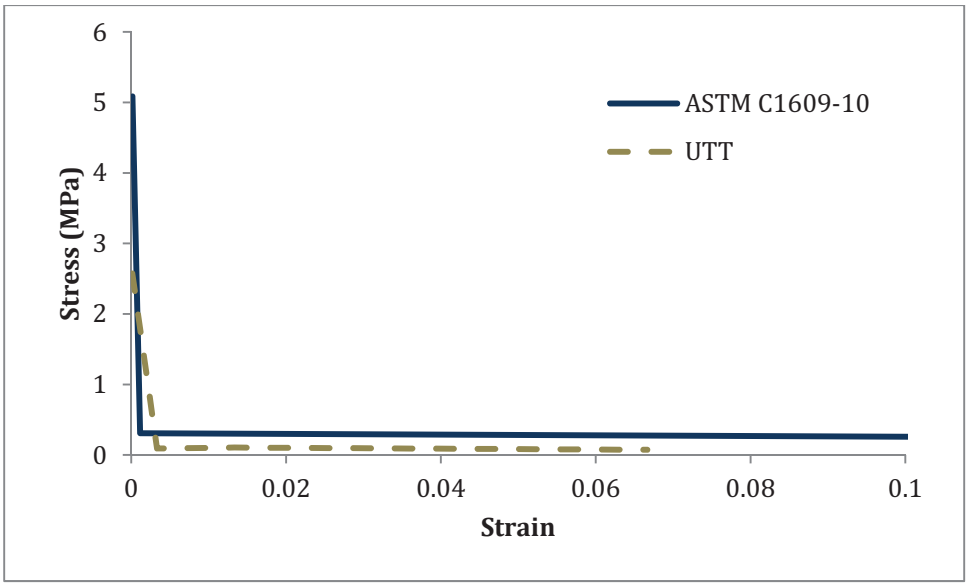

Figure F.17 – Comparison of σ–ε responses: HDPE, 11% PVDF, and 20% MAH, 3.0 kg/m^3.

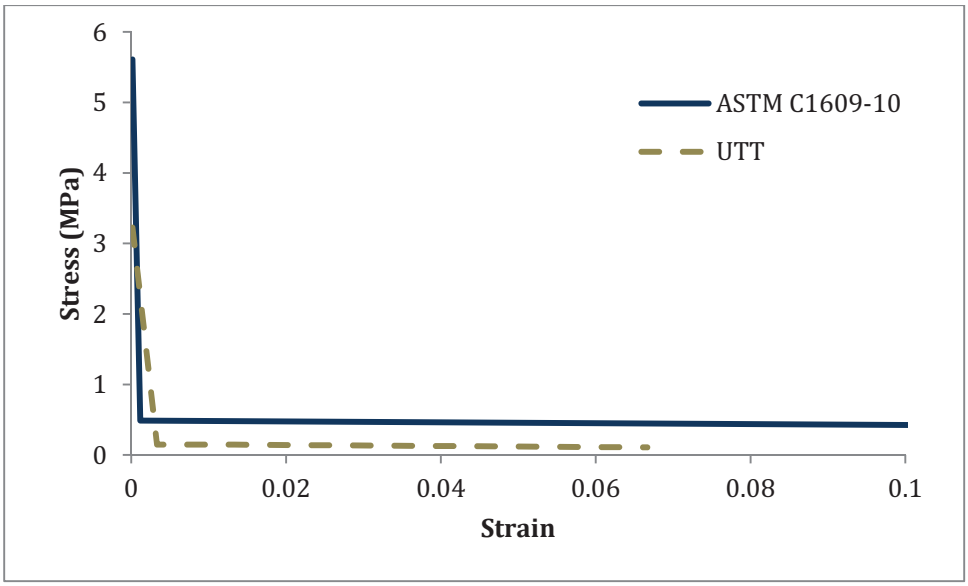

Figure F.18 – Comparison of σ–ε responses: 80% PP, 10% PE, and 10% EVA, 3.0 kg/m^3.

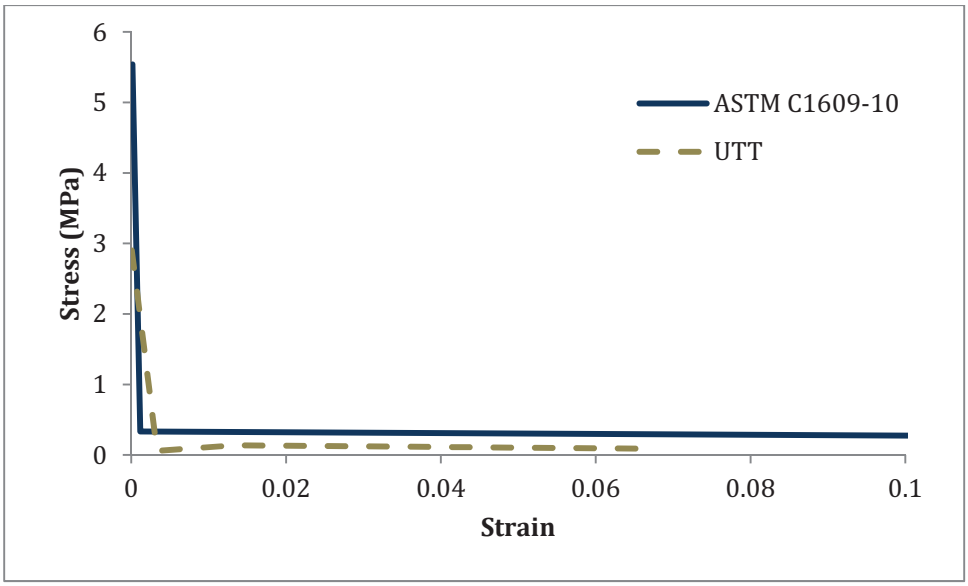

Figure F.19 – Comparison of σ–ε responses: 100% HDPE, 3.0 kg/m^3.

APPENDIX G – ADDITIONAL PLOTS FOR COMPARISON OF FLEXURAL RESPONSE

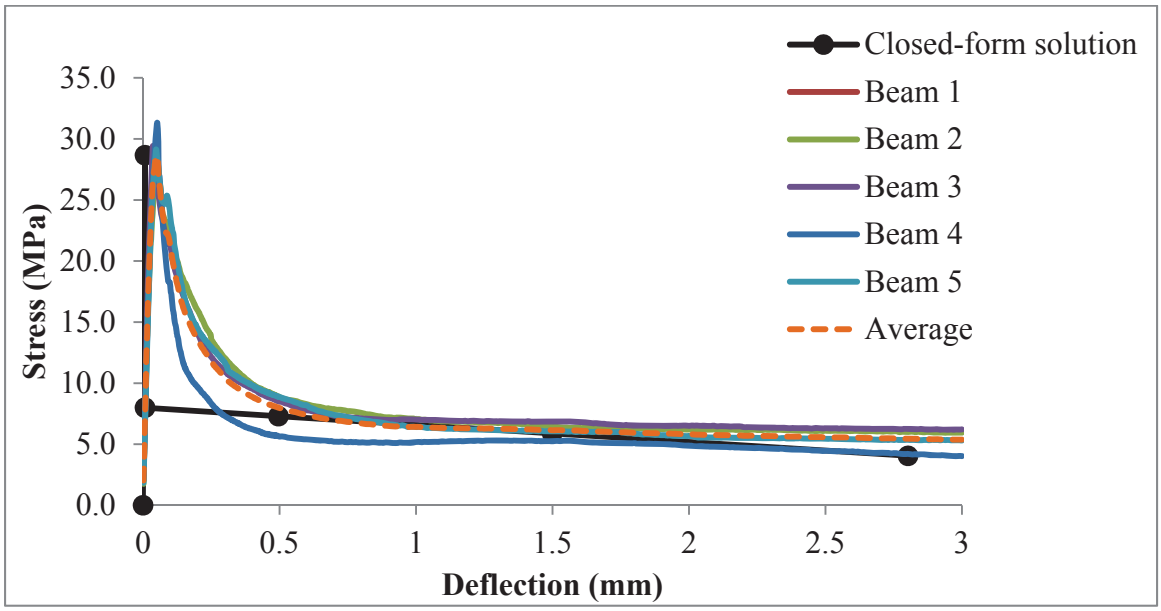

Figure G.1 – Comparison of flexural responses: Tuf-Strand SF (mix truck), 1.8 kg/m^3.

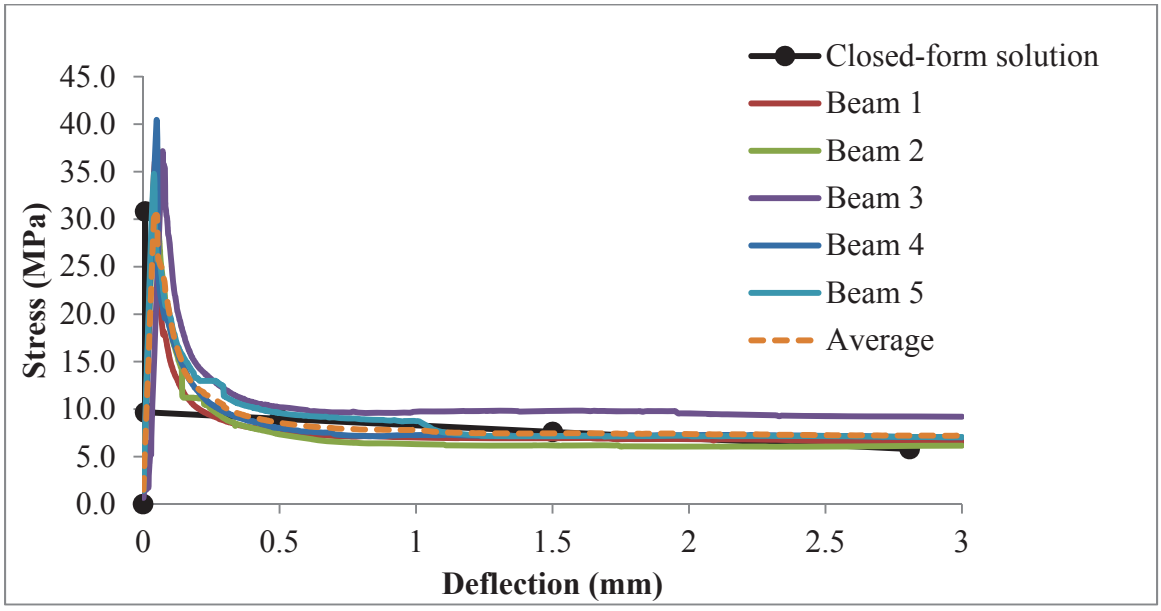

Figure G.2 – Comparison of flexural responses: Tuf-Strand SF (mix truck), 2.4 kg/m^3.

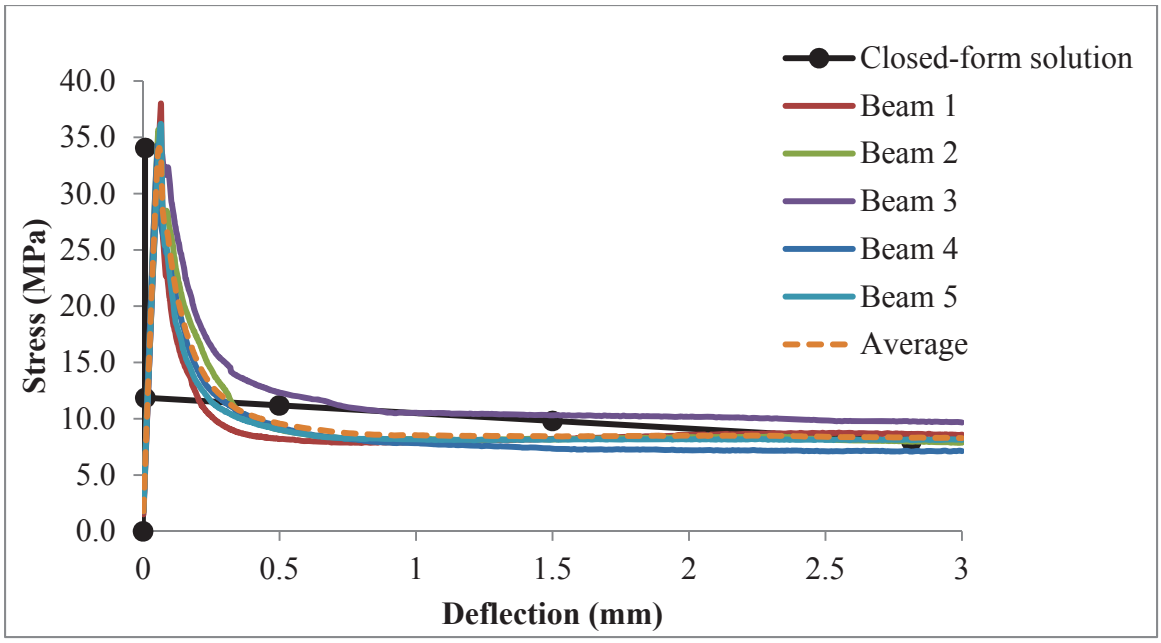

Figure G.3 – Comparison of flexural responses: Tuf-Strand SF (mix truck), 3.0 kg/m³.

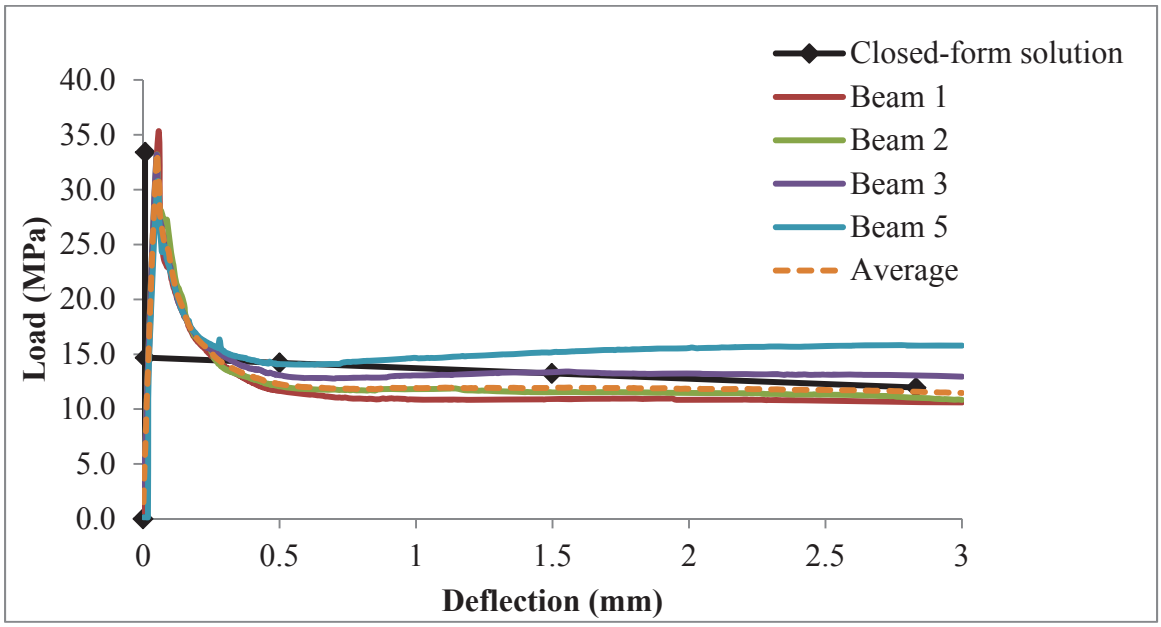

Figure G.4 – Comparison of flexural responses: Tuf-Strand SF (mix truck), 4.6 kg/m³.

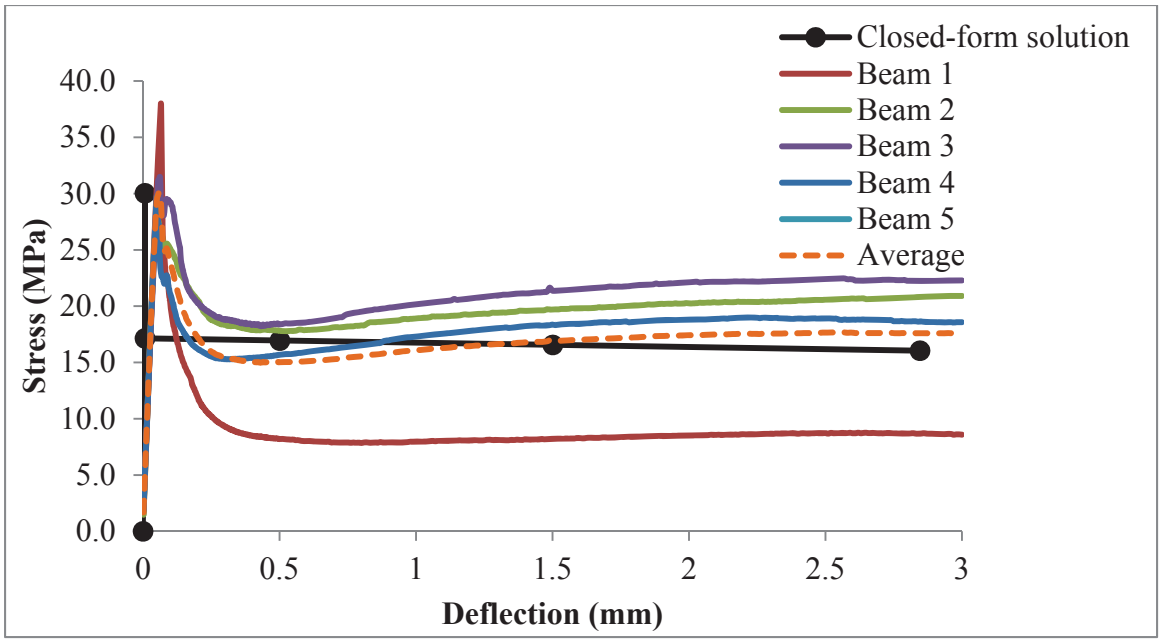

Figure G.5 – Comparison of flexural responses: Tuf-Strand SF (mix truck), 6.9 kg/m³.

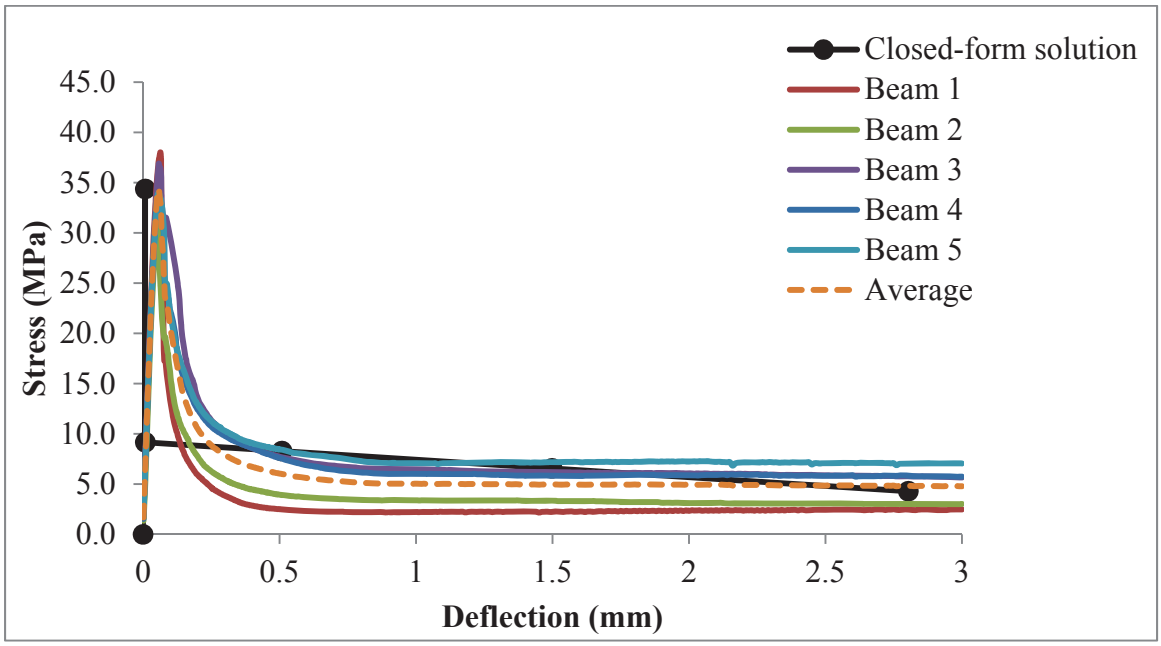

Figure G.6 – Comparison of flexural responses: Tuf-Strand SF (drum mixer), 1.8 kg/m³.

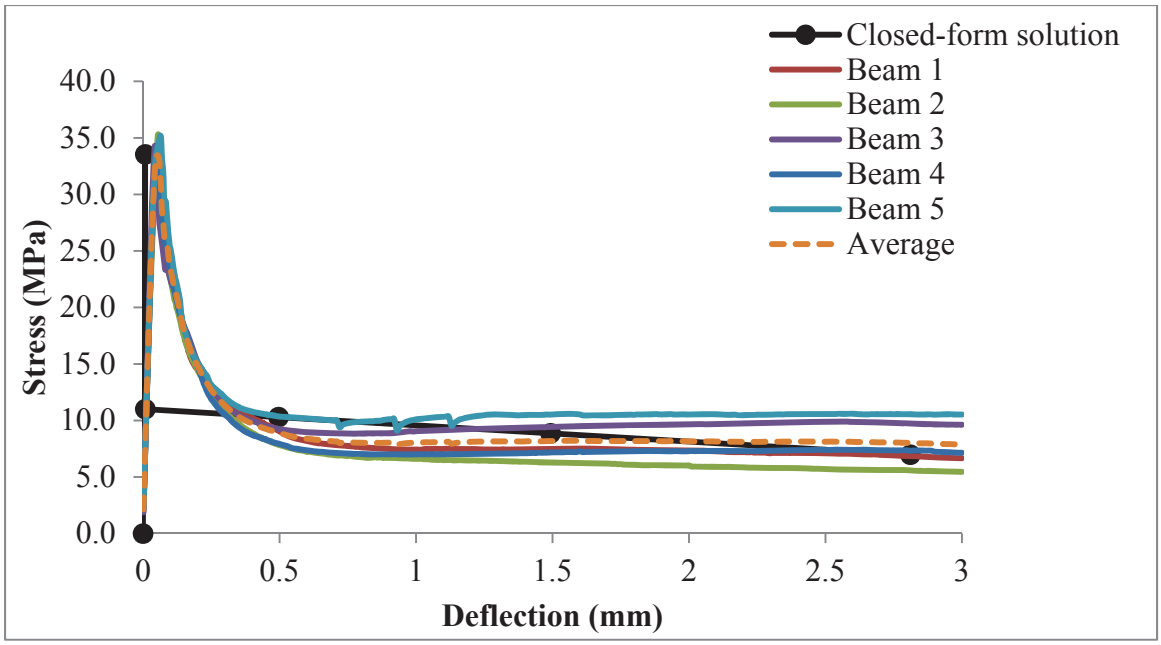

Figure G.7 – Comparison of flexural responses: Tuf-Strand SF (drum mixer), 3.0 kg/m^3.

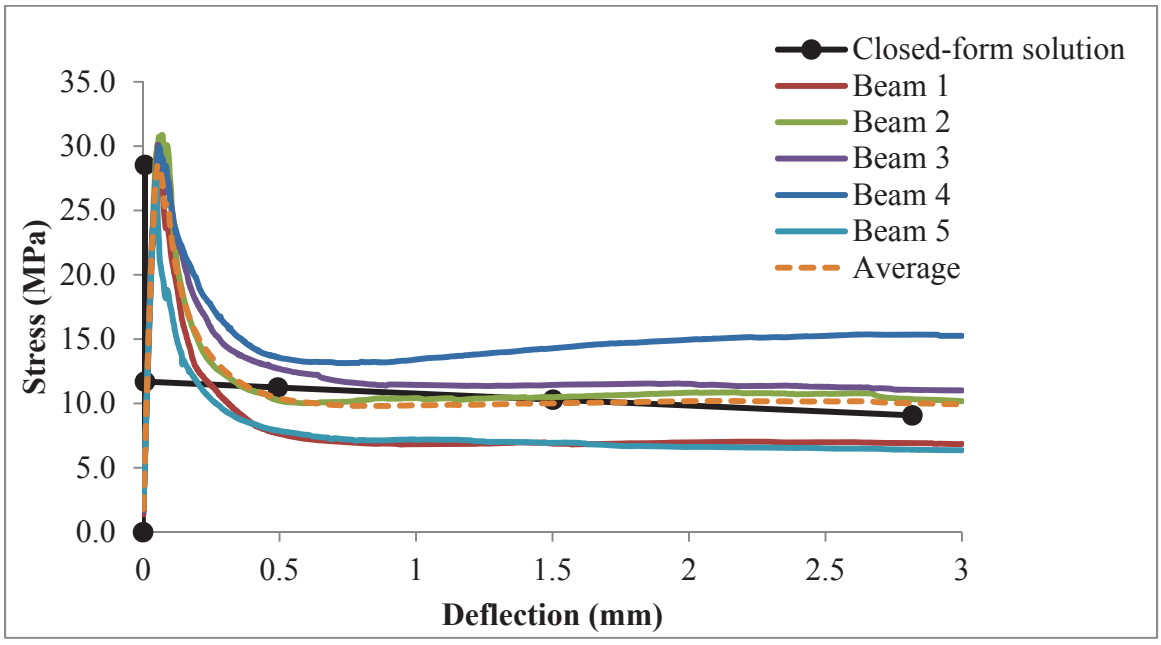

Figure G.8 – Comparison of flexural responses: Tuf-Strand SF (drum mixer), 4.6 kg/m^3.

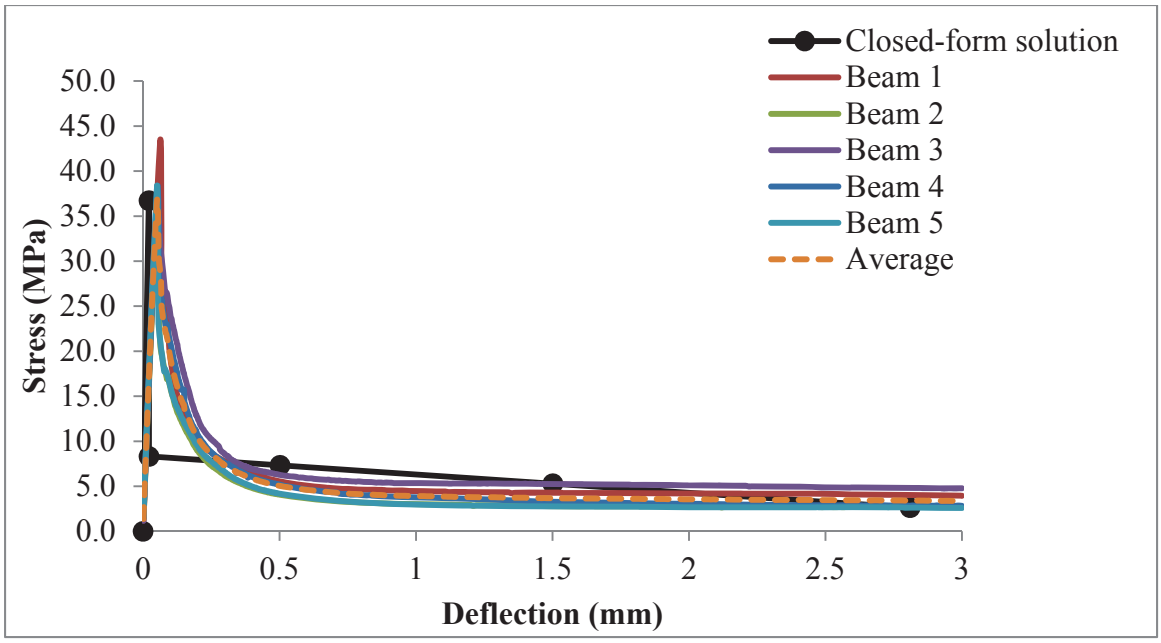

Figure G.9 – Comparison of flexural responses: HDPE and 10% EVA, 1.8 kg/m^3, 38 mm length.

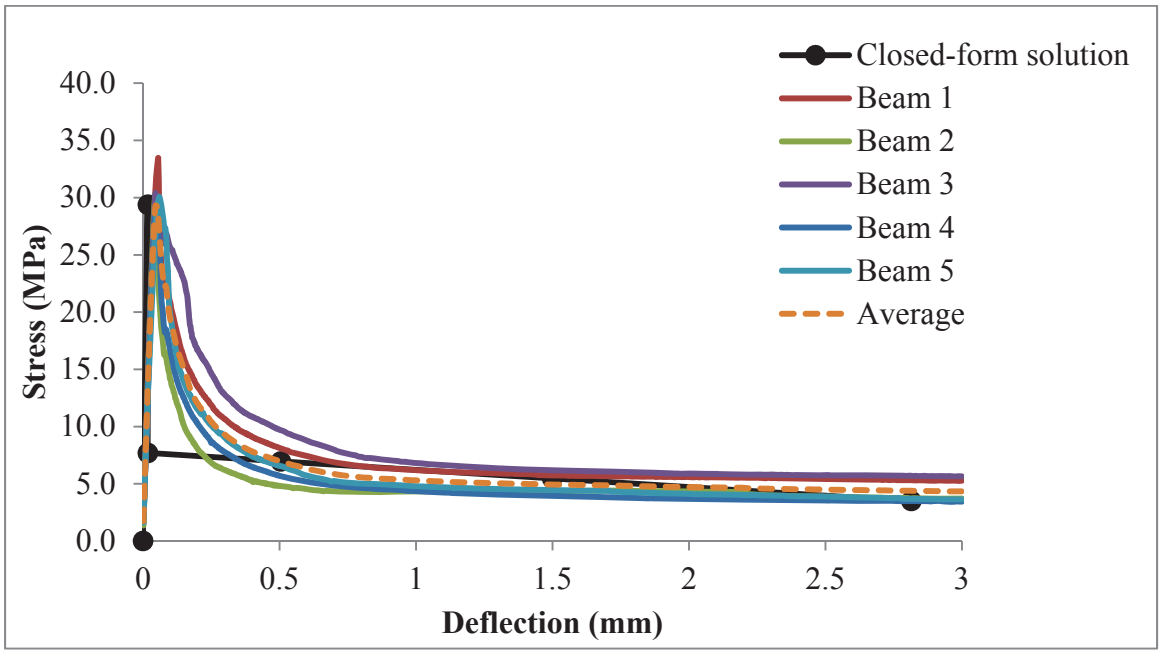

Figure G.10 – Comparison of flexural responses: HDPE and 10% EVA, 3.0 kg/m^3, 38 mm length.

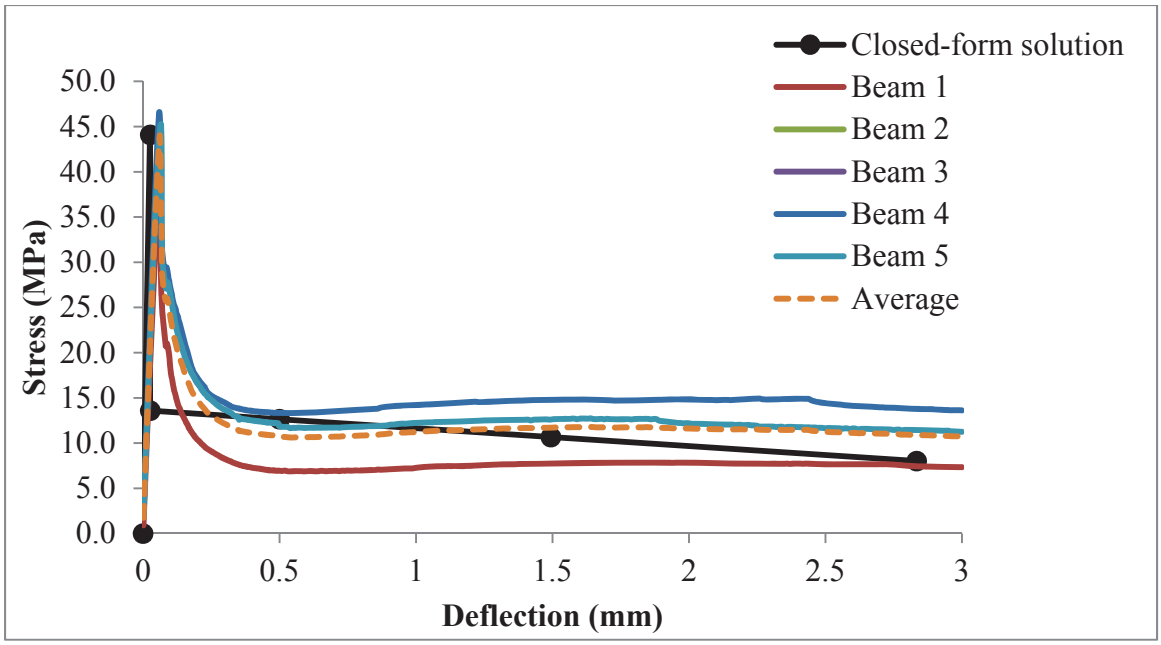

Figure G.11 – Comparison of flexural responses: HDPE and 10% EVA, 4.6 kg/m^3, 38 mm length.

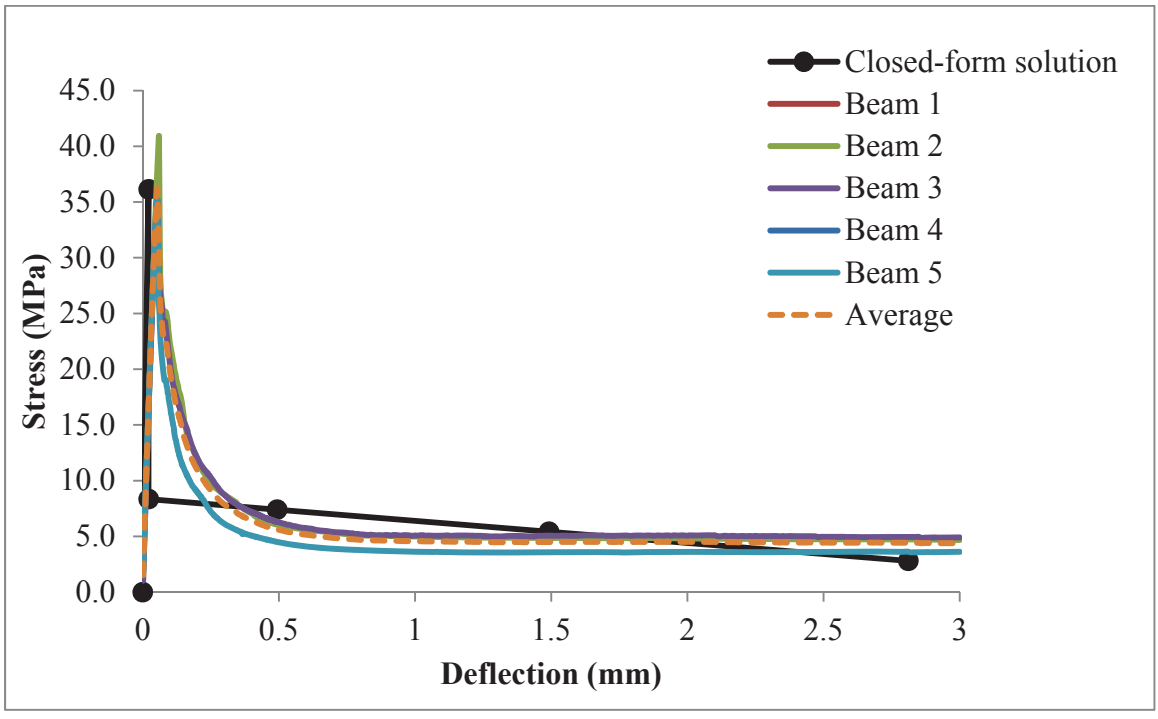

Figure G.12 – Comparison of flexural responses: HDPE and 10% EVA, 1.8 kg/m^3, 50 mm length.

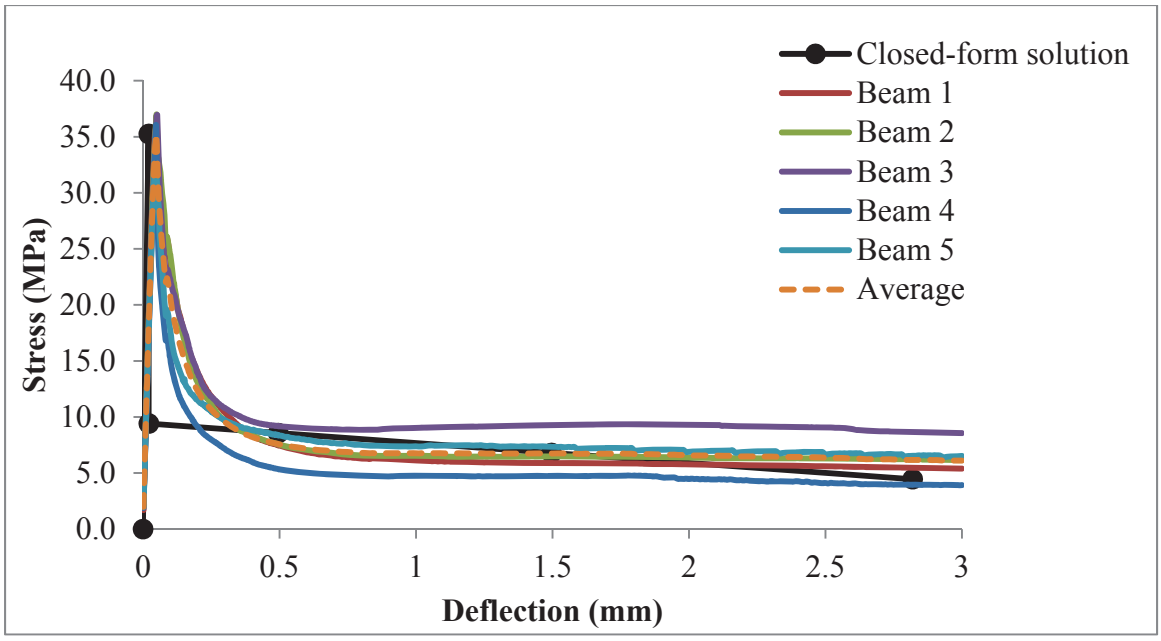

Figure G.13 – Comparison of flexural responses: HDPE and 10% EVA, 3.0 kg/m^3, 50 mm length.

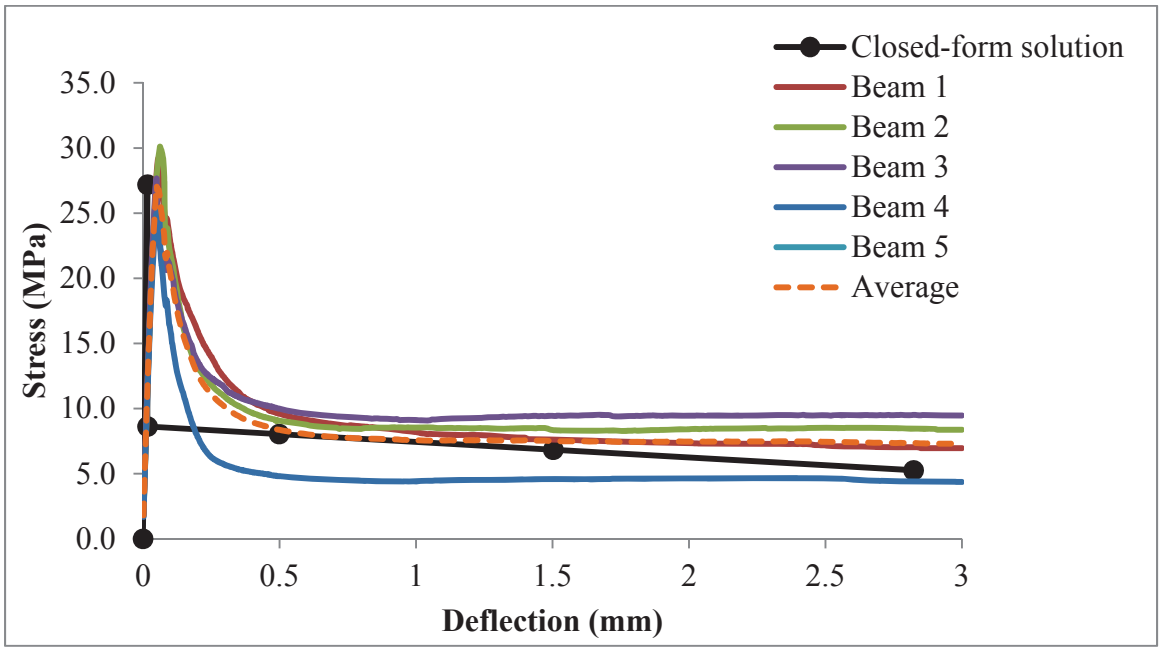

Figure G.14 – Comparison of flexural responses: HDPE and 10% EVA, 4.6 kg/m^3, 50 mm length.

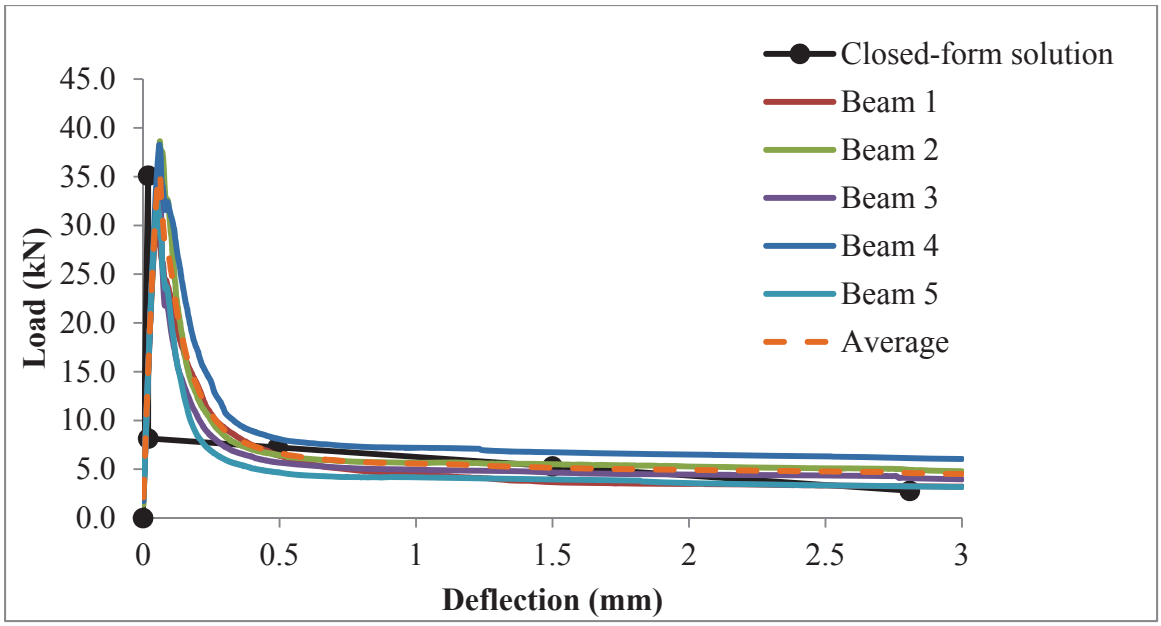

Figure G.15 – Comparison of flexural responses: HDPE and 3% PVDF, 3.0 kg/m^3.

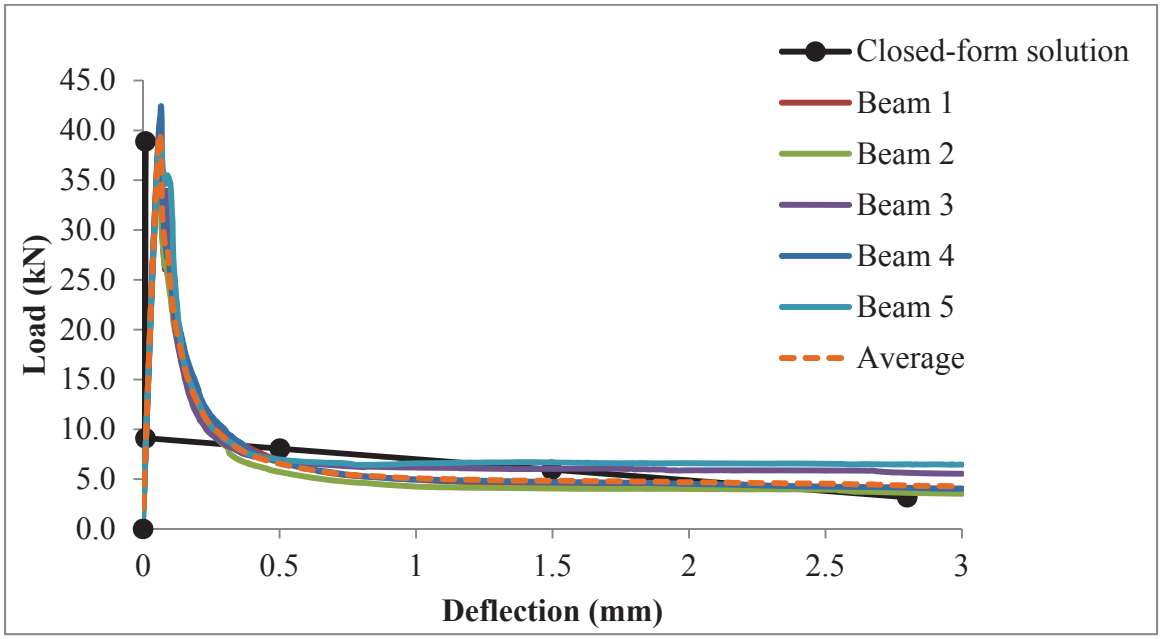

Figure G.16 – Comparison of flexural responses: HDPE, 5% PVDF, and 10% MAH, 3.0 kg/m^3.

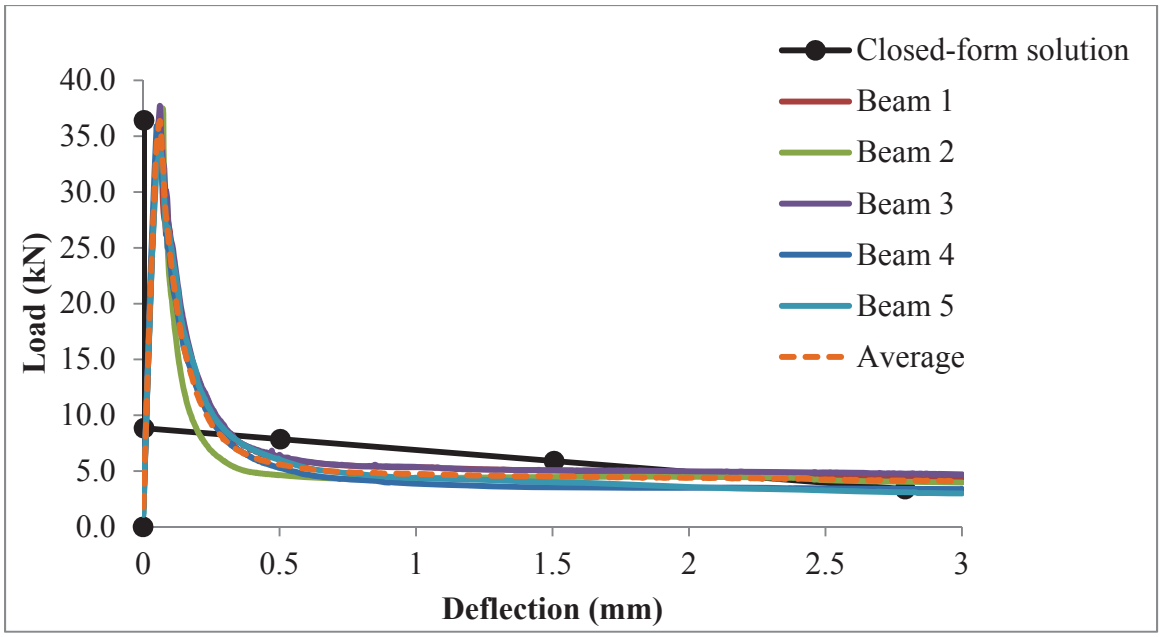

Figure G.17 – Comparison of flexural responses: HDPE, 11% PVDF, and 20% MAH, 3.0 kg/m^3.

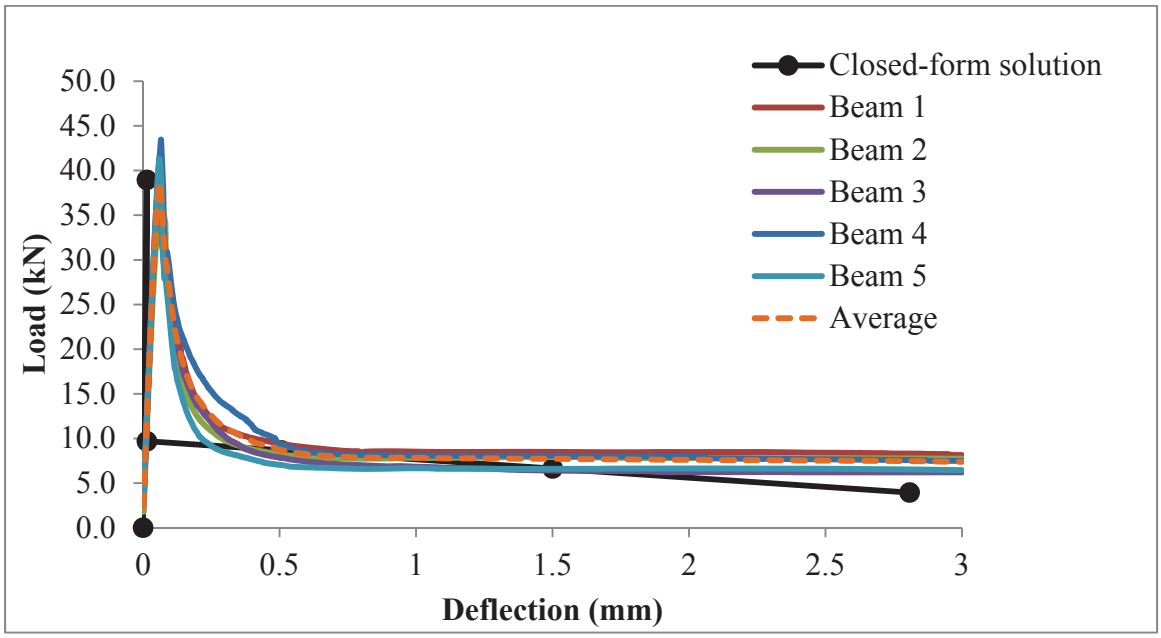

Figure G.18 – Comparison of flexural responses: 80% PP, 10% PE, and 10% EVA, 3.0 kg/m^3.

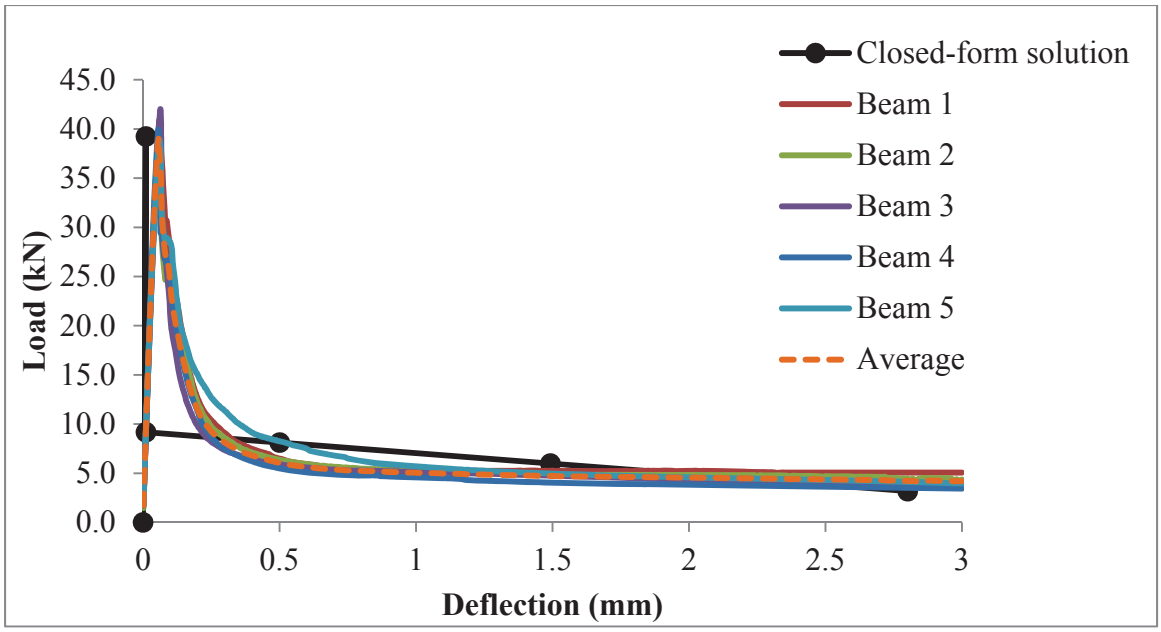

Figure G.19 – Comparison of flexural responses: 100% HDPE, 3.0 kg/m^3.